

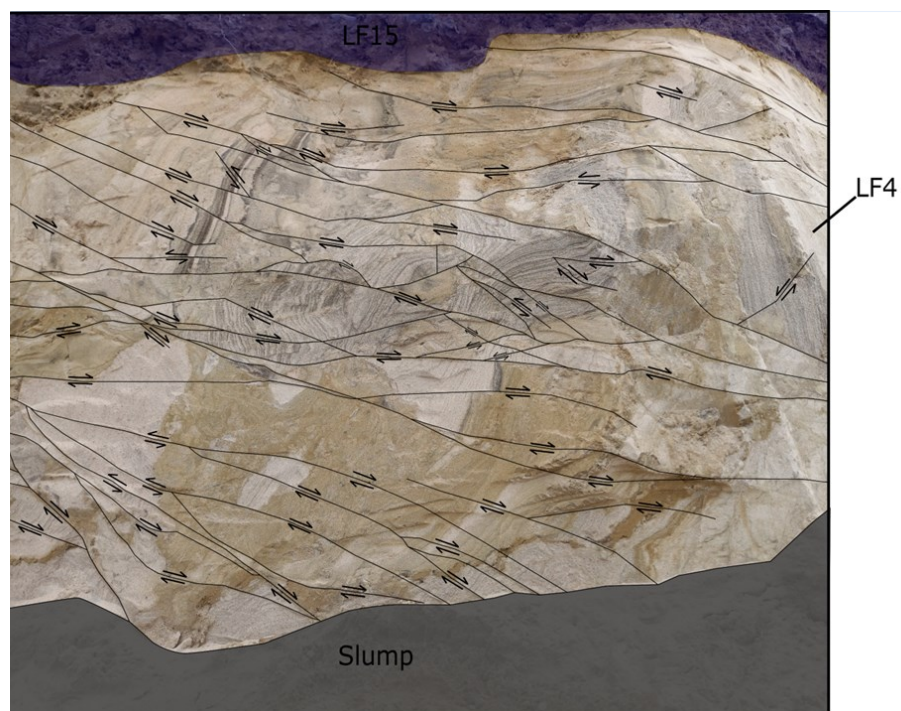
# The glaciotectonic evolution of Ven, Sweden: insights from a comprehensive structural, sedimentological, and geomorphological analysis

***Sebastian Nilsson***

Dissertations in Geology at Lund University,

Master's thesis, no 674

(45 hp/ECTS credits)



Department of Geology  
Lund University  
2024



# **The glaciotectonic evolution of Ven, Sweden: insights from a comprehensive structural, sedimentological, and geomorphological analysis**

Master's thesis  
Sebastian Nilsson

Department of Geology  
Lund University  
2024

# Contents

|   |           |
|---|-----------|
| <b>1 Introduction</b> .....   | <b>7</b>  |
| <b>2 Aim of study</b> .....   | <b>7</b>  |
| <b>3 Litterature review of previous studies on Ven</b> .....                                      | <b>7</b>  |
| <b>4 Methods</b> .....  | <b>9</b>  |
| 4.1 Geomorphological mapping  | 9         |
| 4.2 Fieldwork based material and methods  | 10        |
| <b>5 Results</b> .....  | <b>10</b> |
| 5.1 Geomorphological mapping  | 10        |
| 5.2 Overview of the glacial sedimentology of Ven´s NW cliff exposures                             | 15        |
| 5.2.1 Lithofacies 1   | 22        |
| 5.2.2 Lithofacies 2   | 25        |
| 5.2.3 Lithofacies 3   | 25        |
| 5.2.4 Lithofacies 4   | 26        |
| 5.2.5 Lithofacies 5   | 27        |
| 5.2.6 Lithofacies 6   | 27        |
| 5.2.7 Lithofacies 7   | 27        |
| 5.2.8 Lithofacies 8   | 29        |
| 5.2.9 Lithofacies 9   | 31        |
| 5.2.10 Lithofacies 10   | 32        |
| 5.2.11 Lithofacies 11   | 32        |
| 5.2.12 Lithofacies 12   | 37        |
| 5.2.13 Lithofacies 13   | 37        |
| 5.2.14 Lithofacies 14   | 41        |
| 5.2.15 Lithofacies 15   | 41        |
| <b>6 Fine gravel analysis</b> .....   | <b>41</b> |
| <b>7 Interpretation of depositional environments</b> .....  | <b>43</b> |
| <b>8 Lithostratigraphy of Ven</b> .....   | <b>45</b> |
| <b>9 Tectonic evolution of Vens strata</b> .....  | <b>49</b> |
| <b>10 Conceptual model for the tectonic evolution of the norhern cliff exposures of Ven</b> ..... | <b>53</b> |
| <b>11 Discussion</b> .....  | <b>57</b> |
| <b>12 Conclusion</b> .....  | <b>61</b> |
| <b>13 Acknowledgements</b> .....  | <b>62</b> |
| <b>14 References</b> .....  | <b>62</b> |

**Cover Picture:** Complex system of riedel shears. Picture taken by Sebastian Nilsson.

# The glaciotectonic evolution of Ven, Sweden: insights from a comprehensive structural, sedimentological, and geomorphological analysis

Sebastian Nilsson

Nilsson, S., 2024: The glaciotectonic evolution of Ven, Sweden: insights from a comprehensive structural, sedimentological, and geomorphological analysis. *Dissertations in Geology at Lund University*, No. 674, 77 pp. 45 hp (45 ECTS credits) .

**Abstract:** This study presents the results from the first detailed structural analysis of glaciotectonic structures of the northern cliff exposures on Ven alongside the first coherent interpretation of the glaciotectonic evolution of the island. Additionally, the study presents the findings of the first geomorphological mapping of surface features on Ven. The primary objective of this study was to fill gaps in our knowledge regarding the influence of successive advancements of the SIS in the area and address previous claims regarding the surface geomorphology of the island. This was accomplished using a standard sedimentological and geomorphological approach along with detailed structural investigations of glaciotectonic structures.

Fifteen distinct lithofacies were identified throughout the northern cliff exposure, which can be summarized as three subglacial till beds connected to the two last glacial advances of the SIS during the late Weichselian, separated by discontinuous layers of deformed outwash and glaciolacustrine deposits. Overall, the interpreted sedimentary succession is interpreted to represent the upper sedimentary succession of the Alnarp Valley fill, one of Scania's most valuable groundwater resources. Measurements of deformational structures alongside the sedimentological revealed a substantial glaciotectonic influence from the last two glacial advances on island's stratigraphic succession. The findings show that our preexisting knowledge pertaining to the glaciotectonic evolution of the island only show a simplistic overview. This study presents two conceptual models to explain the evolution of the glaciotectonic structures and the sedimentological findings seen in the northern cliff exposures.

Furthermore, previous claims of Ven being a prime example of a cupola hill complex could not be entirely dismissed but are shown to be an unlikely interpretation based on the evidence from the geomorphological analysis of the island. Additionally, 10 subtle long-stretched ridges are located throughout the island's otherwise flat surface. The origin of these ridges could not be determined but are postulated to be derived from agricultural activities.

This study concludes that additional analysis of the Alnarp valley fill, employing alternative investigative techniques like seismic and ground-penetrating radar, is necessary. Glaciotectonic structures within these sediments are likely overlooked due to the predominant use of sedimentary coring. Furthermore, continued exploration of Ven is recommended to gain a comprehensive understanding of the island's glaciotectonic evolution.

**Keywords:** Glaciotectonic structures, Structural analysis, Sedimentological analysis, Geomorphological mapping, Deformational structures, Cupola hill complex, Alnarp valley fill, Glaciotectonic evolution, Glaciotectonism

**Supervisor(s):** Sven Lukas

**Subject:** Quaternary Geology

*Sebastian Nilsson, Department of Geology, Lund University, Sölvegatan 12, SE-223 62 Lund, Sweden. E-mail: nilssonsebastian7@gmail.com*

# Den glaciotehtoniska utvecklingen av Ven, Sverige; Insikter från en omfattande strukturell, sedimentologisk och geomorfologisk undersökning

SEBASTIAN NILSSON

Nilsson, S., 2024: The glaciotehtonetic evolution of Ven, Sweden: insights from a comprehensive structural, sedimentological, and geomorphological analysis. *Examensarbeten i geologi vid Lunds universitet*, Nr. 674, 77 sid. 45 hp.

**Sammanfattning:** Denna studie presenterar resultaten från den första detaljerade strukturanalysen av glaciotehtoniska strukturer på de norra klippexponeringarna på Ven tillsammans med den första sammanhängande tolkningen av öns glaciotehtoniska utveckling. Dessutom presenterar studien resultaten av den första geomorfologiska kartläggningen av land former på Ven. Det primära syftet med denna studie var att fylla kunskapsluckor gällande påverkan av successiva framsteg av SIS i området och adressera tidigare påståenden angående öns morfologi. Detta uppnåddes med hjälp av en standard sedimentologisk och geomorfologisk metodik tillsammans med detaljerade strukturella undersökningar av glaciotehtoniska strukturer.

Femton distinkta litofacies identifierades genom hela de norra klippexponeringarna, vilket kan sammanfattas som tre subglaciala tillsångar som är kopplade till de två senaste glaciala framstegen av SIS under sena Weichsel, åtskilda av diskontinuerliga lager av deformerade avrinnings- och glaciolakustrina avlagringar. Övergripande tolkas den sedimentära successionen som den övre sedimentära successionen av Alnarp dalen, en av Skånes mest värdefulla grundvattenresurser. Mätningar av deformerande strukturer tillsammans med sedimentologin avslöjade en betydande glaciotehtonisk påverkan från de två senaste glaciala framstegen på öns stratigrafiska succession. Resultaten visar att vår befintliga kunskap om öns glaciotehtoniska utveckling endast ger en förenklad översikt. Denna studie presenterar två konceptuella modeller för att förklara utvecklingen av glaciotehtoniska strukturer och de sedimentologiska fynden i de norra klippexponeringarna.

Vidare kunde tidigare påståenden om att Ven skulle vara ett utmärkt exempel på en cupola hill inte helt avfärdas, men visar sig vara en osannolik tolkning baserat på bevis från den geomorfologiska analysen av ön. Dessutom finns det 10 subtila långsträckta åsar som finns genom öns annars platta yta. Ursprunget till dessa åsar kunde inte fastställas men antas vara härledda från jordbruksaktiviteter.

Denna studie drar slutsatsen att ytterligare analyser av sedimenten i Alnarp dalen med användning av alternativa undersökningsmetoder som seismik och markpenetrerande radar, är nödvändiga. Glaciotehtoniska strukturer inom dessa sediment tros vara förbisedda på grund av den dominerande användningen av borrhning. Vidare rekommenderas fortsatt utforskning av Ven för att få en omfattande förståelse av öns glaciotehtoniska utveckling.

**Nyckelord:** Glaciotehtoniska strukturer, Sedimentologisk analys, Geomorfologisk kartläggning, Deformationsstrukturer, Cupola hill, Alnarp Dalen, Glaciotehtonisk evolution, Glaciotehtonism

**Handledare:** Sven Lukas

**Ämnesinriktning:** Quaternary Geology

*Sebastian Nilsson, Geologiska institutionen, Lunds Universitet, Sölvegatan 12, 223 62 Lund, Sverige. E-post: nilssonsebastian7@gmail.com*

# 1 Introduction

The Quaternary period, comprising the Pleistocene (2.6 Ma to 11.7 ka) and the Holocene (11.7 ka to present) series, is characterised by repeated glacial and interglacial climate cycles, which caused the growth and decay of ice sheets in the Northern Hemisphere (NH) (Willieit et al., 2019; Batchelor et al., 2019; de Boer & van de Wal, 2021). The early stages of the Pleistocene (2.6–0.8 Ma) were characterized by short glacial cycles to insubstantial too produce large ice sheets in the NH (Ehlers et al., 2018). It was not until the mid-Pleistocene transition between roughly 1.25 and 0.7 Ma, that there was a shift in cyclicity in the dominant periodicity regime to the 100 ka orbital cycle (Willieit et al., 2019; Baker et al., 2022), which caused long-lasting glacial cycles enabling the formation of large continental ice sheets in the NH.

Subsequent glacial periods during the Pleistocene saw the formation of the Scandinavian Ice Sheet (SIS) with its accumulation area in the Scandinavian Mountain range. The SIS has on numerous occasions during the Quaternary covered large parts of Sweden, Finland and the NW Russian plain and reached its last glacial maximum during the late Weichselian period (26–20 ka). Several periods of glacial advance and retreat of the SIS have moulded and shaped the northern European landscape into its current form. Understanding how subsequent SISs have altered and structured the sediment succession of the landscape has proven to be vital for improvements in our understanding of glacial dynamics and glacial processes. The study of glacial and interglacial sediments has also been shown to have had huge societal applications, in terms of infrastructure, agriculture and understanding groundwater systems (Lloyd 1983; Freeze and Cherry, 1979; Engel, 1914; Saad, 2008; Earle, 2019).

Ven is a small island between Sweden and Denmark in the middle of the Öresund strait (Fig. 1) and consists entirely of Quaternary deposits directly deposited on the bedrock (Adriellsson, 1984). These Quaternary deposits have a thickness of 110 m on the island, whereas merely 50 m of this are exposed above sea level (Adriellsson, 1984). The Quaternary deposits at Ven are part of the Alnarp valley fill, a Quaternary sediment-filled graben complex, which is one of Scania's most valuable groundwater resources, consisting of fine-grained fluvial deposits known as the Alnarp-sediment, overlain by and interfingering with different till beds (Ringberg, 1980; Gustafsson, 1983). The Quaternary deposits at Ven can be found clearly exposed and easily accessible along parts of the coastline of Ven, making it a suitable site for detailed sedimentological studies.

Several sedimentological studies have been done on coastal outcrops with exposed Pleistocene sediment all around Northern Europe in countries such as Sweden, Denmark, Poland, Norway, and Germany (Krzyszowski & Koszka-Maron 2018; Hoffmann & Reichert, 2012; Houmark-Nielsen, 1994; Raunholm et al., 2002). However, even though there is a high possibility for detailed studies to reconstruct the island's local deposition history, Adriellsson (1984), just

under 40 years ago, conducted and published the last detailed sedimentological study of the island with a focus on establishing a lithostratigraphy and interpreting the paleoenvironmental conditions during the time of deposition of the categorised units in the Ven-Glumslöv area. Despite Adriellsson's (1984) effort and other previous studies (Erdmann, 1883; Holmström 1879; Markgren, 1961), still much remains to be understood concerning the extent of the deformation of the glacial sediments on the islands caused by the advancement of the SIS during the late Weichselian. Thus, new studies are needed to get a deeper insight into the formation and evolution of Ven's strata.

Furthermore, Ven has been stated by Aber et al. (1989) to be a prime example of a glaciotectionic phenomenon called cupola hills, which are defined as irregular hills consisting of glacially reworked Quaternary sediments, commonly found in regions composed of soft sediments that have been the subject of multiple glacial advances. As such, a cupola hill is characterised by a disconnection between surface features and sedimentary units, because the final shaping of the land surface postdates the initial deformation at depth and so leaves local to regional unconformities (Phillips, 2018). However, Aber et al.'s (1989) statement was made without scientific backing except for referencing parts of Adriellsson's (1984) sedimentological study, which in turn does not provide any such data in support of this (re-)interpretation. Aber et al.'s (1989) statement has since been incorporated into more recent textbooks such as Evans and Benn (2010) and Phillips (2018), in both cases without further scrutiny, which makes the need for an independent reassessment of Ven's sedimentary record more pressing.

Due to the two aforementioned gaps in our understanding, a re-investigation of the cliffs on Ven is overdue.

## 2 Aim of study

To close aforementioned gaps, this study aims to further improve our understanding of the glacial deposits at Ven through renewed investigations that emphasize the use of structural geological methods and employ a systematic detailed sampling approach. The main objective of this study is to understand the influence of successive advancements of the SIS in the area. This will be achieved through: 1. Mapping of any surface features on the island, enabling thorough testing of hypotheses; 2. Systematic sedimentological logging of different lithofacies as they are currently exposed, partly to allow a comparison with the changed cliff-lines from Adriellsson (1984); 3. Investigation of glaciotectionic signatures preserved in the stratigraphy; 4. Reconstruction of both palaeo-ice flow and palaeo-ice dynamics throughout the sections on Ven through time; 5. To test the glaciotectionic hypotheses posed in previous publications.

## 3 Literature review of previous studies on Ven



Figure 1. A) Overview map of the location of Ven marked with the small red box. The black lines mark the outline of the Alnarp valley. B) Aerial photograph of Ven. The red box shows the position of the closed-up photo of “C”. C) Close-up aerial photo to showcasing the locations of the studied cliff sections. The red line marks the location of Section 1 and the green line and blue line marks the location of Section 2 and 3. Aerial photograph: ©Lantmäteriet 2019.

The quaternary deposits at Ven have previously examined by Holmström (1879), Erdmann (1883), Markgren (1961), Rasmussen (1973), and most recently by Adrielsson (1984). The earlier research, following Adrielsson's (1984) studies, primarily focused on small-scale sedimentological analyses and papers addressing broad observations of cliff sections.

Holmström (1879) observed the stratigraphy of the eastern side of Ven and found that it was largely made of a blackish-gray till overlain by a yellow till bed. These till beds were occasionally found to be separated by well sorted, deformed layers of sand (Holmström, 1879). Holmström (1879) found a significant difference in lithological makeup between the two till beds, where the blackish-gray till was noted to lack any inclusions of sedimentary rocks such as shale and chalk, while the upper yellowish till bed was found to contain a substantial amount of these lithologies. This discrepancy was later attributed by Holmström (1879) to have been caused by differences in the source material's provenance, brought to the

island by ice sheets with two different flow directions. Holmström (1879) tentatively proposed that the lower till bed was deposited from an ice sheet flowing from the N-NE, while the upper till was deposited by an ice sheet that traversed upwards through Oresund from the SE to NW. These directions of ice movement of the ice sheet that deposited the two till beds initially proposed by Holmström (1879), in later studies correlated to the main glacial advance and the young Baltic ice advance dating back to the late stages of the Weichselian (Johnsson, 1956; Markgren 1961; Rasmussen 1973; Adrielsson 1984).

Erdmann (1883) continued with the study of the stratigraphy of the Ven and Glumslöv area, examining 5 different cliff sections located throughout the NNE coast and the western coast of Ven in combination with several cliff exposures along the cliffs of Glumslöv. Much like Holmström (1873), Erdmann (1883) found the same two till beds in the same stratigraphic position, but Erdmann also found that the upper till bed predominantly laid with an unconformity above a thick



bed of deformed sandy clay in most of the studied cliff sections. This overarching stratigraphic sequence by Holmström (1879) and Erdmann (1883) were later also found in the southern and southwestern part of the Island by Rasmussen (1973). Prior to Adrielsson (1984) the stratigraphy of the island was predominantly understood through several small-scale sedimentological studies as seen above, and it was not until after that a well-rounded understanding of the stratigraphy sequence of Ven was achieved and separated into different groups representing different paleoenvironmental conditions.

The northern tip of Ven, where this study was located, has exclusively only been studied in detail by Adrielsson (1984), and was determined to consist of three lithofacies association named Västernäs till member, Laebrink till member and the Glumslövs member.

The Glumslöv member is seen deformed across large parts of the island's cliff exposures consisting of a mixture of sand, clay and silt, and is correlated to be the same unit discussed by Erdmann (1883) in the NNE sites. The silt and clay beds were found by Adrielsson (1984) to be occasionally massive but mostly laminated to cross-laminated containing occasional outsized clasts. The sands are either planar laminated or cross-bedded (Adrielsson, 1984). The Glumslöv member was interpreted to be derived from a braided river environment and a glacial lake environment (Adrielsson, 1984).

The Västernäs till member was characterized to consist of three beds of diamicts interwoven with discontinuous facies of sand and gravel (Adrielsson, 1984). The blackish-gray till bed and the sorted sediment located on top of the till, described by both Holmström (1879) and Erdmann (1883), was correlated to this member by Adrielsson (1984). The different beds of diamicts were subdivided by Adrielsson (1984) into a basal part consisting of a homogenous fissile diamict with inclusions of stringers of sand, followed by a homogenous diamict, and lastly the upper partly stratified diamict. The sorted beds of gravel and sand were located between the upper diamict and the middle diamict in synformal depression formed in the upper part of the basal diamict (Adrielsson, 1984). Three fabric measurements were taken in the basal part of the diamict which showed a preferred clast long axis orientation towards the NW, which had 90° offset from measurements on striated boulders which were directed towards the NE (Adrielsson, 1984). All the diamicts' fine gravel composition was found to be homogenous consisting primarily of crystalline grains. The two diamicts located at the basal part of the section was interpreted as subglacial till beds and the upper diamict was interpreted as a melt out till, all of which were connected to the NE glacial advance. Furthermore, the sorted sediments

located between the two lower till beds were interpreted as sediments that had been deposited prior to the second advancement of the ice sheet. The sorted sediment on top of the melt out till consisted of a wide array of different sediments which were interpreted as outwash sediments deposited through flowing water in a braided stream environment.

The Laebrink till member at the northern sites consists of a homogenous fissile diamict which lies with an unconformity above the lower dislocated strata of the Västernäs member and the Glumslöv member (Adrielsson, 1984). The diamict shows a distinct lithological assemblage compared to the Västernäs till beds and contain high amounts of Cretaceous limestone and display a variance in the clast long axis orientation of the fabrics (Adrielsson, 1984). The diamict is interpreted as subglacial till, deposited during the young Baltic advance. Furthermore, above the homogenous fissile diamict are occasionally two additional beds of diamicts which displayed a lateral variance in texture and were interpreted as till flows (Adrielsson, 1984). This till was correlated to be the same as the basal till beds described by Holmström (1879) and Erdmann (1883).

## 4 Methods

### 4.1 Geomorphological mapping

In order to systematically inventories the landform record on Ven, geomorphological mapping was employed. Surface features such as possible ridges, lineations and scars related to mass movements were mapped using input data such LiDAR based digital elevation models (DEM) with a horizontal resolution of 1 m and a vertical resolution of 0.1 m, combined with aerial photographs, available at Lantmäteriet (Lantmäteriet, 2019). These input data were analysed and mapping conducted using the graphical user interface QGIS following the recommendations of Chandler et al. (2018), with the interpreted geomorphological features traced on the input imagery, such as the DEM.

This study used a shaded relief DEM (Hillshade) to improve the visual display of the relevant information by using a normal greyscale band. During mapping, the solar illumination (azimuth angle and solar elevation) of the DEMs was altered throughout the mapping procedure to optimise the visual information and avoid azimuth biasing, which have been shown to greatly affect the visibility of elongated features in particular (e.g. Smith, 2011). Additionally, slope, topographic and aspect maps were constructed using built-in features in QGIS from the LiDAR DEM. This was done as slope maps have been found to better highlight linear features in the landscape independent of illumination azimuth (Malmborg, 2022), and the aspect maps and topographic maps were constructed as a complement to the DEM and slope map. The conceptual workflow for the mapping of palaeo ice sheet geomor-

phological imprints presented by Chandler et al. (2018) was adopted in combination with their general recommendations for geomorphological mapping.

## 4.2 Fieldwork based material and methods

Fresh exposures through the cliff section were manually dug out using a shovel and trenching tool and then cleaned using a trowel, which exposed the undisturbed sediment beneath. After the section had been cleaned, an outline of the cliff section was drawn to scale using tape measures to ensure planimetric accuracy. The log of the cliff section was drawn in a systematic manner following Evans and Benn (2021), first focusing on broader elements such as unit boundaries and then on more progressively smaller details such as individual large boulders and distinct sedimentary structures within individual lithofacies units. In the field, different lithofacies units were identified based on their properties, e.g. grain size characteristic, sorting, sedimentary contacts, and internal sedimentary structure, which may include depositional, erosional and deformation structures. These units were then given lithofacies codes for ease of visual communication (Evans and Benn, 2010; Evans and Benn, 2021). Photographs of the cliff section were taken to compile a mosaic of the cliff section; this was later used as an overlay with the drawn outline of the cliff section in Inkscape, facilitating the addition of numerous individual clasts to the drawn sketch to further enhance its visual representation of geological features in the 2D-logs. The two-dimensional logs were later complemented by vertical profile logs, using a modified version of Krüger and Kjær's (1999) model (see Appendix A figure 1-9). Modifications to this model were made to include further information regarding fine gravel analyses (see below) as well as additional symbols of various structures and features.

To augment interpretations, quantitative data, such as clast microfabric and additional measurements on deformational structures such as folds and faults were taken and plotted in Stereonet (Allmendinger et al., 2012; Cardozo & Allmendinger, 2013), to gain a better insight into the deformation history of the sediments. A-axis fabrics was measured and plotted in Stereonet with the calculated eigenvalue (S1), using the methodology described in Benn & Lukas (2021), measuring a minimum of 50 clasts with a distinguished A-axis from a 25x25cm window. A-axis fabric measurements were done on diamicts and gravel units in the studied area to decipher possible depositional or deformational processes.

Lastly, in addition to fabric and structural measurements, several ~500 g bulk samples were collected from different units in the study area. In the laboratory, individual bulk samples were sieved to examine the lithological content of the fine gravel fraction (2-4mm) using a stereo microscope, of which a minimum of 300 grains were counted for each sample (cf. Adrielsson, 1984). Fine gravel analysis was conducted to aid in the differentiation of different diamict units and for the

determination of lithological provenance of the material.

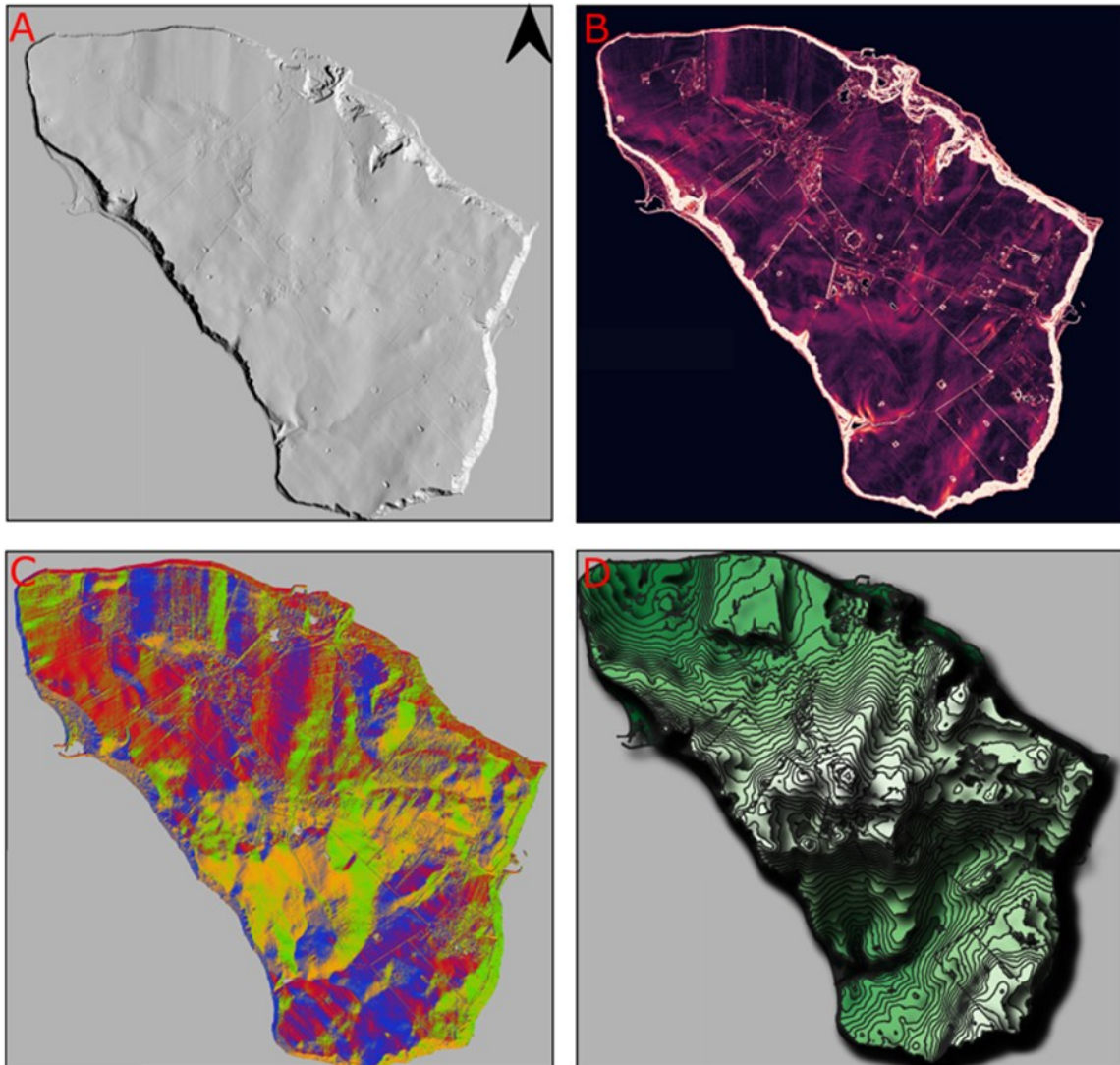
## 5 Results

### 5.1 Geomorphological mapping

The geomorphological mapping procedure revealed a rather uniform and flat surface at Ven evident from the low slope angles and the diverse aspect in respective map (Fig. 2). The highest point of the island lies around 50 m above sea level and is found in the middle of the island. Steep cliffs are found all along the perimeter of the entire island. These are nearly vertical in places, but the majority of the cliffs have a slope between 30-50°. The height of these cliffs exceeds 30 m above sea level in the southern half of the island while they do not exceed 20 m in the northern half. The average height difference between the top of the cliffs and the highest point on Ven (Fig. 2) is only around 20-30 m.

Landslide scars of various sizes can be seen around the entire coast but are concentrated along the southern and western coast of the islands (Fig. 3). Several small depressions can be seen irregularly scattered across the island and are filled with water. Additionally, long irregularly-shaped depressions can be seen in the SW part of the islands sloping toward the sea. Additional linearly-shaped depressions can also be seen in the SW and E part of the islands positioned in agricultural fields.

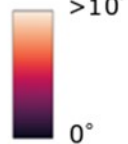
A total of 10 ridges was identified (Fig. 3). These ridges are small, not spanning more than 740 m with a gradually sloping ridge crest's of less than 10° on either side of the ridgeline (Fig. 2-3). The ridge profiles display a height of the ridges ranging between 1-5 m from its surroundings and with a width spanning between 80-250 (Figs. 4, 5). The lengths of the ridges show a great variance, with some ridges as small as 130 m in length and the largest 740 m (Fig. 4). The ridgeline of the mapped ridges has three distinct directions the most prevalent of which is SW-NE followed by SSW-NNE lastly SE-NW. The average calculated elongation ratio of the mapped ridges is 2.98 (Fig. 4), which indicates a clear elongated nature of the ridges.



**Symbology: B**

Slope map:

Degree of slope



**Aspect map: C**

Direction of slope

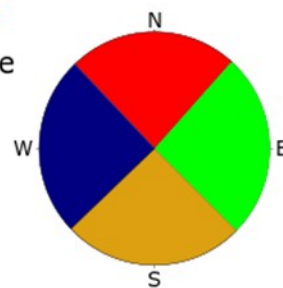
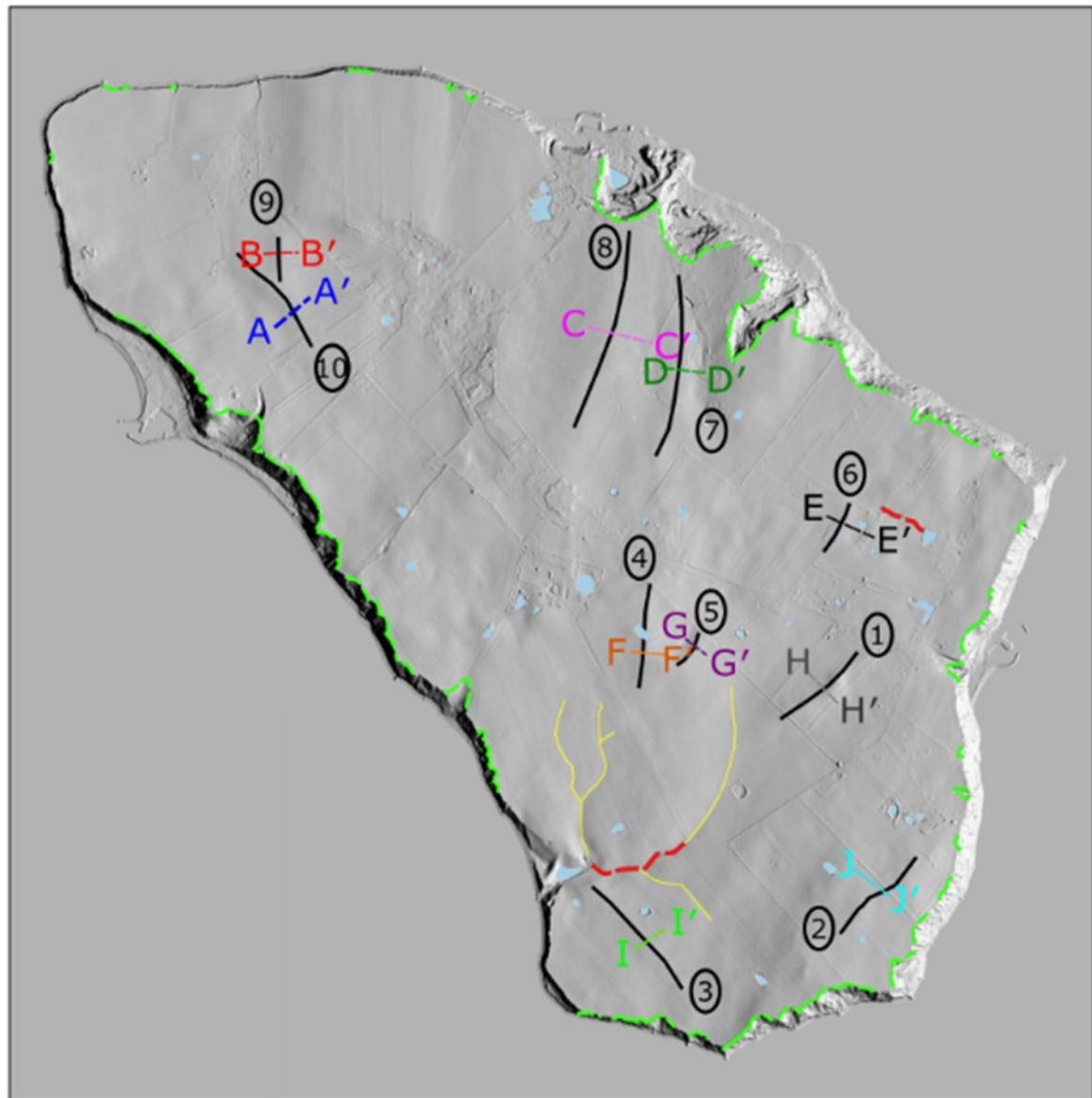


Figure 2. Maps of the island of Ven A) Hill shaded DEM. B) Slope map. C) Aspect Map. D) Topographic map



- Symbology:
- Lakes
  - - - Artificial drainage ditch
  - Paleochannel
  - - - Landslide scar
  - Ridges
  - ⓐ Ridge number
  - - - A-A' Ridge profile

Figure 3. Geomorphological map of Ven containing interpreted geomorphological features

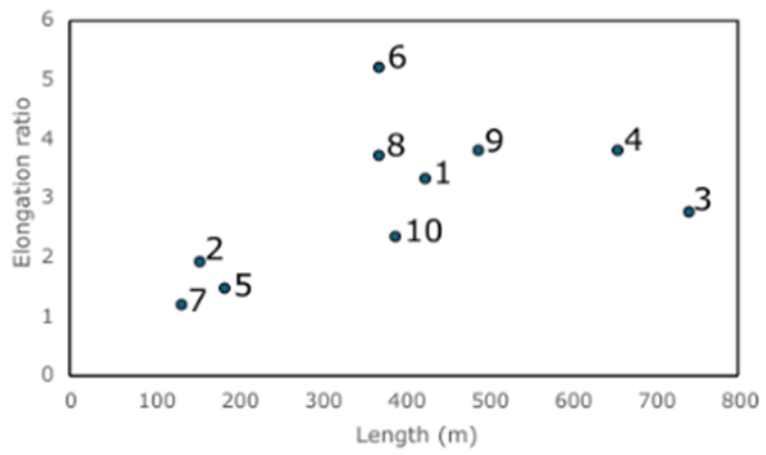


Figure 4. Length-to-elongation ratio of individual ridges in figure 3. The black numbers refer to the ridge number in figure 3.

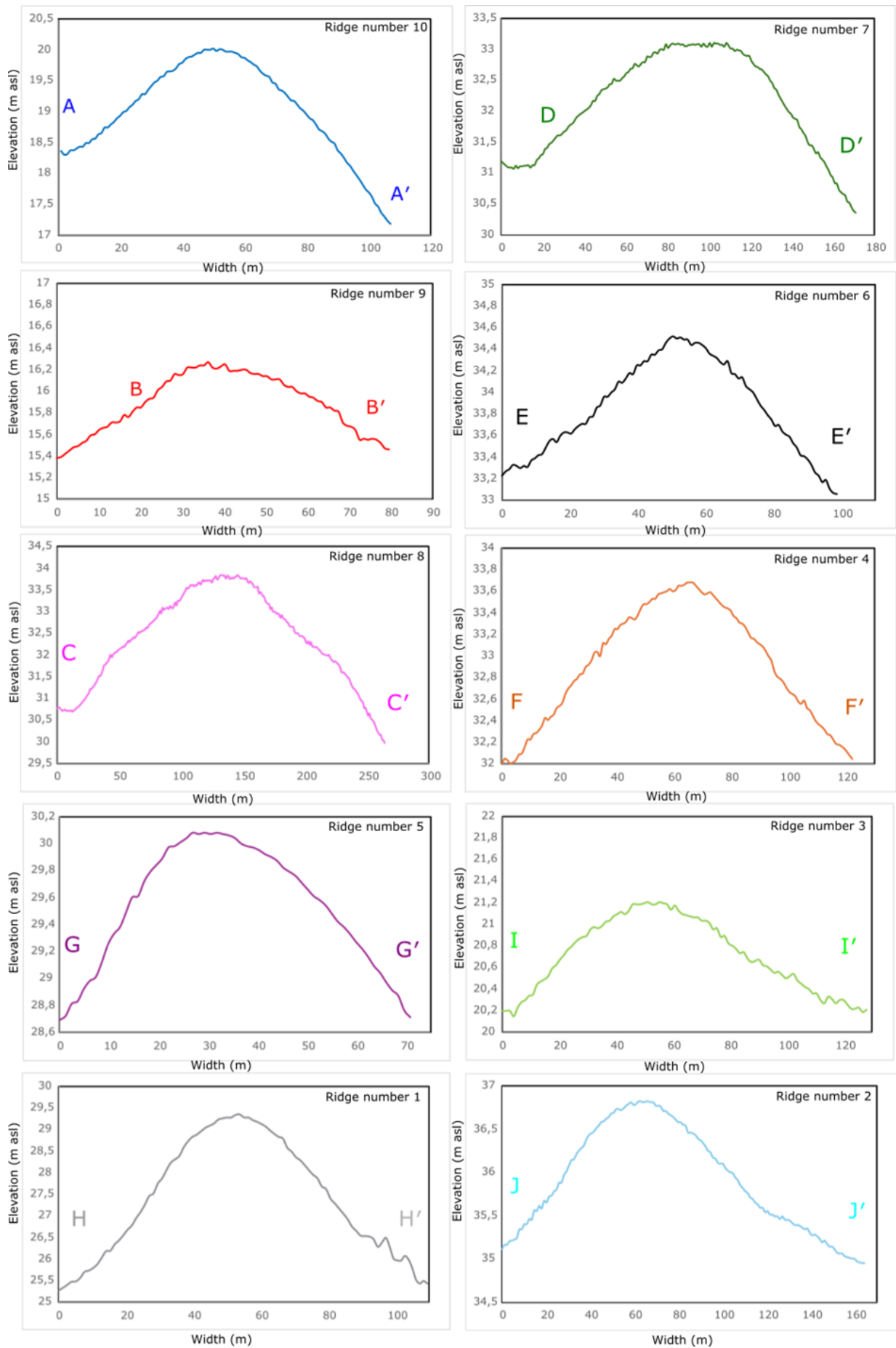


Figure 5. Ridge profiles showing the height and width of individual ridges. Note differences in scales.

### 5.1.1 Interpretation of geomorphological mapping

Four types of geomorphological structures were observed on the island. These structures consist of landslide scars, long-stretched irregular depressions, linear depressions, and ridges. The depressions that were found to be linear and the positioned in agricultural fields are interpreted as artificial drainage ditches, important management tools that farmers often employed to increase crop-yield (Christensen, 2019). Furthermore, the irregular long stretched depressions that are seen to lead out into the sea are interpreted as remnants of past channels, most likely formed through the drainage of excess surface water during heavy rain-storms.

Furthermore, 10 ridges of various sizes were located throughout the island. These ridges were very subtle in nature and long stretched. A firm interpretation of these ridges cannot be adequately made considering that no onsite visit was conducted to examine these ridges. Longstretched ridges found along the western coast Scania consists mostly of eskers and drumlins (Floren and Ohlsson, 2006; Juliusson, 2021; Berglund and Rapp, 1988; Yrgård, 1980).

Drumlins are a landform loosely defined as an oval-shaped hill formed in previously glaciated regions (Spagnolo et al., 2012), and can be made of a variety of different substances including till, stratified sediments, and bedrock cored (Stokes et al., 2011). The elongation ratio of drumlins varies (Clarke et al., 2009; Maclachlan and Eyles, 2013), with the average elongation ratio of drumlins being 2.9 based on a sample size of 35 000 drumlins from England and Ireland (Clarke et al., 2009). The length of the drumlins is found by Clarke et al. (2009) to vary between 250-1000 meters with a minimum length of roughly 100 m, and the width between 120-300 m.

Eskers are ridges composed of glaciofluvial sediments such as sand and gravel which are deposited by flowing water in subglacial conduits (Brennan, 1994). Eskers are often formed in groups and can occasionally be laterally connected to one and another (Dewald et al., 2021). The length of eskers has been observed by Dewald et al. (2021) to vary between 200 m to >3500 m. The average elongation ratio is 2.82 measured based on a sample size of >1400 eskers in across the Fennoscandia and Keewatin, Canada (Dewald et al., 2021)

The ridges being a set of eskers are an unlikely interpretation based on Quaternary deposits maps from Ven which have concluded that the subsurface mainly consist of till with minor inclusions of postglacial sand deposits (Adriellsson et al., 1981). This leaves drumlins as a likely explanation for the observed ridges, considering that the ridges are most likely made of till based on the findings presented in Adriellsson et al. (1981), and the observed average elongation ratio as well as length and width of the ridges are in line with

what is presented by Clarke et al. (2009). However, an equally possible explanation of the ridges is that they are derived from agriculture activity connected to ploughing considering the height and the fact that the ridges are located in agricultural fields.

No firm conclusion can be made regarding the ridges based on the geomorphological mapping presented in study alone, due absence of field excursions to examine the ridges in person. However, the ridges can either be explained as drumlins or ridges formed through agricultural activities.

## 5.2 Overview of the glacial sedimentology of Ven's NW cliff exposures






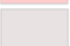

The examined outcrop is located on NW tip of Ven (Fig. 1). In total three different sections of the NW cliff outcrop were logged which includes the main with a recorded sediment sequence 355 m long, with a maximum height of 11 m and is referred to as section 1, and two smaller outcrops located just East of section 1 referred to as section 2 and 3. The examined cliff exposure of section 1 can be divided into two parts based on outcrop orientation, one facing NW and trends SW-NE and a second part of the outcrop that faces W and trends N-S. The change in orientation occurs around 170 m from the start of the 2d-log (Fig.7). The cliffs are nearly vertical but in places the cliffs slope at an angle of 40-60°. The vegetation cover is poor on parts of the cliffs that are vertical. On the sloping parts of the cliff section the vegetation cover is denser and in places the sediments are completely covered by grass. Furthermore, a talus and slumped material of varying thickness occurs along the entire main log limiting access to the lower parts of the exposure.

Furthermore, the two additional sections that were logged just east of section 1 (Fig. 1), are 7 and 8 m wide and are just over 10 m apart. Moreover, both section's trends in a N-S direction whereas the logged outcrop is facing west and has a height between 5-6 m. The Lower parts of the cliffs in the two additional sections are mostly inaccessible due to the large amounts of slump caused by landslides.

In total 15 lithofacies were identified across all the examined cliff sections which have been colour coded to better highlight their lateral distribution. These lithofacies consists of a mixture of three diamicts labelled LF9, LF12 and LF15. Between these, there are strata consisting of gravel and a mixture of sand and silty sand, all of which have undergone varies levels of glacial tectonism. These tectonically altered sediments exhibits varies degrees of deformation that feature a wide range of different deformation structures consisting of faulting, folding, boudinage and shearing. Symbology for the 2d-logs is shown in Figure 6 which is followed by the 2D-logs (Fig. 7, 8, and 9), and later by a detailed description of each lithofacies followed with the interpretations of each section.

## Symbology

### Lithofacies numbers and colours:

|   |      |   |      |   |       |   |       |
|---|------|---|------|---|-------|---|-------|
|  | LF 1 |  | LF 5 |  | LF 9  |  | LF 13 |
|  | LF 2 |  | LF 6 |  | LF 10 |  | LF 14 |
|  | LF 3 |  | LF 7 |  | LF 11 |  | LF 15 |
|  | LF 4 |  | LF 8 |  | LF 12 |   |       |

### Lithofacies codes:

Dmm- Diamicton (matrix-supported, massive)

Dmf- Diamicton (matrix-supported, fissile)

Gms- Gravel (matrix-supported, massive)

Gm- Gravel (clast-supported, massive)

Gh- Gravel (horizontally-bedded)

Gd- Gravel (deformed bedding)

Gfu- Gravel (upward-fining)

Sp- Sand (planar cross-bedded)

Sh- Sand (horizontally-bedded)

Sm- Sand (massive)

Sd- Sand (deformed)

SiSh- Silty Sand (horizontally-bedded)

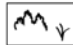

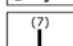



SiSd- Silty Sand (deformed)

Fm- Fines (massive)

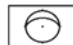


...(d)- with dropstones

...(w)- with dewatering structures

### Additional features:

|   |                                       |
|---|---------------------------------------|
|  | Slump                                 |
|  | Boulders                              |
|  | Location of Vertical profile number X |
|  | Bulksample X                          |
|  | Fabric measurement X                  |
|  | Figure. number X                      |

### Structural measurements

|   |                |
|---|----------------|
|  | Folds          |
|  | Faults         |
|  | Bedding planes |

### Lithofacies code for diamictic sediments used in the Vertical profiles:

#### Diamictic sediments

D Diamict

#### General appearance:

m Massive, homogeneous

h Heterogeneous

b Banded/stafified

#### Matrix:

M Medium-grained, silty-sandy

F Fine-grained, clayey-silty

#### Clast/matrix relationship:

(m<sub>1</sub>) Matrix-supported, clast poor

(m<sub>2</sub>) Matrix-supported, moderate

(m<sub>3</sub>) Matrix-supported, clast-rich

#### Consistence when moist:

1 Loose

2 Friable

3 Firm, difficult to excavate

4 Extremely firm

Figure 6. Symbology used for the 2D-logs and the lithofacies codes used for the vertical profiles.



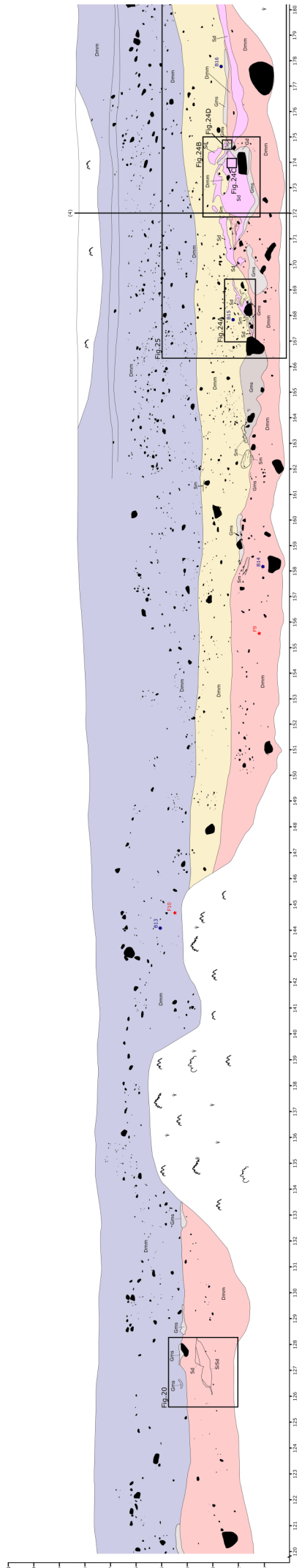
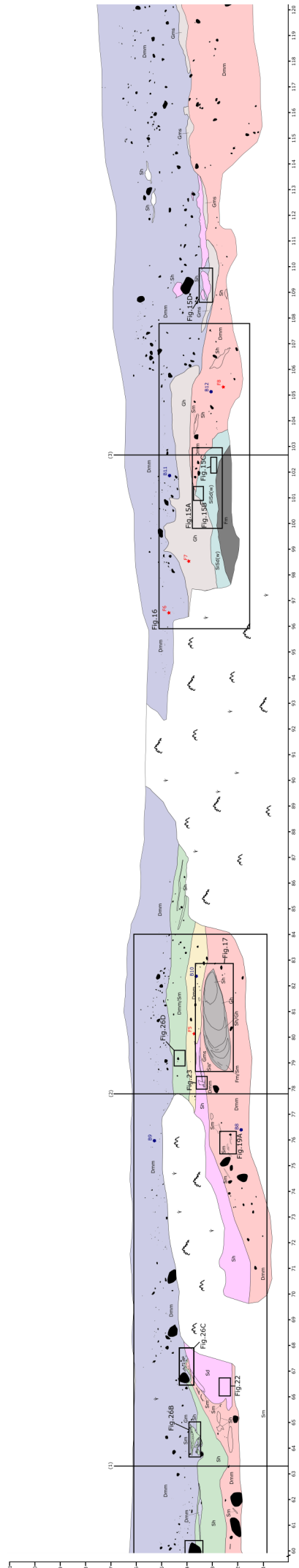
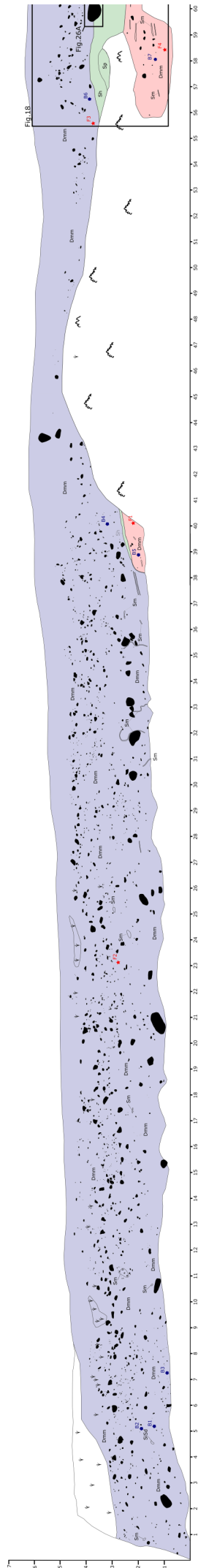


Figure 7. 2d-log section I

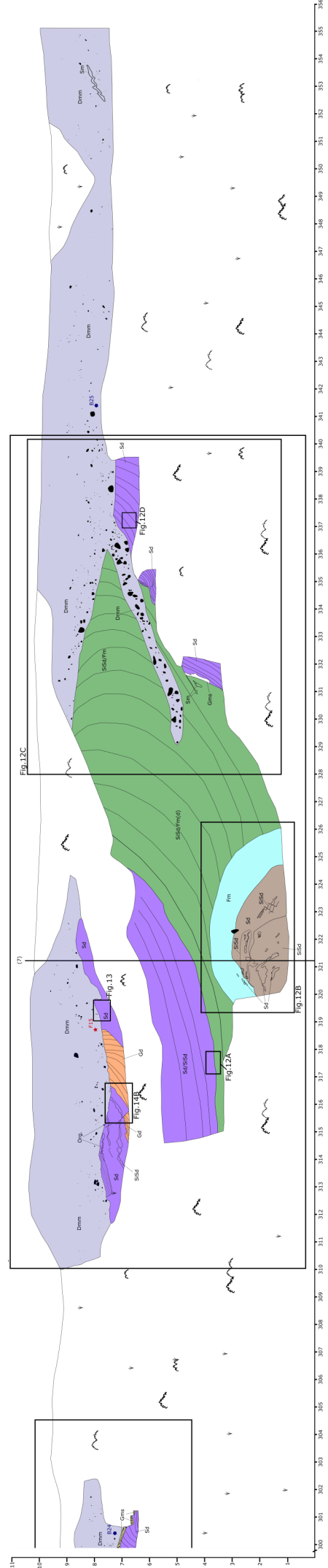
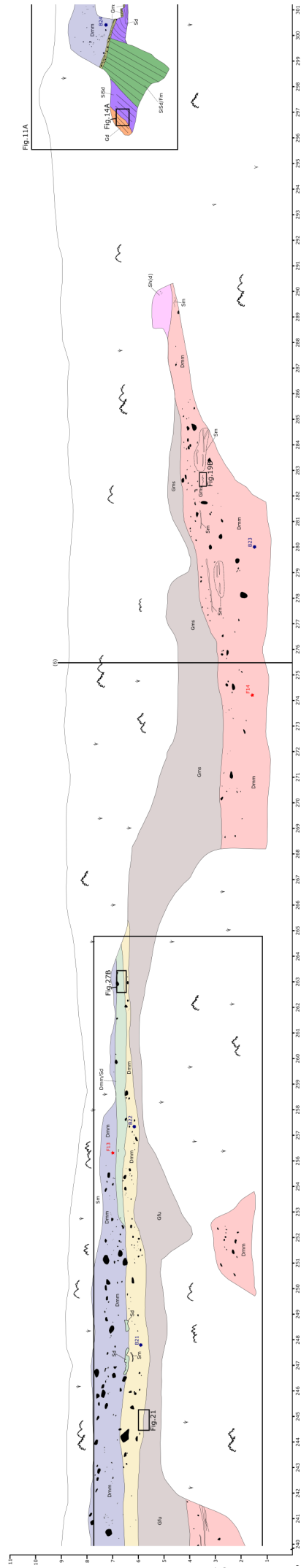
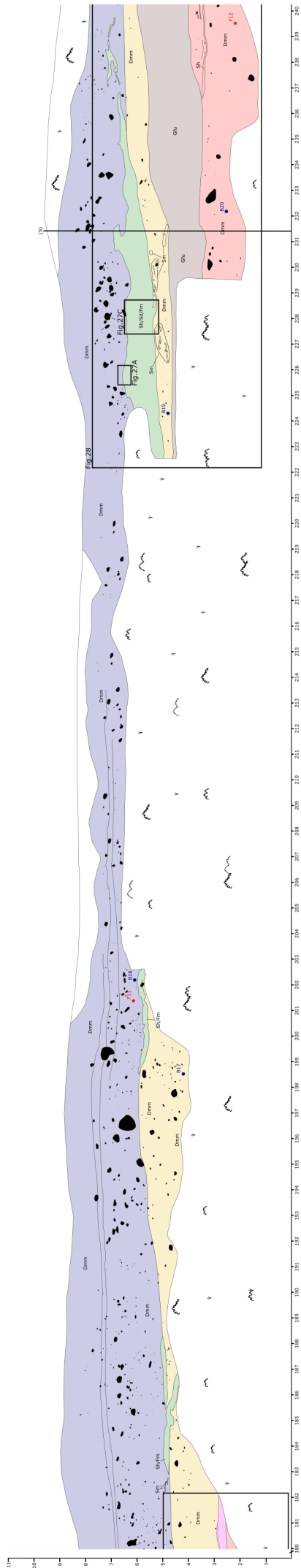


Figure 7. (Continued)

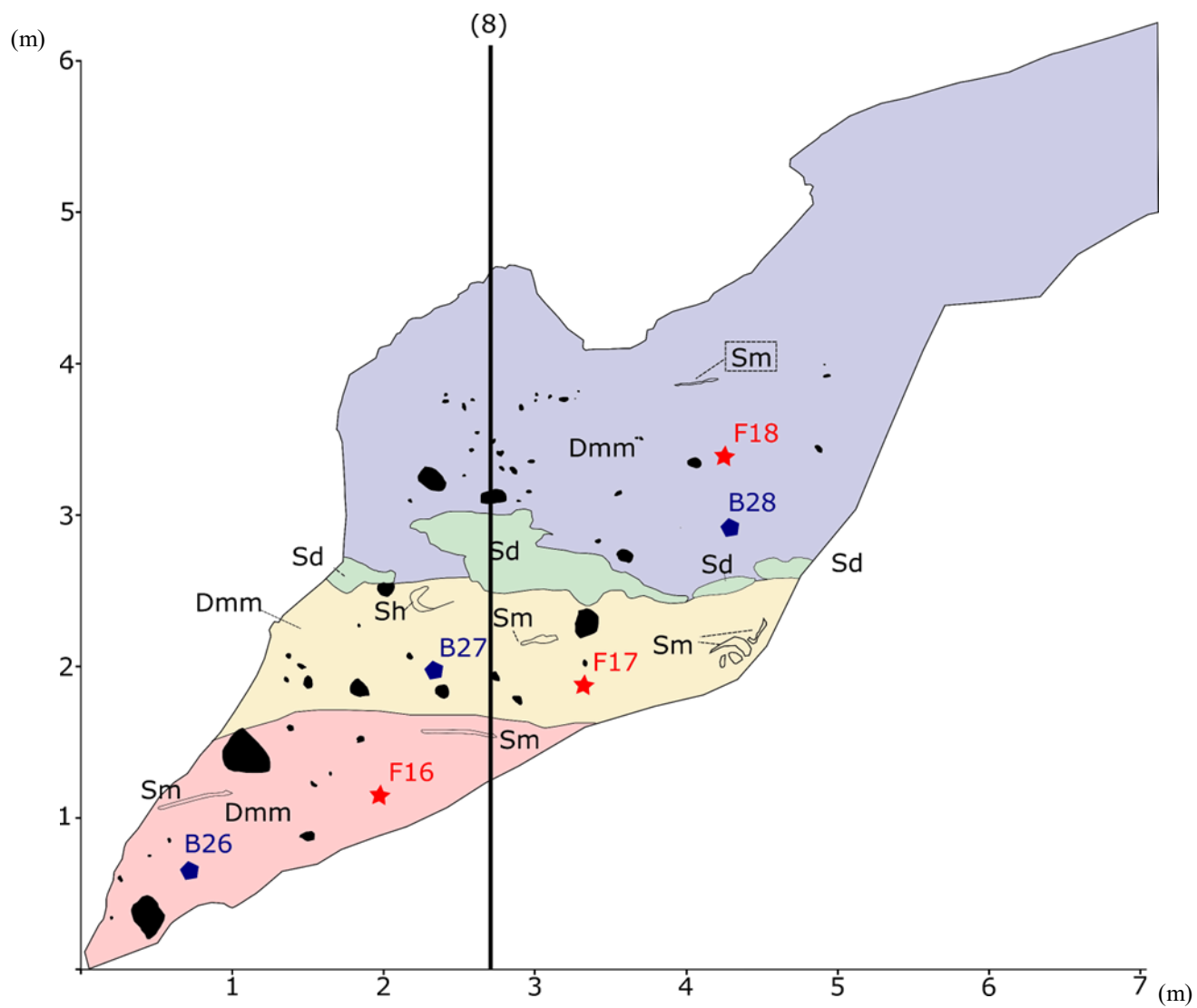


Figure 8. 2D-log Section 2

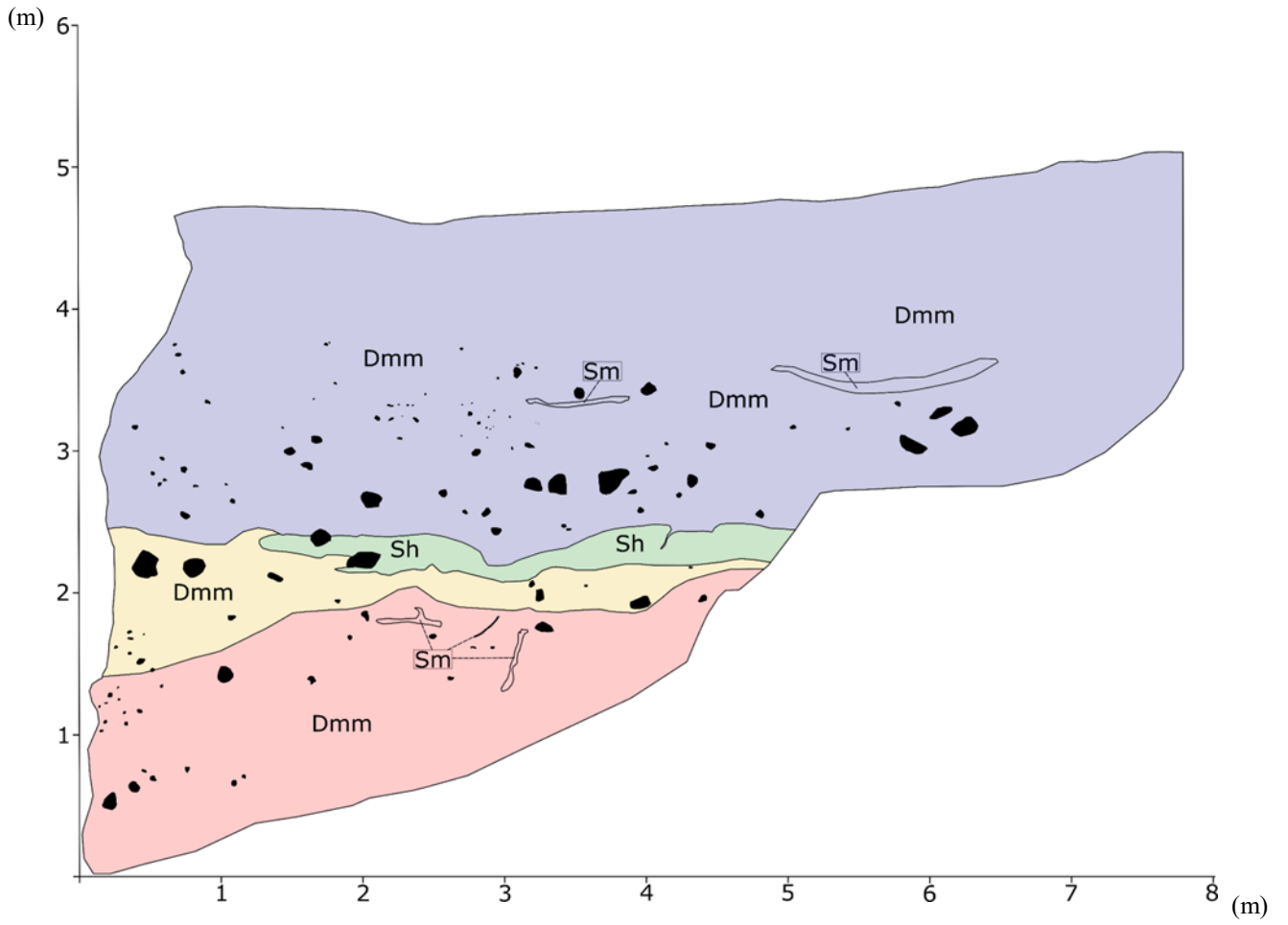


Figure 9. 2D-log Section 3

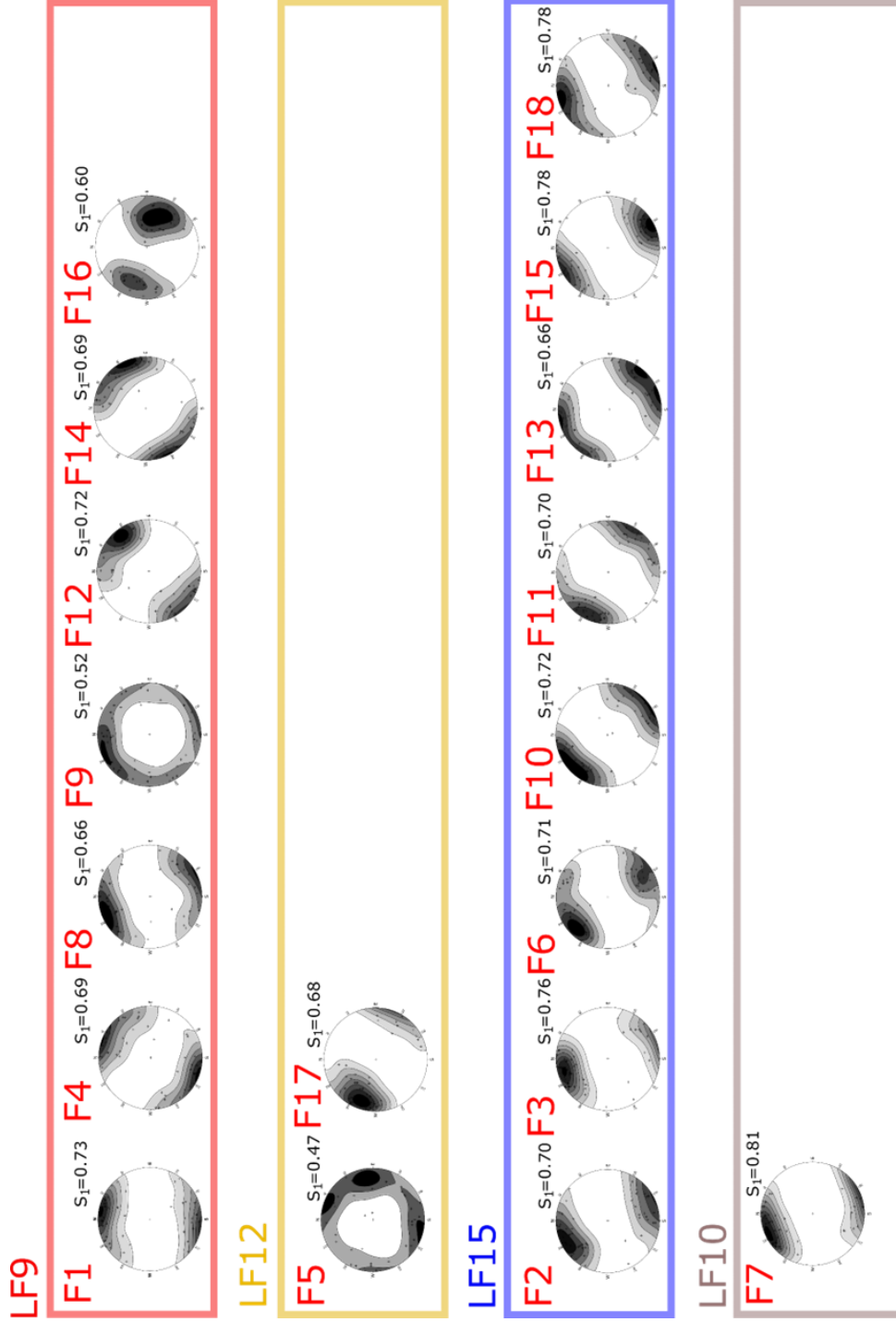


Figure 10. Fabric measurements with eigenvalue ( $S_1$ ). The red capital letter F followed by a number refers to the location of the measurements in the 2D-logs (Fig.7-9).

### 5.2.1 Lithofacies 1

LF1 consists of two distinct beds located between 320-326 m in section 1 (Fig. 6). The lower bed features a massive silty sand unit containing irregularly shaped inclusions of crudely horizontally layered fine to medium sand. The upper part of LF1 consists of a crudely horizontally layered fine sand, including irregularly shaped interbeds of laminated silty sands and horizontal bands of a dark brown clay. Normal faults and drag folds occur throughout the entire exposure.

Five bedding planes were measured which show an average dip of  $51^\circ$  towards the south. Additionally, 10 fault planes display two preferred orientations, one towards the SW and the other towards the NE (Fig.11). The average dip of the fault planes was  $51^\circ$ .

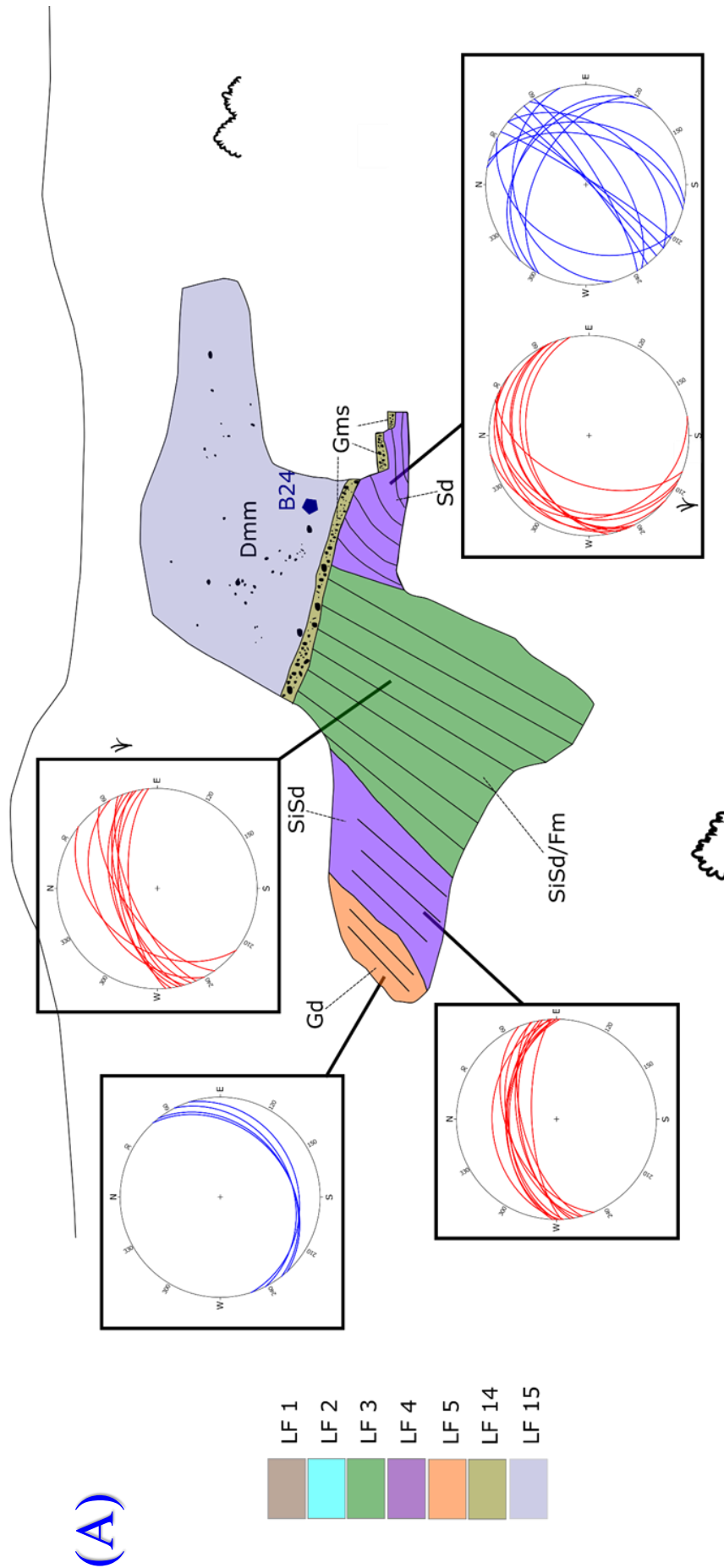


Figure 11. Structural measurements of LF1,3, 4 and 5. A) Detailed figure of section 1 between 295-302 m. B) Detailed figure of section 1 between 310-340 m. The thin black lines inside of lithofacies highlights the overall orientation and direction of the bedding planes. The location of the displayed figures is shown in figure 7.

(B)

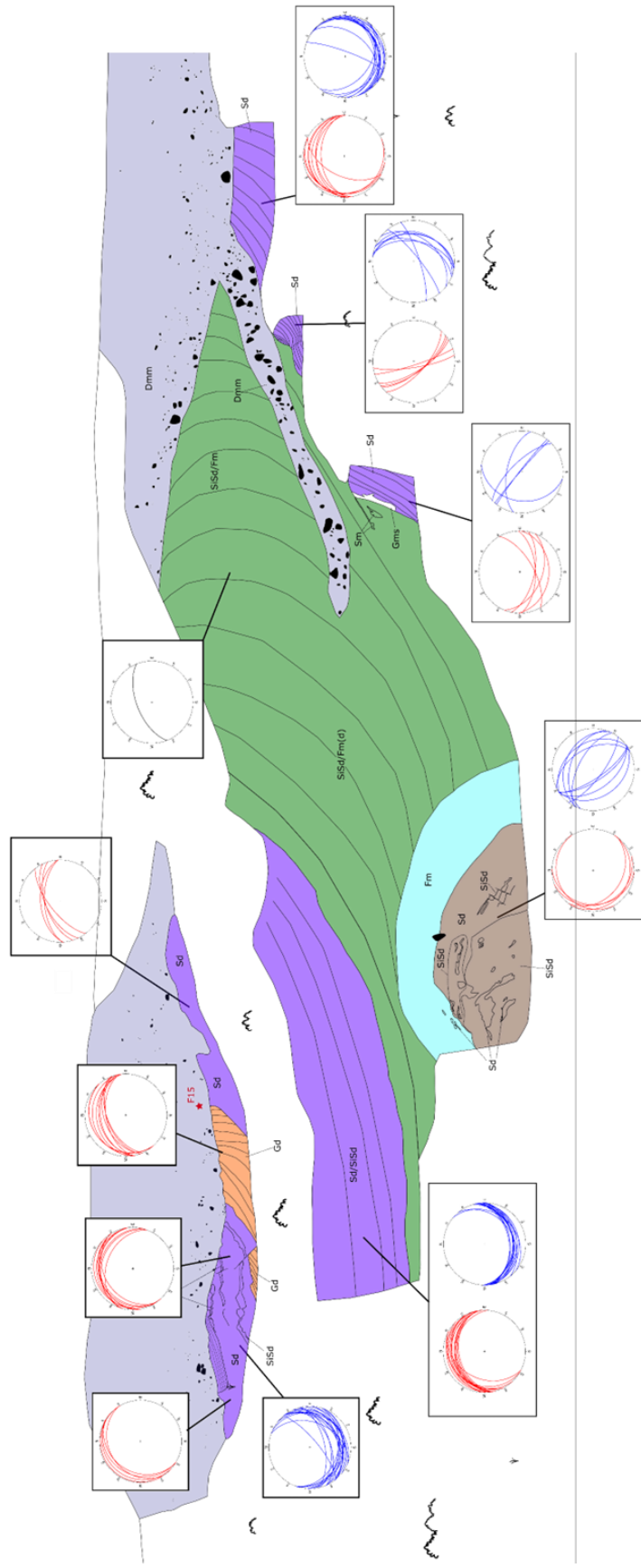


Figure 11. (continued)



### 5.2.2 Lithofacies 2

Lithofacies 2 consists of a heavily compacted dark grey massive clay with a downward dip. LF2 is exposed between 320-326 m in section 1 and is observed to have a maximum thickness of 0.7 m (Fig.12). The contact with the surrounding lithofacies is sharp.

### 5.2.3 Lithofacies 3

Lithofacies 3 is characterized by alternating beds with varying thicknesses, composed of horizontally to laminated silty sand and massive clay. LF3 can be observed in section 1 between 294-297 and 315-336m, reaching a maximum observed thickness of approximately 6 m (Fig. 7). The bedding planes exhibits a upwards dip between, 294-297 m (Fig.11). The contacts with the surrounding lithofacies are sharp, much like the internal contacts between the different beds.

The upper contact with LF15 is observed to form an angular conformity where the bedding planes of LF3 are intersected by LF15. Furthermore, between 315-336 m, LF3 is seen to be folded, with bedding planes transitioning from horizontal to gradually becoming nearly vertical and ultimately overturned (Fig.11, 12C). LF3 can also be seen to be deformed where instances of faults are featured in the unit. A few out-sized clasts were also located within the lithofacies.

10 bedding planes were measured between 294-297 m of section 1 and show an average dip of  $57^\circ$  with a preferred orientation toward NW (Fig.11). The axial plane of the fold observed between 315-336 was calculated through the measurement of 10 contacts of the alternating beds at the horizontal, vertical and overturned parts of the fold. This approach gave an axial plane tilted with a dip of  $67^\circ$  toward the SE (Fig.11).

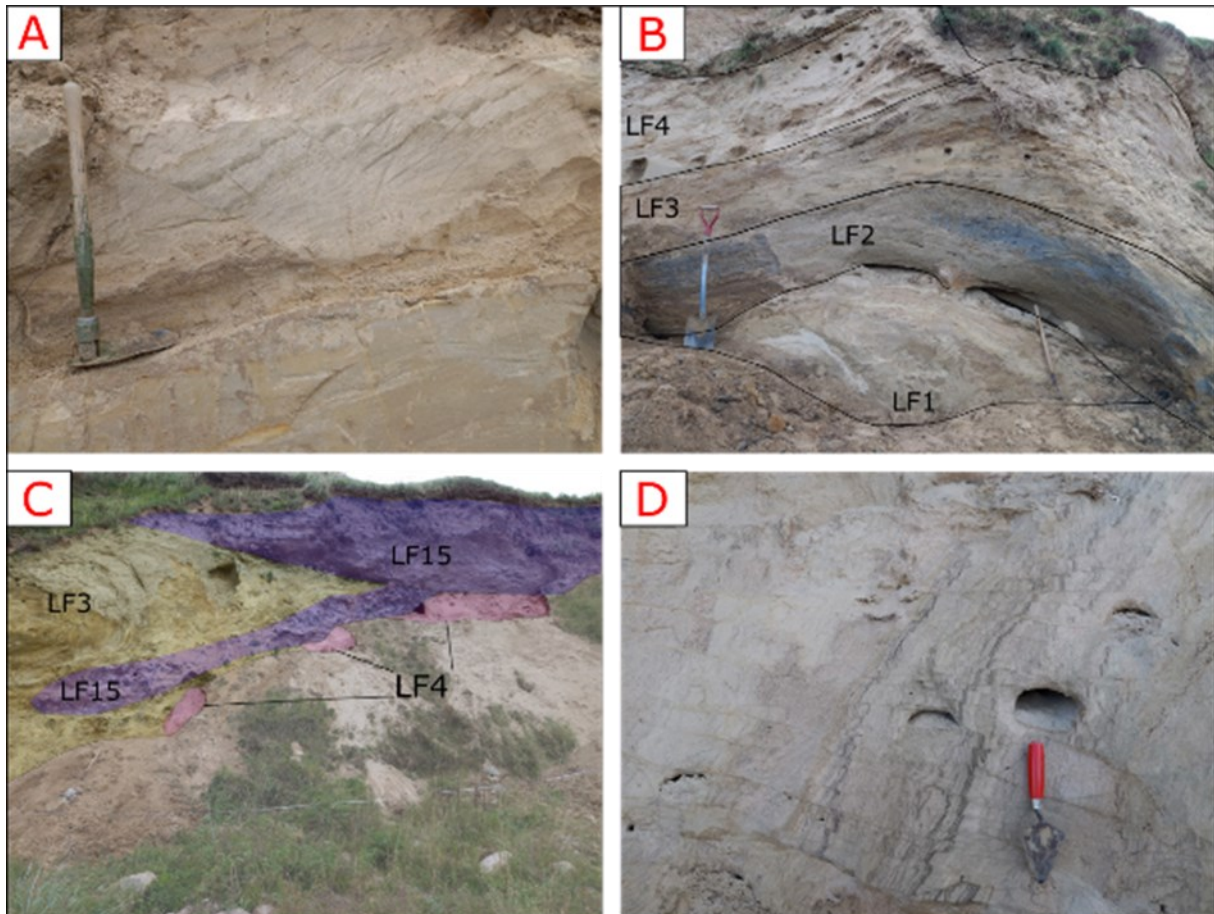


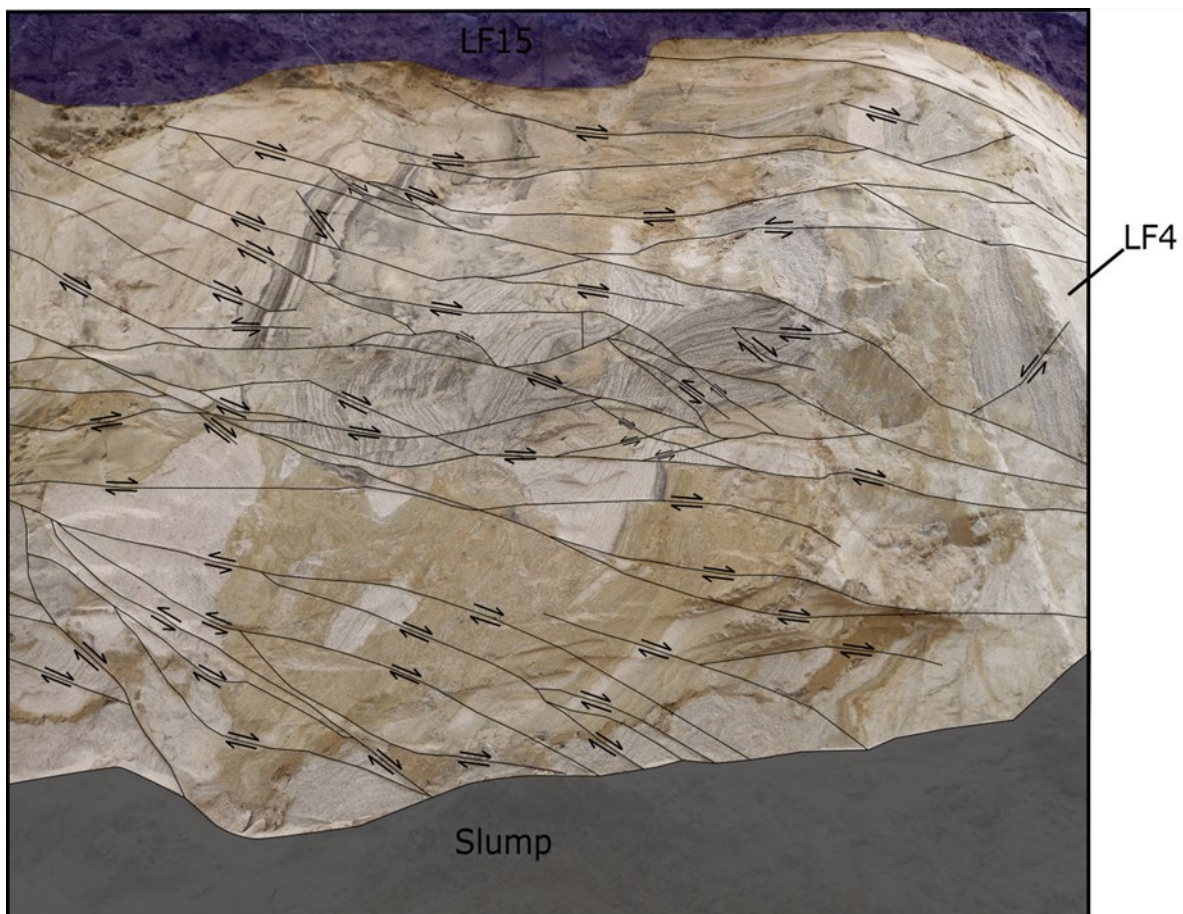
Figure 12. Various structures and lithofacies. A and D) Present a complex network of low-angle faults organized in an echelon pattern within LF4, with a trenching tool (~40cm) and a trowel (~20cm) provided for scale. B) Displays irregularly shaped lenses of medium and silty sand within LF1, with a shovel (~1m) for scale. C) Illustrates overturned bedding planes of LF3 and highlights LF15 extending downward in a wedge-like shape into LF3. The location of each individual photo is indicated in Figure 7.

#### 5.2.4 Lithofacies 4

Lithofacies 4 (LF4), located between 294-340 m in section 1 (Fig. 7), consists of an assemblage of deformed and displaced lithofacies including horizontally layered medium sand, laminated and cross bedded silty sands and laminated fine sand and silt. Additionally, repeated bands of organic material can be seen in the upper part of LF4 between 311-316m (Fig. 7). Overall, LF4 exhibits a coarsening upwards sequence between 311-323m where the basal part of the section predominantly consists of a mixture of horizontally layered fine sand and silty sand (Fig.12A), while the upper parts between 311-317m consists of a mixture of horizontally layered to cross bedded medium to coarse sand (Fig.14B).

The deformation structures consist of a network of low angled faults structured in an echelon pattern (Fig.13, 12A, D), some of

which exhibits drag folding. The degree of deformation is seen to steadily increase from 318-323, where the highest degree of deformation progressively increases toward the upper parts of LF4 between 320-323 m. This zone displays a complex network of faults and nearly vertical bedding planes (Fig.13). Additionally, the degree of tilt in the bedding planes can also be seen to steadily increase toward the later part of the upper section particularly between 318-323 m. In this interval, between 320-323 m, the bedding planes are nearly vertical, and towards the top of the section they are faulted, transitioning from a nearly vertical to horizontal arrangement. The contacts between LF4 and LF5 are sharp while the contact between LF4 and LF3 are more gradual. The upper contact with LF15 is observed to form an angular conformity where the bedding planes of LF4 are intersected by LF15.



A total of 91 fault planes was measured at various locations, detailed in figure 11, revealing two preferred orientations: one towards the SE and another towards the NE, with the SE direction being most prevalent (Fig.11). The tilt of the fault showed a great variance, but their combined average dip is 34°. Alongside the faults, 103 bedding planes were measured at several locations, also outlined in figure 26, indicating a dominant trend of the bedding planes dipping toward the NE (Fig.11). However, a more SW direction is also observed in certain parts of the exposure (Fig.11).

### 5.2.5 Lithofacies 5

Lithofacies 5 is composed of horizontally layered, well-sorted gravel consisting of alternating beds of fine gravel and gravelly sand (Fig. 14A,B). LF5 appears in the later parts of section 1 (Fig. 6), between 293-294 m and 314-319 m. The bedding planes exhibit a gentle upwards dip at a roughly 40° angle, transitioning to nearly vertical at 318-319 m. An angular unconformity can be seen between 314-319 m where the bedding planes are intersected by LF15 (Fig. 24W). The contacts with the surrounding lithofacies are sharp. This unit also exhibits low angled normal faults, and a single reverse fault highlighted in red in figure 14A. Four fault planes of the normal faults were measured between 293-294 m which showed an average dip of 28° toward the SE (Fig.11).

### 5.2.6 Lithofacies 6

Lithofacies 6 (LF6) is composed of an unconsolidated, massive dark grey coloured clay that can be seen in the basal part of section 1 between 98-103 m (Fig. 7). The basal contact of the unit could not be located

due to slump.

### 5.2.7 Lithofacies 7

LF7, positioned between 98-103 m in section 1 (Fig.7) is composed of a horizontally layered silty sand, that gradually transitions into a coarse sand in the upper parts of the section (Fig. 6). Brittle and ductile deformational structures are present within the unit, such as sheath folds and a series of normal faults (Fig. 15A-C). The external and internal structure of the unit also shows a subtle pinch and swell structure, with the pinch occurring at 100 m in section 1 and with the swell formation occurring on either side. Dewatering structures are present throughout the entire unit, superimposed and intersecting with preexisting deformation and bedding plane structures in the unit (Fig. 15A,C).

The maximum exposed thickness of the unit is roughly 1 m, and it has a sharp contact with the overlying units LF10 and LF9. While the bedding planes are predominantly horizontal, the eastern side of the unit displays a downward dip beneath LF9 (Fig. 16).

Three measurements were taken on the sheath folds, indicating a dip of the axial plane toward the SW for two of the measurements and a tilt toward the NE for one (Fig.16). Furthermore, a total of 20 bedding planes were measured, ten of which were taken in the part of the section which tilted downwards, while the other was of the horizontally layered bedding planes. The bedding planes that were tilted downward had an average tilt of 33° toward SWW (Fig 16). In contrast, the bedding planes taken at the horizontal part had an average dip of 10° and the trend of the bedding planes were found to be diverse including some toward NW and the majority toward NNE. Ten fault planes were measured which had two dominant trends: one toward

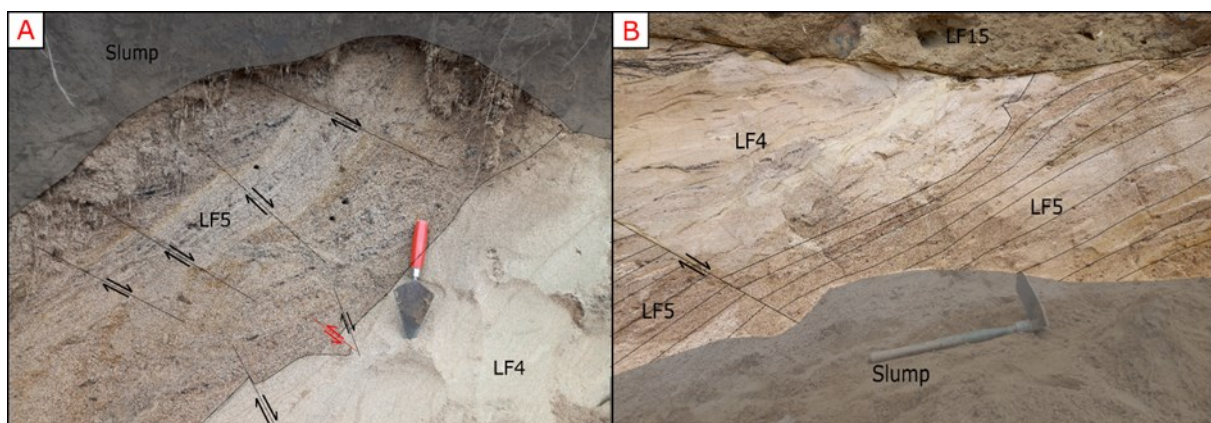


Figure 14. Faults within LF5. A) Illustrates a cluster of minor low-angled normal faults within LF5, with one notable reverse fault highlighted in red, with a trowel for scale (~20cm). B) Depicts a large normal fault observed in LF5 and LF4 with a trenching tool for scale (~40cm). The directional displacement is indicated by black and red arrows, while the corresponding photo locations are referenced in Figure 7.

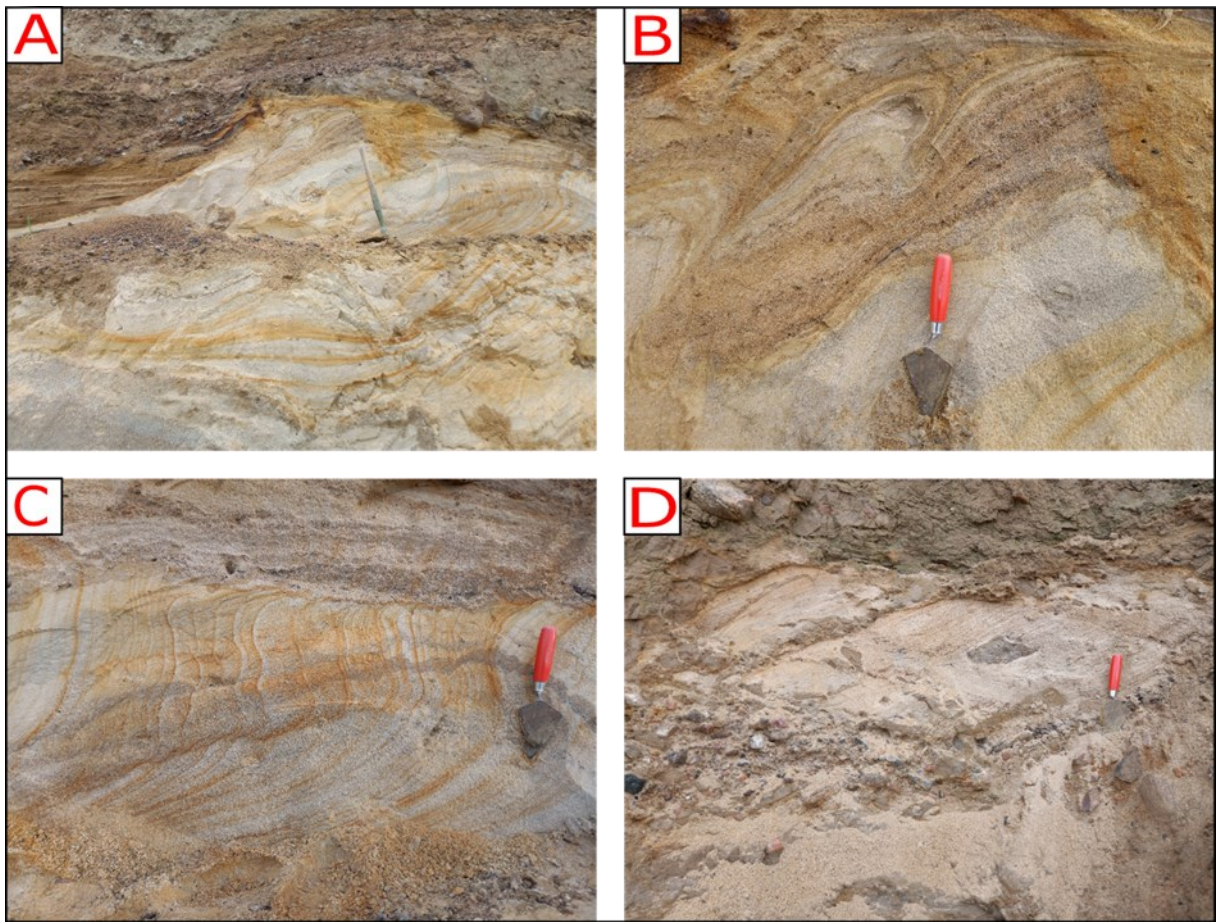


Figure 15. Deformational structures in LF7 and LF10. A) Emphasizes dewatering structures within LF7, with a trenching tool provided for scale (~40cm). B) Presents a sheath fold observed within LF7, with a trowel included for scale (~20cm). C) Illustrates a sequence of minor normal faults superimposed by the dewatering structures, with a trowel for scale. D) Demonstrates two augen-shaped lenses of LF7 with a trowel for scale. The photo locations are indicated in Figure 7.

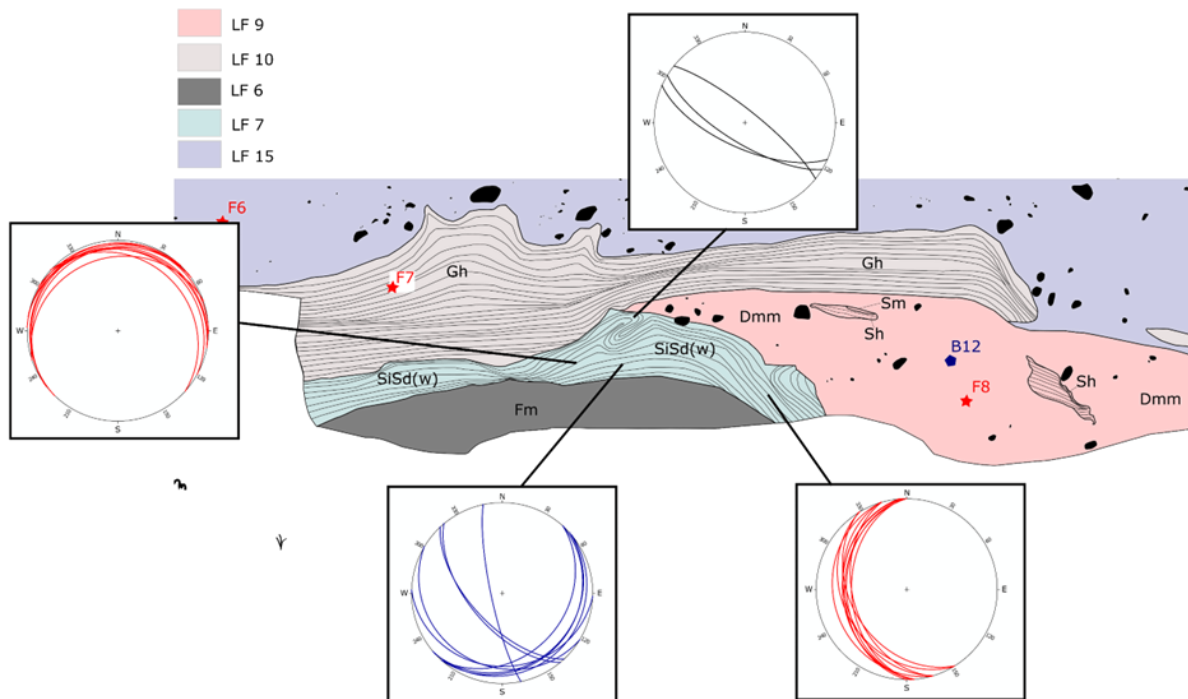


Figure 16. Detailed figure of section 1 at 96-110 m (Fig.7), highlighting the overarching directions and orientations of the bedding planes in LF7 and LF10 and structural measurements.

the SW and the other toward the SE (Fig. 16). The degree of the dip varied between the two different trends where the fault planes trending toward the SW had a average dip of 55 ° while the bedding planes trending toward the SE had a lower average dip of 19°.

#### 5.2.8 Lithofacies 8

LF 8 consists of several different units which are located as lenses inside LF9 (Fig. 7: 78-83 m). LF8 is characterized by a wide range of different lenses including silty sand containing inclusions of fine to medium sand, followed by gravelly sand, and lastly fine to medium sand (Fig. 6, 17). All lithofacies are layered except for the silty sand unit with its sandier components/parts that are all massive. Occasional small bands of coal can be found across the gravelly sand and the fine to medium sand layers (Fig.17).

All the encompassed lithofacies show signs of ductile deformation and collectively form a recumbent fold,

which is on the verge of transitioning into an enclosed fold, and further into advanced stages of boudinage (Fig. 17). Three axial planes were calculated based on measurements of different unit boundaries inside the fold. Two axial planes were seen to be tilted towards the NW-NNW and the last axial plane had a tilt towards the SEE (Fig. 18).



Figure 17. LF8 with a trenching tool for scale (~40cm). The location of the photo is displayed in figure 7 between 78-83 m.

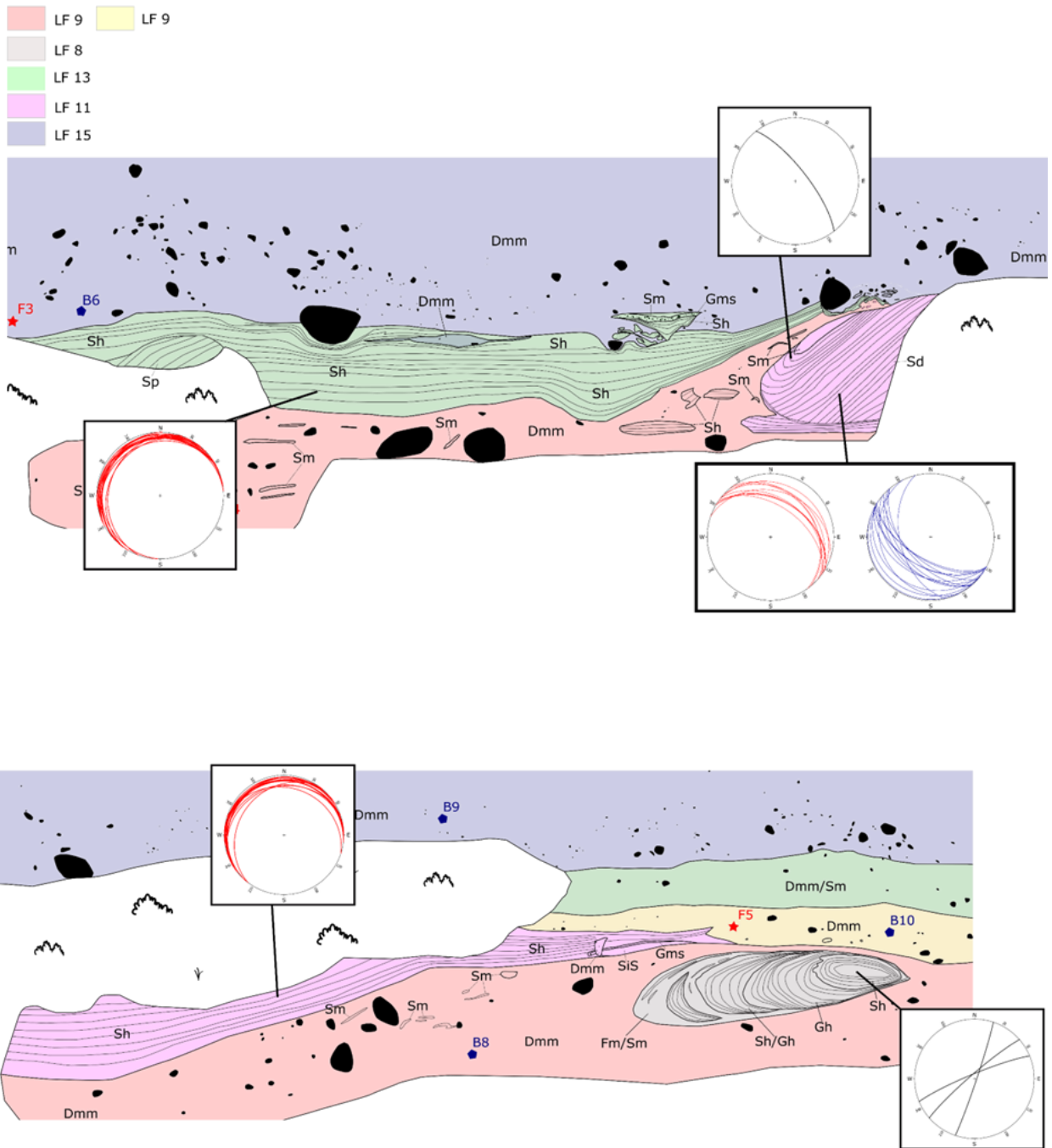


Figure 18. Structural measurements of LF11, 8 and 13. Thin black lines within lithofacies delineate the orientation and direction of... The position of the depicted figure is indicated in figure 7.

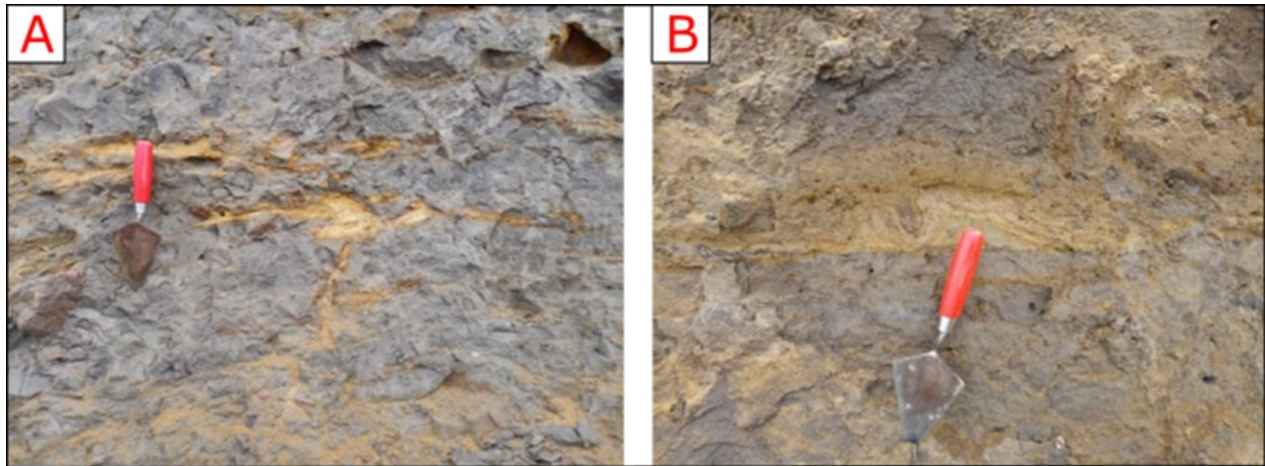


Figure 19. Deformed stringers: A) illustrates a folded stringer comprised of massive sand. B) showcases a folded stringer made of massive gravel. Both stringers are situated within LF9, with their respective photo locations indicated in Figure 7. The trowel is used for scale and is approximately 20 cm long.

### 5.2.9 Lithofacies 9

Lithofacies 9 (LF9) consists of a dark grey matrix supported, bi-modal diamiction with a fine-grained matrix identified in field to consist of silt and clay. LF9 can laterally be discontinuously traced in the lower parts of the section from 38-291 m (Fig. 7). The maximum thickness of the unit is 3.5 m. A lateral variability in the diamict was observed where parts of the unit showed a faint level of low angle fissility between 38-84 m of section 1 (Fig. 7). Additionally, a lateral variability in compaction was also noted where parts of the diamiction were loose and friable while other parts of the unit exposure were considerably firmer and difficult to excavate. LF9 is clast poor, with clasts predominantly consisting of either granite or gneiss. However, amphibolite and sandstone do also occur albeit at lower frequencies.

Partings of sand and gravel were observed throughout the entire exposure in a stochastic and evenly dispersed manner. These partings of sand consist of stringers and lenses of various thicknesses and lengths. The stringers consist predominantly of massive sand, but occasionally massive fine gravel, have a thickness of >3 cm and can be continuously traced for 1-2 m. Furthermore, the stringers are observed to occur in groups at the same location. The stringers are mostly elongated and lie horizontally and at an angle, and some are found to be folded (Fig. 19).

The lenses consist predominantly of sand, but small inclusions of gravel do also occur. The lenses show a large variation in external structure where some are bi-convex, circular, augen shaped and other display a much more irregular exterior shape. Additionally, the sizes of these lenses also show a great variation with the largest measuring 2.3 m wide and with a thickness of 0.6 m, but on average these lenses are more subtle. The internal structure of the lenses is massive and horizontally layered sand and faulting can be observed in some lenses. Eight fault planes were measured in the

sand lens located inside LF9 between 126-129 m in section 1 (Fig.20). The fault planes in the sand lens showed a diverse set of orientations with the SW and SE being the most prevalent followed by NE (Fig. 20). The surrounding contacts of the sand partings and the diamiction are all sharp.

A total of seven fabric measurements were taken at regular intervals and showed a discrepancy of the preferred orientation of the clast long axis and in fabric strength between some samples (Fig. 10). Four out of seven samples (F1, F4, F12 and F14) showed a preferred clast long axis orientation toward the NE-SW while two fabric measurements displayed a preferred orientation of SE-NW. Additionally, one fabric measurement (F9) showed a large variance in the clast orientation, with the majority of clast long axis dipping toward the NW. Furthermore, a discrepancy in fabric strength between each sample is observed and the S1-value ranges between 0.52 to 0.73, with an average of 0.66.

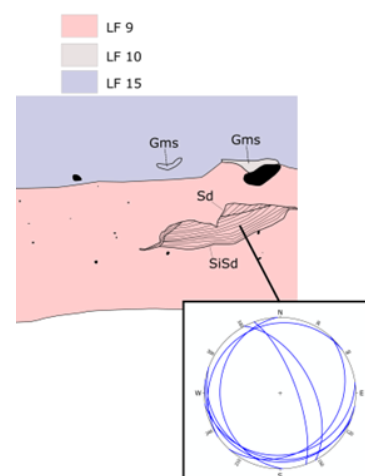


Figure 20. Structural measurements of fault planes in a sand lens located within LF9.

#### 5.2.10 Lithofacies 10

Lithofacies 10 exhibits a poorly sorted gravel, discontinuously traceable from 96 m to 179 m in section 1 but continuously present between 222-286m (Fig. 7). The maximum observed thickness is 3.5 m observed at 268 m, though the upper contact could not safely be examined due to the steepness of the cliff (Fig. 7). Despite its thickness between 229-286m, other exposures of LF10 show a more subtle nature, not exceeding 1 m in thickness except for at 97-101 m where it can be seen to be just shy of 2 m.

Its discontinuous part (107-179 m) is dominated by irregular to augen shaped lenses consisting of massive gravel that contains variously sized boulders and pebbles, with a matrix consisting of coarse sand to fine gravel. Between 96-106m, LF10 consists of a finer and better sorted gravel that displays a faint horizontal layering. The upper part of LF10 in this section is irregularly shaped, extending upwards in to LF15, where the bedding planes in the vicinity are folded upwards into LF15. A fabric measurement was taken at 98 m in the upper part of the unit, which showed a preferred long axis orientation toward the NE and has an eigenvalue of 0.81 (Fig.10).

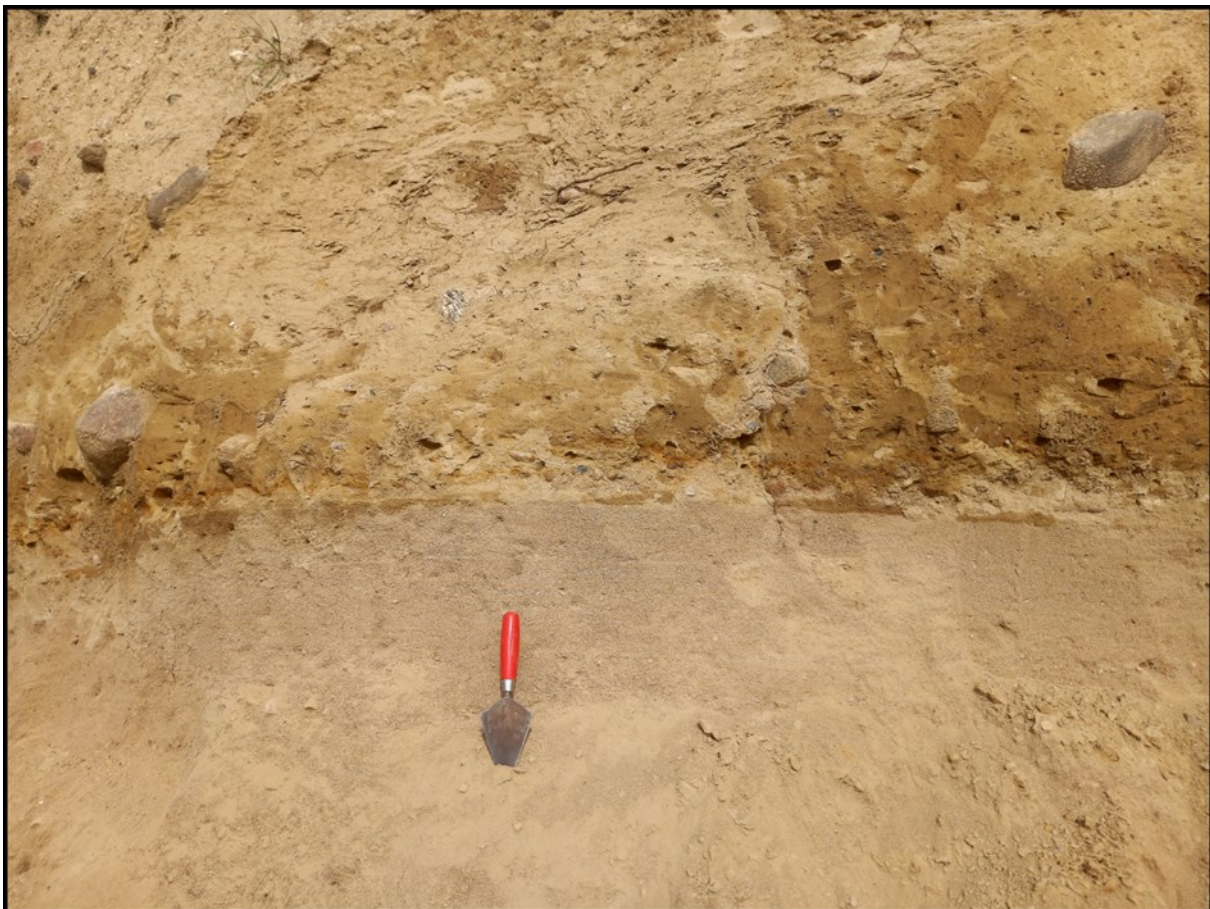
LF10 between 222-286 is characterized by a fining upwards sequence, with the basal part of the cliff consisting of a massive gravel with a high content of cobbles and boulders. The upper part of the section is characterized by a crudely horizontally layered gravelly sand (Fig. 21). The basal contact of this unit with LF9 is seen to be sharp and at places erosive.

#### 5.2.11 Lithofacies 11

Lithofacies 11 (LF11) consists of a well-sorted, stratified sand that can be intermittently located near the basal part of section 1, located directly on top of LF9 and overlain by LF12 and LF15. (Fig. 6). LF11 is exposed at four separate locations in section 1 (Fig. 7). Below follows a detailed description of the individual exposures of LF11.

##### LF11 65-68m

LF11 located between 65-68 m of section 1, is seen to be located between LF9 and LF15 (Fig. 7). LF11 in the given interval mainly consists of a well-sorted, stratified, and deformed, fine to medium sand with inclusions of finer grains such as bands of silty sand and massive clay.



*Figure 21.* Upper portions of LF10 displaying the finer grained and partially horizontally layered characteristics of the upper segment of the unit, along with the sharp unit boundary with LF12. A trowel is used for scale (~20cm) and the location of the photo is shown in Figure 7.



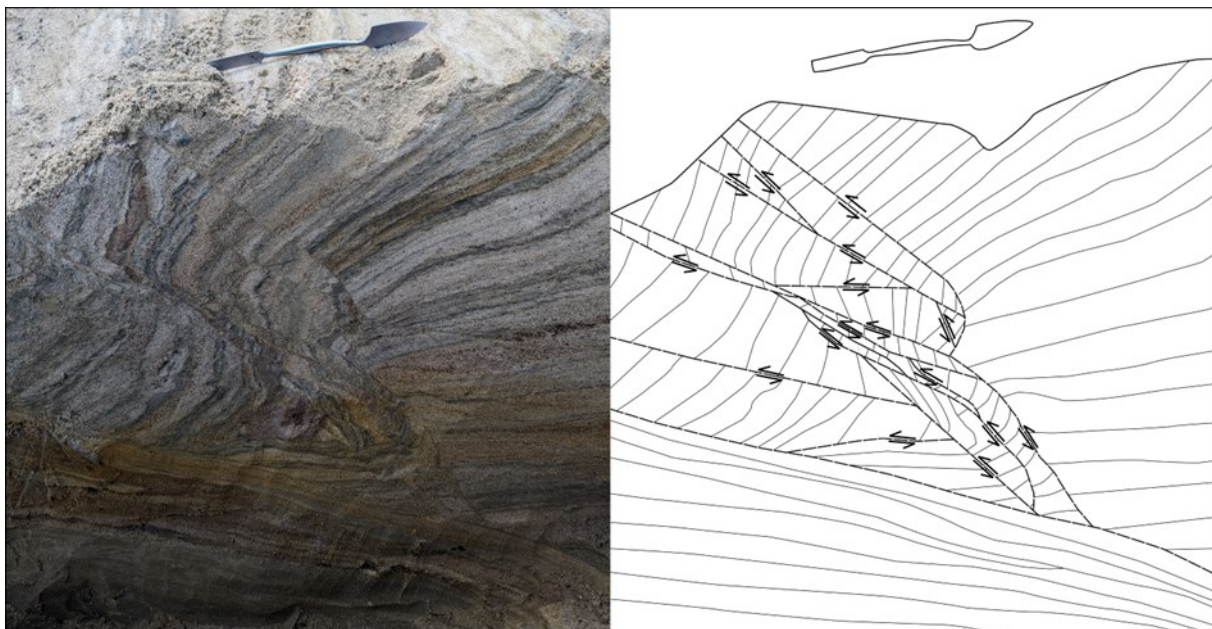
The contacts with the surrounding units are sharp. The present deformation structure of LF11 consists of a complex mixture of ductile and brittle deformation. Furthermore, the brittle deformation consisted of a network of reverse faults, whereas the degree of brittle deformation in the unit steadily increases towards the bottom of the LF11 (Fig. 22). The deformed bedding planes can be seen tilted in the upper parts of the unit where the bedding planes become increasingly faulted and dragged or folded into an increasingly more horizontal plane matching the lower parts of the unit (Fig.22). The contact between the upper and lower part of LF11 is undulating and sharp. Small scale folding can also be seen in the upper left part of the section where the bedding planes toward the contact with LF9 are folded upwards (Fig. 18). Moreover, a small section in the upper parts of the unit is found to be massive (Fig. 7; Fig. 18).

Ten different bedding planes was measured throughout the upper parts of the unit and showed a average dip of  $28^\circ$  toward the NE (Fig.18). Furthermore, a total of 15 fault planes was measured where the average fault plane had a dip of  $41^\circ$  tightly clustered toward the SW. One fold in the section was measured and the calculated axial plane has a dip of  $76^\circ$  and a strike of  $321^\circ$  (Fig.18). The variance in the data plots for both the bedding plane and faults plane measurements was low and the spread in the direction of dip was only a few degrees off between each measurement. No bedding

plane measurement were taken in the lower part of the exposure.

#### LF11 69.5-80m

LF11 between 69.5-80m consists of a horizontally bedded medium sand, but inclusions of bands consisting of coarse sand to fine gravel in the upper parts of the unit. The bedding planes can be easily traced across the entire unit which can be seen to mimic the contours of the upper contact of LF9 (Fig.18). The second part of the exposed LF11 is observed to thin towards the south. Compared to the initial exposed parts of LF11, the exposure between 69.5-80 m is overlain by LF12. The contacts with the surrounding lithofacies are sharp. Additionally, a small interbed of additional lithofacies such as gravel, diamiction and silty sand is sighted towards the end of LF11. These inclusions lie at the boundary with LF9, with the horizontally layered silty sand layer at the bottom followed by a thin unit of massive gravelly sand. The inclusion of diamiction is in the shape of a wedge that discontinuously extend downward from the LF12 and cuts LF11 and the gravelly sand and silty sand (Fig. 23). A total of 15 bedding planes measurements was taken and shows an average dip of  $12^\circ$  towards NNE (Fig.18).



*Figure 22.* The basal part of LF11 between 65-68 m, showing a network of reverse faults. The black arrows show the direction of the vertical displacement of the bedding planes and the thin black lines illustrates the orientation of bedding planes. A small trowel, approximately 20 cm long, provides scale. The location of the photo is displayed in figure 7.



Figure 23. Small interbeds of diamict, gravel and sand located within LF11, with a trowel for scale (~20cm). The location of the photo is displayed in figure 7.

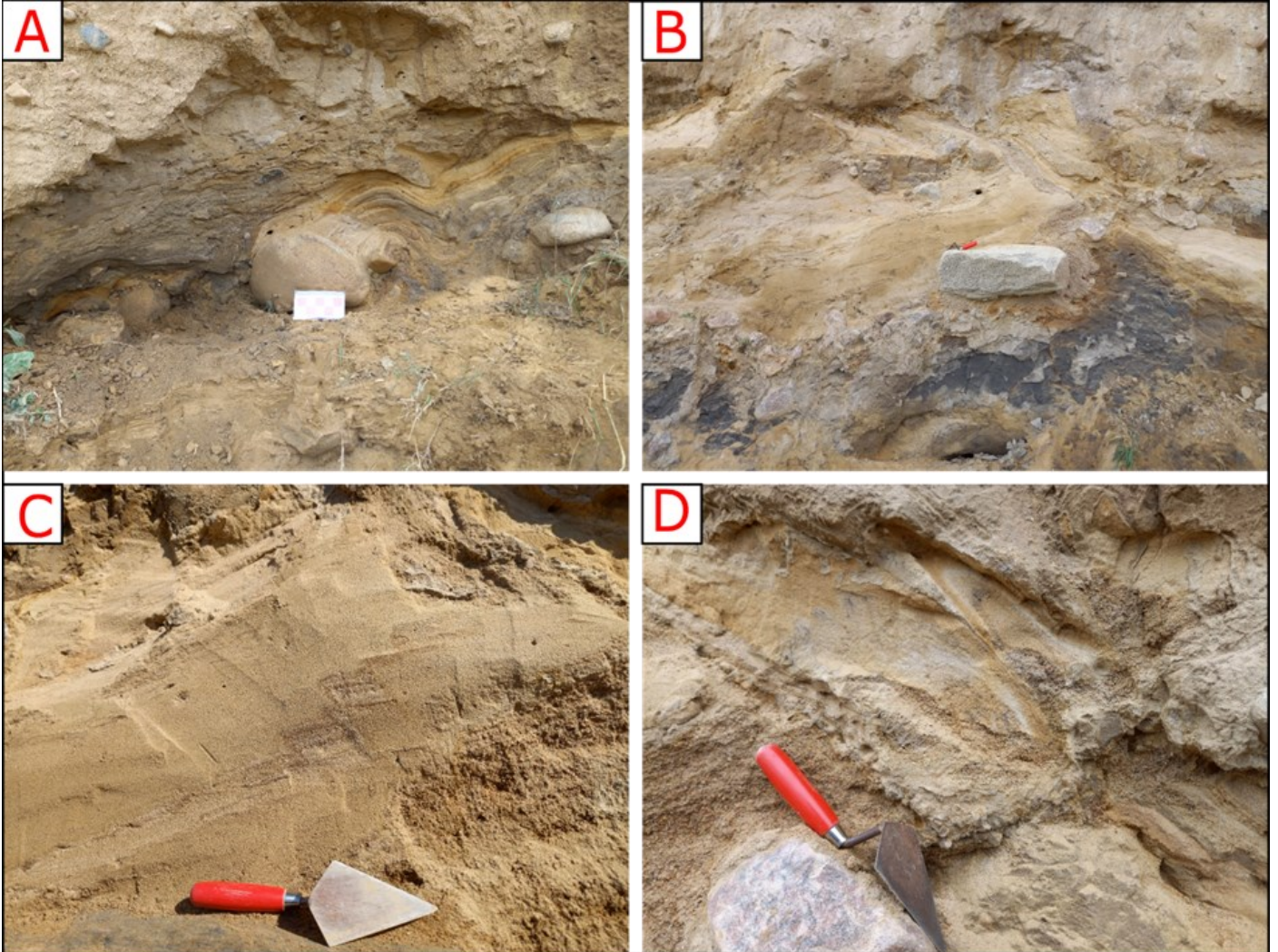
#### LF11 167-182m

LF11 comprises several smaller, irregularly shaped outcrops featuring layered fine to medium sand, with occasional bands of massive clay and silt. Both its internal and external structure exhibit clear signs of both brittle and ductile deformation (Fig. 24; Fig 25). LF11 between 167-182 m is located at the boundary between LF9 and LF 4, where parts of LF11 can be seen to extend into LF12. The contact between the surrounding units is sharp.

Within this section, two different types of folds, sheath, and asymmetric folds (Fig. 24A, B) were observed alongside a series of step faults. The step faults, characterized by a sequence of reverse faults (Fig. 24C), some of which led to the formation of drag folds, are concentrated between 172-174 m (Fig 7). In total five folds were measured with three in the asymmetric fold and two in the isoclinal fold

The axial planes of the asymmetric folds were all tilted towards the SE while the isoclinal folds axial planes displayed varied orientations- one was tilted towards the SE and the other was tilted towards the NW (Fig. 25). Furthermore, 8 fault planes were measured all of

which had a dip between 38-62 ° towards the SSE (Fig.25). Fifteen bedding planes were measured between 172-174 m and showed a predominant tilt of 18° towards the SE (Fig. 25).



*Figure 24.* Deformational structures in LF11 located between 167-182 m in section 1 (Fig. 7). A) Depicts two smaller asymmetrically folded interbeds composed of layered sand. B) Illustrates the irregularly shaped external structure of LF11. C) Shows step faults comprising a series of small reverse faults. D) Displays a small sheath fold. A trowel, approximately 20 cm long, is included for scale. The locations of all depicted photos are indicated in Figure 7.

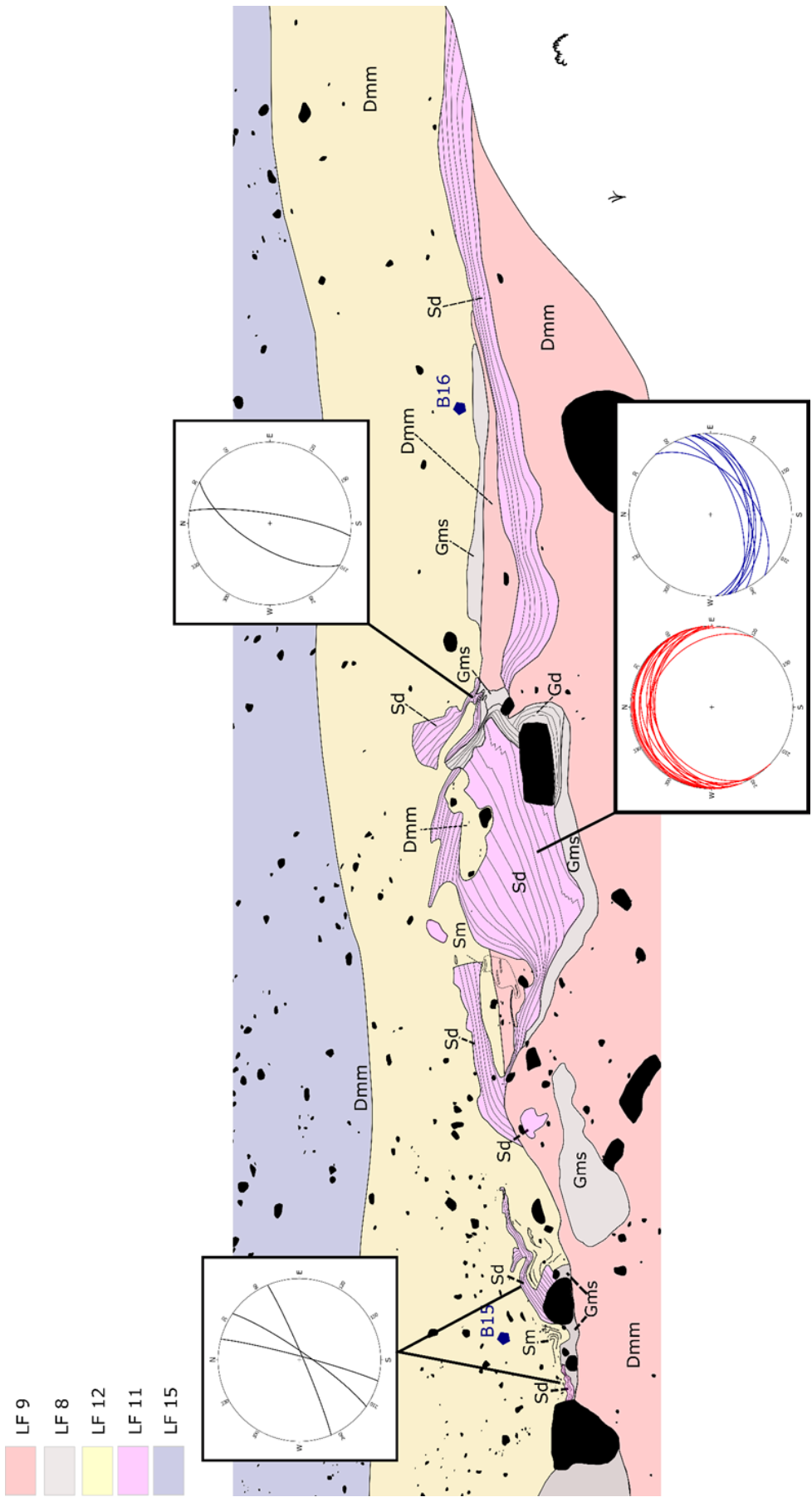


Figure 25. Detail of section 1 at 166-182 m of section 1 (Fig.7), highlighting the overarching directions and orientations of the bedding planes and structural measurements of folds, faults and bedding planes.

### 5.2.12 Lithofacies 12

Lithofacies 12 (LF12) comprises a matrix supported, bi-modal diamict, with a light taupe-coloured fine to medium grained matrix. LF12 can be discontinuously observed between 77-266 m in section 1 (Fig. 7) but can also be seen in section 2 and section 3 (Fig 7, 8). The maximum observed thickness of LF12 is 2 m and the thickness is found to vary laterally. The diamiction displayed varying levels of compaction, evident in section 1 where it is notably loose between 77-85 and 222-262 m, but considerably firmer between 145-202 m. Much like LF9, LF12 is also observed to be clast poor whereas the lithological makeup of the exposed clasts is identical to LF9.

Furthermore, LF12 overlies the underlying lithofacies LF9, LF11 and LF10 with a predominantly sharp basal contact. However, there is a significant variation observed in the contact with LF9 across the studied sections, where the contacts are sometimes more gradual but predominantly erosive. The upper contact of LF12 with LF15 in section 1 between 145-182 m of section 1 could only be assessed at certain locations of the given interval due to the morphology of the cliff section at this location. Consequently, the mapping of the upper contact of LF12 is mostly based on observations in the visual transitions of the lithological content of exposed clasts in LF12 and LF15. However, at places where the contact could be examined it was found to be erosive. Overall, the contacts with the other overlying lithofacies are predominantly sharp, but LF12 can be seen to be interfingering with LF13 in a complex fashion between 77-87 and 253-264 m of section 1.

Several partings of sand are observed throughout LF12 in sections 1 and 2. A small cluster of irregularly shaped interbeds can be seen at section 2, consisting of horizontally layered medium sand with a sharp contact to the surrounding unit (Fig. 7). Near the middle part of section 2 exists two additional interbeds of sand, one planar-shaped consisting of massive medium sand, and one folded with an axial plane measured to have a strike of 105° and a dip of 82°. Moreover, several differently shaped and sized partings of sand were also observed in section 2, while LF12 is seen to be homogeneous in section 3.

The sand partings in section 1 in LF12 are found to be a mixture of stringers and irregularly shaped lenses all of which are composed of massive sand. Both the lenses and stringers are observed to occur in clusters located between 162-169 and 226-232 m (Fig. 6). The stringers have a thickness of >2 cm and can be continuously traced for roughly 0.5-1 m. Some of them are found to be folded, with the highest degree of folding occurring between 167-169 m of section 1 (fig. 7, 15, 16). Due to the subtle nature of the stringers no measurements could be taken on the folds in this zone. The lenses are small in nature with a width of <40 cm and a thickness of <30cm.

Two fabric measurements were taken in the middle diamict, one in section 1 at 80 m (F5, figure 9), and the other was taken in the middle of section 2 (F17, figure 9). The fabric measurement taken in section 1 showed a diverse set of orientations of the clast long axis, the most common being NE, SSW and E. The second fabric measurement demonstrates a preferred orientation of the clast long axis towards the NWW and SE, with the majority of clasts dipping towards the NWW.

### 5.2.13 Lithofacies 13

Lithofacies 13 (LF13), consists of a well-sorted, layered sand that can be intermittently traced near the upper parts of stratigraphic succession at sections 1, 2, and 3. LF13 exposed at three separate locations in section 1 and across Section 2 and 3 (Fig. 6). Along these exposures LF13 is observed to be positioned on top of LF9 but mainly on LF12 and overlain by LF15. Below follows a detailed description of each exposure.

#### LF13 56-68m

LF13 consists of well-sorted stratified medium sand that overlies LF9 and at places LF12. LF13 is predominantly composed of a horizontally layered sand (Fig. 7). However, LF13 between 56-59 m of section 1 consists of planar cross bedded medium to fine sand. Additionally, bands of coarser fractions identified as gravelly sand are observed in the upper parts of the unit.

The upper and lower contacts of the unit are both sharp. While the upper contact is mainly sharp, in certain parts LF13 and LF15 are seen to be interfingering. The maximum thickness of the cleaned section of LF13 was determined in the field to be 1.6 m and can be seen to thin out towards the east of the section.

Deformation structures are seen across the upper parts of the unit beneath big boulders with a diameter of roughly 90 cm. These deformation structures consist of distorted and compacted bedding planes that wrap around the boulders (Fig.26A). Additionally, behind one of these boulders LF13 between 66-67 at the conjunction with LF9 and LF15, is a tectonically juxtaposed structure where LF13 alongside LF11 consists of a complex system of irregularly shaped and sheared lenses surrounded by the two diamicts (Fig.26C). Additional deformation structures consist of a single sheath fold located at 60.5 m of section 1 (Fig. 7). No measurements could be taken of the fold due to its small size.

At 60-63 m at section 1 in LF13 exists a bi-convex-shaped lens consisting of a diamicton. This lens exhibits long tails on either side, that horizontally spreads and thins outward approximately one m on either side. The lens has a maximum thickness of 0.3 m and a

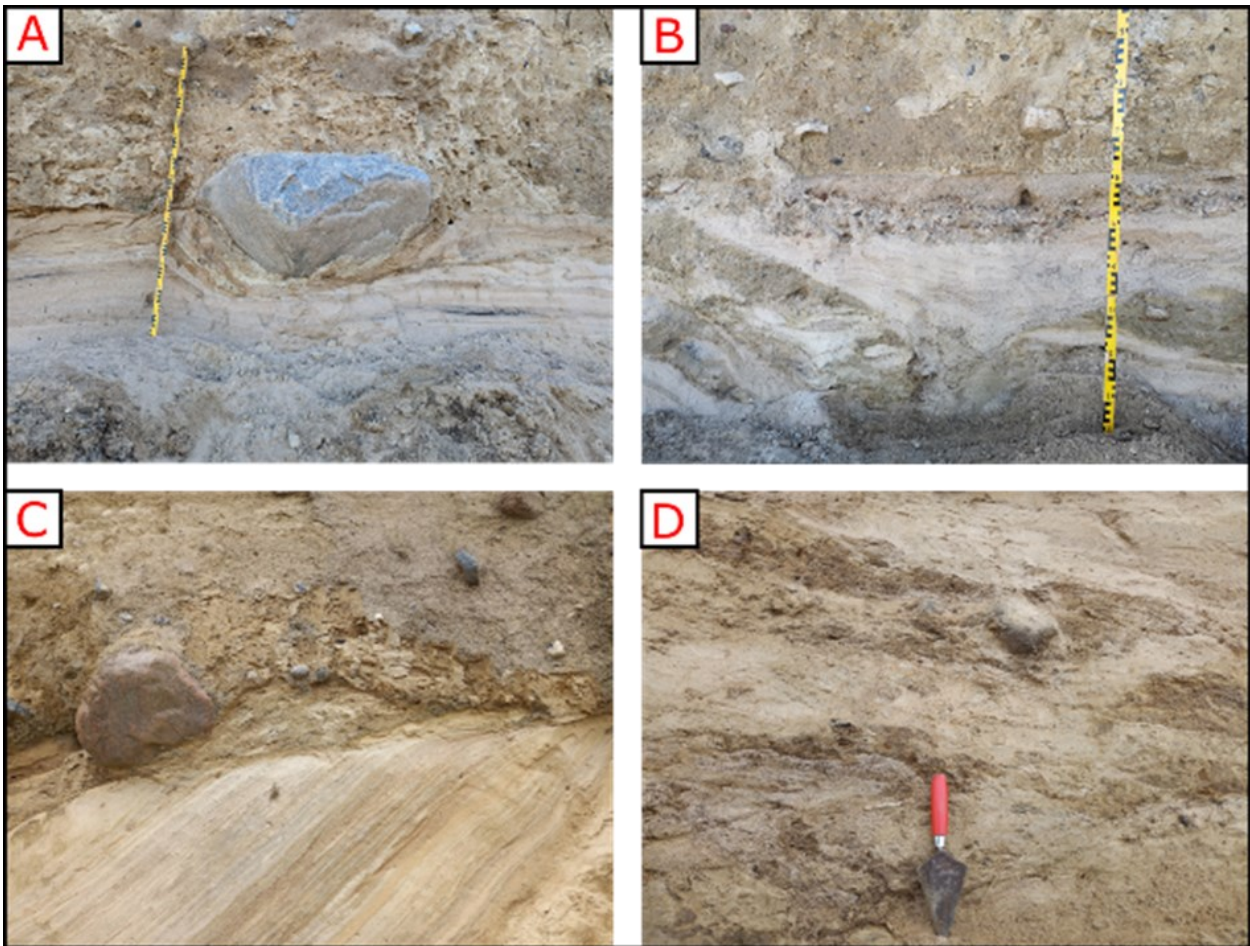


Figure 26. Deformational structures within LF13: A) Distorted and compacted bedding planes in LF13 wrapping around a boulder within LF15. B) Triangular-shaped unit located in the upper segments of LF13. C) Network of irregularly shaped and sheared lenses of sand. D) Complex amalgamated zone within LF13 comprising diamicton and sand, with a trowel for scale (~20cm). The location of the images are shown in figure 7.

width of 1.2 m.

At 64-65 m in LF13 there is an triangular-shaped unit (Fig. 26B), partially located inside LF15. The internal structure of the unit comprises three lithofacies: a sequence of stratified medium to fine sand, followed by a thin clast-supported bi-modal gravel sheet overlaid by a massive coarse sand to fine gravel. The maximum thickness of this unit is about 0.5 m, while the width of the top of the structure is around 2 m. The contact point between the surrounding LFs including the lower part of LF13 are sharp. The internal contact between the massive gravel and the layered sand at the base of the unit is sharp, while the boundary between the clast-supported gravel and the overlying coarse sand is significantly more gradual. To the left of this segment are several irregularly shaped lenses of layered medium sand that are located inside of LF15 (Fig.26B).

A total of 20 different bedding planes were measured in the lower parts of the unit, which showed an average tilt of  $11^\circ$  with a preferred orientation toward the NW (Fig.18).

#### LF13 77-87m

LF13 between 77-87 m in section 1 is characterized by a complex amalgamated zone of massive sand and

diamict(Fig. 26D). While the sand is predominantly massive, parts with deformed bedding planes occur within this section. The sand is composed of a mixture of fractions ranging from fine to coarse sand. The basal contact between LF13 and LF12 is complex where LF12 is seen to be interbedded with LF13. The upper contact of LF13 and LF15 are gradual. This complex zone can be easily traced from 77 m but gradually skews, where individual parts of sand become sparser and the basal part of LF15 gradually becomes increasingly sandier.

#### LF13 182-264m

LF13 is discontinuous but can be traced from the beginning of 182 m until 264 m as previously mentioned in section 1. However, the largest continuous exposure where the unit can be examined from top to bottom is between 222-236 m. LF13 is seen be superimposed on LF12 but at 184-187 a small section of LF13 can be seen to extend into LF12. The greatest exposed thickness of LF13 at the given interval is roughly 1.5 m.

Two discontinuous lenses of LF13 are observed between 182-188m and 198-203m. These lenses consist of fine sand to coarse silt with interbeds of clay.

LF13 between the 222-236 m is characterised by a fining upwards sequence where the basal part of the unit consists of horizontally layered medium sand which gradually transitions into a horizontally laminated silty sand. Above the laminated silty sand is clay and fine sand to coarse silt interwoven in a complex amalgamated fashion (Fig. 27A,C). The clay in the upper part of the section is massive and its internal structure at certain places in the upper part is composed of horizontal pillars. Furthermore, the sand in the upper part of the unit is interbedded with small bands of clay, which are indistinguishable from the two smaller exposures between 182-188 and 198-203 m previously explained.

At roughly 228 m a small section of LF13 is seen to extend downwards into LF12 where it cuts the basal part of a unit consisting of horizontally layered medium sand (Fig. 27C, D). Additionally, the laminated silty sand can also be seen to cut into LF12 in a wedge-like manner. The bedding planes in the basal medium sand part near this cut can be seen to be deformed and partly folded downward at either side. The contact point between the laminated silty sand and the horizontally layered sand are sharp in the parts that extend downwards. The bedding planes of the laminated silty

sand that extend downwards show a complex pattern where the bedding planes can be seen to be folded downwards.

LF13 between 222-236 m is seen too thin toward the south and dissipates at 236 m before reappearing in the form of several smaller irregularly shaped lenses located inside of LF15 and at the border between LF12 and LF15. These irregularly shaped lenses are made of silty sand and the internal structure is made up of heavily plastically deformed bedding planes. A complex heterogeneous zone can be seen at 253-264m in section 1 (Fig.7), consisting of a network of these sand lenses interbedded with diamict (Fig.27B).

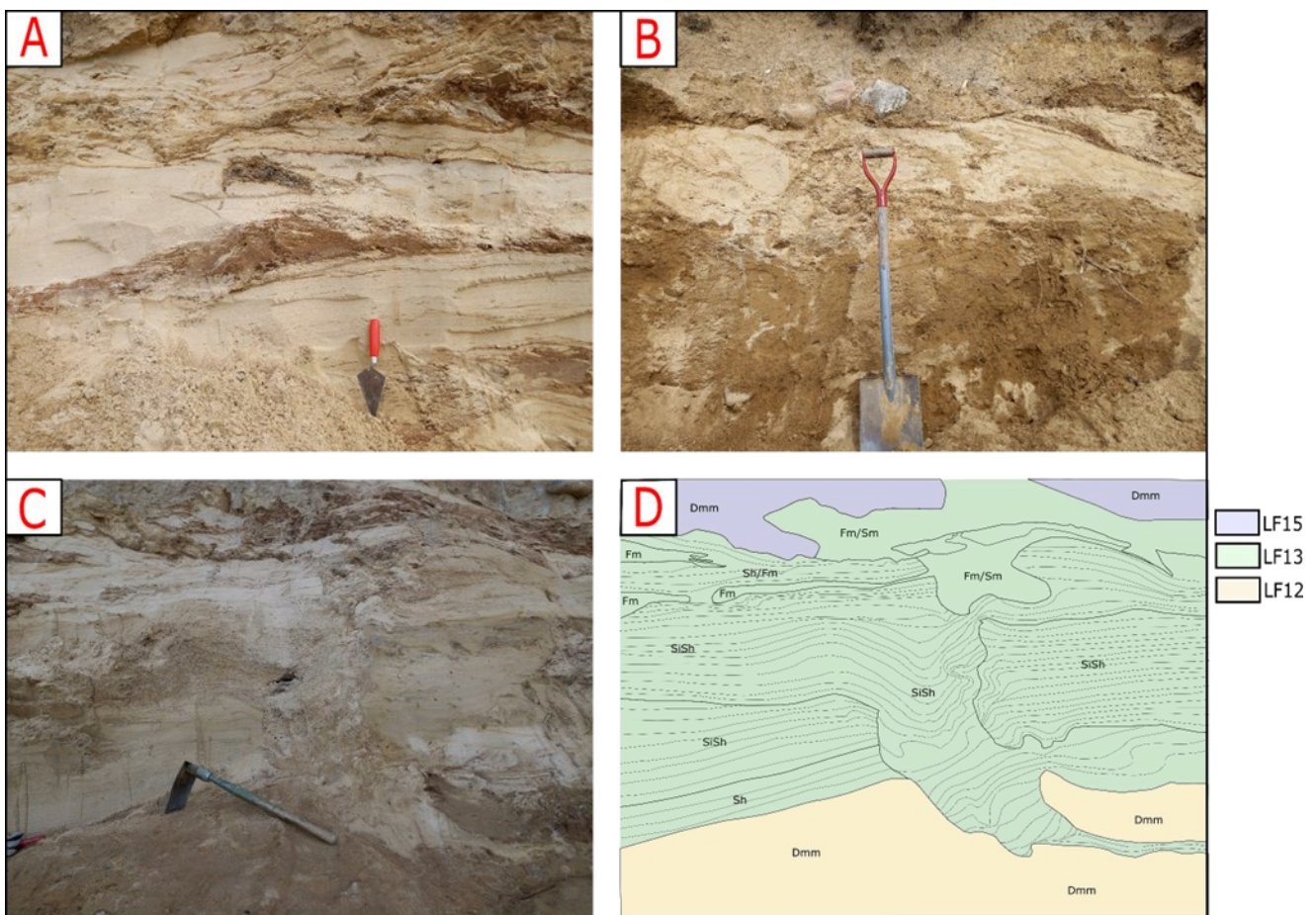


Figure 27. Deformational structures within LF13: A) A complex network of interwoven sand and clay, with a trowel for scale (~20 cm). B) Lenses of sand interbedded with diamict, with a shovel for scale (~1 m). C) Upper segments of LF13 descending into LF12 in a wedge-like fashion, intersecting preexisting bedding planes of the lower parts of LF13. The trenching tool is included for scale (~40 cm). D) Sketch corresponding to picture "C," illustrating the orientation of the bedding planes. The location of each photo is shown in Figure 7.

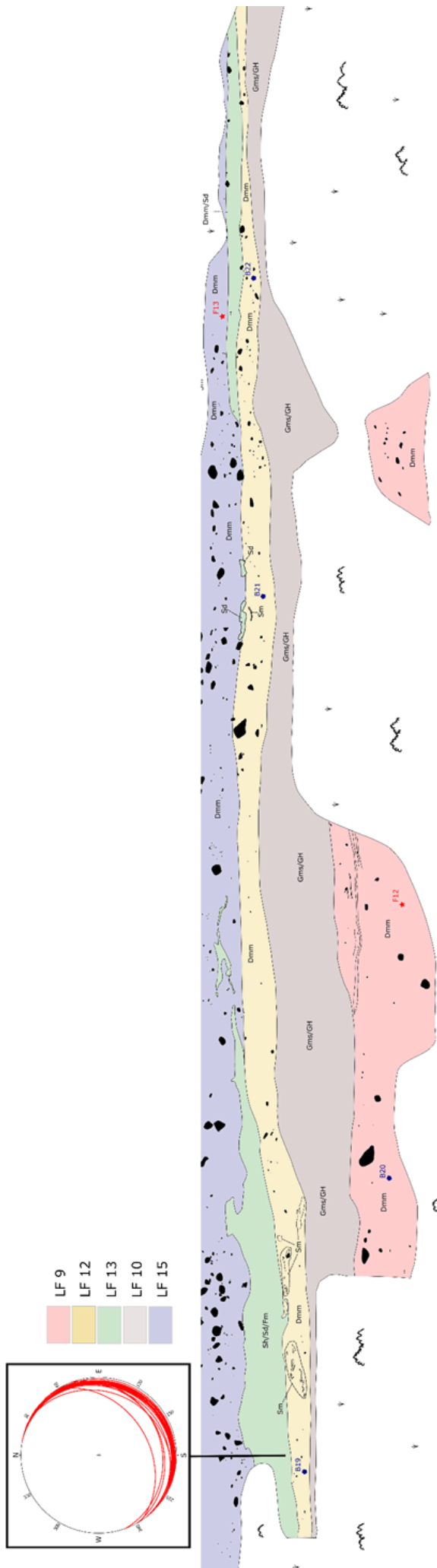


Figure 28. Detail of section 1 222-264 m of section 1 (Fig. 7), highlighting the overarching directions and orientations of the bedding planes.



### LF13- Section 2

LF13 in section 2 is characterized by discontinuous lenses of layered medium sand, broken into four individual parts that lies at the boundary of LF12 and LF15 (Fig. 8). The sand parting to the south of the section consists of deformed medium sand, where the bedding planes are clearly folded. This is followed by a small biconvex shaped parting of horizontally bedded sand. Additionally, the largest part of sand is in the middle of the section and is irregularly shaped. The bedding planes of this part have been subjected to soft deformation where the bedding planes can be seen to be deformed and follows the lenses irregularly shaped exterior. Lastly, lens located in the most northern part consists of horizontally layered sand, but worth mentioning is that only parts of the lens is visible due to erosion of the cliff section. The size of the different lenses varies where the largest lens in the middle of the section is almost 2 m wide and 0.5 m tall, and the other lenses being considerably smaller (Fig. 8). The surrounding contacts with LF12 and LF15 and LF13 are all sharp.

### LF13- Section 3

LF13 in section 3 is characterised by two subunits. The basal unit which consists a bright orange heavily compacted medium to coarse grained sand with faint horizontally layering, with interspersed darker layers consisting of organic material. The basal unit is followed by a light beige coloured crudely horizontally layered, loose medium sand. Moreover, LF15 can be seen to extend into the upper parts of unit LF13 in a thin wedge-like shape at 4 m in section 3 (Fig. 9). The maximum observed thickness of the LF13 is ~40 cm. Furthermore, a faint pinch and swell structure is observed within LF13, with the pinch occurring at 3 m of section 3 and with the swell formation on either side but most pronounced on the right-hand side (Fig. 9). The contacts with the surrounding diamictions, LF12 and LF15, are exclusively sharp much like the internal contact between the two subunits.

#### 5.2.14 Lithofacies 14

LF 14 consists of a massive, poorly sorted gravel consisting of boulders and cobbles enclosed in an unsorted matrix consisting of gravelly sand. The unit is exposed at 295-299 m of section 1 and lie directly beneath LF15 (Fig.7). The basal contact is erosive where LF14 can be seen to intersect the bedding planes of LF3 forming an angular conformity. Additionally, the upper contact of the unit with LF15 is sharp.

#### 5.2.15 Lithofacies 15

LF15 is composed of a light brown massive, matrix-supported bi-modal diamict, with a medium grained matrix. The diamict is situated at the top of the stratigraphy throughout all examined sections and can be

continuously traced from 0 to 265 m in section 1 where it can then be discontinuously traced between 295-355 m due to slumping (Fig. 7). LF15 shows a lateral variability in terms of its thickness where the maximum observed thickness is 5.6 m. LF15 is found to be enriched in clasts compared to the other diamictions LF9 and LF12, where the clast lithology are found to consist of crystalline and sedimentary rocks such as flint, chalk, and limestone. The basal contact of LF15 is sharp, and at places the upper diamict can be seen to be incorporated with the underlying units. Due to the height and morphology of the cliffs the upper parts of LF15 could not be properly examined, therefore not much can be said in regard to the diamictions properties in the upper parts of section 1. However, examination of the upper parts of LF15 along section 2 and 3 revealed a homogenous nature of the diamict from top to bottom. Furthermore, pseudo lamination is observed in the basal part of LF15 between 0-38 m in section 1 (Fig.7).

Partings of sand can be seen sparingly across the basal part of the diamiction, consisting of thin stringers (maximum thickness <1.5 cm) and small lenses of sand and silt that can be laterally traced over a distance of 2 m. The stringers are predominantly horizontal but between 30-36 m in section 1 they can be seen to be vertical and wrapping around boulders. Furthermore, the observed lenses are small in nature, often only a few centimetres in width and thickness. The lenses are a mixture of small spherical to near circular and irregularly shaped lenses, consisting of massive silt and sand.

LF15 between 329-337 m is seen to extend downward into LF3 in a wedge-like fashion intersecting bedding planes in LF3 and 10 (Fig. 12C). The surrounding contacts with the other lithofacies are sharp.

Eight fabric measurements were taken at regular intervals of LF15 (Fig 9). These fabric measurements indicate a preferred clast long axis orientation of NW and SE with the most common orientation being NW. Compared to the fabric measurements taken in the other diamicts, LF15 exhibits on average a much stronger fabric with the average eigenvalue of 0.73 (Fig.10).

## **6 Fine gravel analysis**

A total of 28 bulk samples were taken for fine gravel analysis, collected from regular intervals throughout LF9, LF12 and LF15 at section 1 and 2 (Fig. 7; Fig. 8). The lithological assemblage of each bulk sample is illustrated in figure 29 and the amount of the bulk samples collected from each diamict in the different sections is shown in Table 1.

Table 1- Number of bulk samples collected from each diamicton in section 1, 2, and 3.

| Lithofacies: | Bulk samples (n): |           |           |
|--------------|-------------------|-----------|-----------|
|              | Section 1         | Section 2 | Section 3 |
| LF9          | 7                 | 1         | 0         |
| LF12         | 7                 | 1         | 0         |
| LF15         | 11                | 1         | 0         |

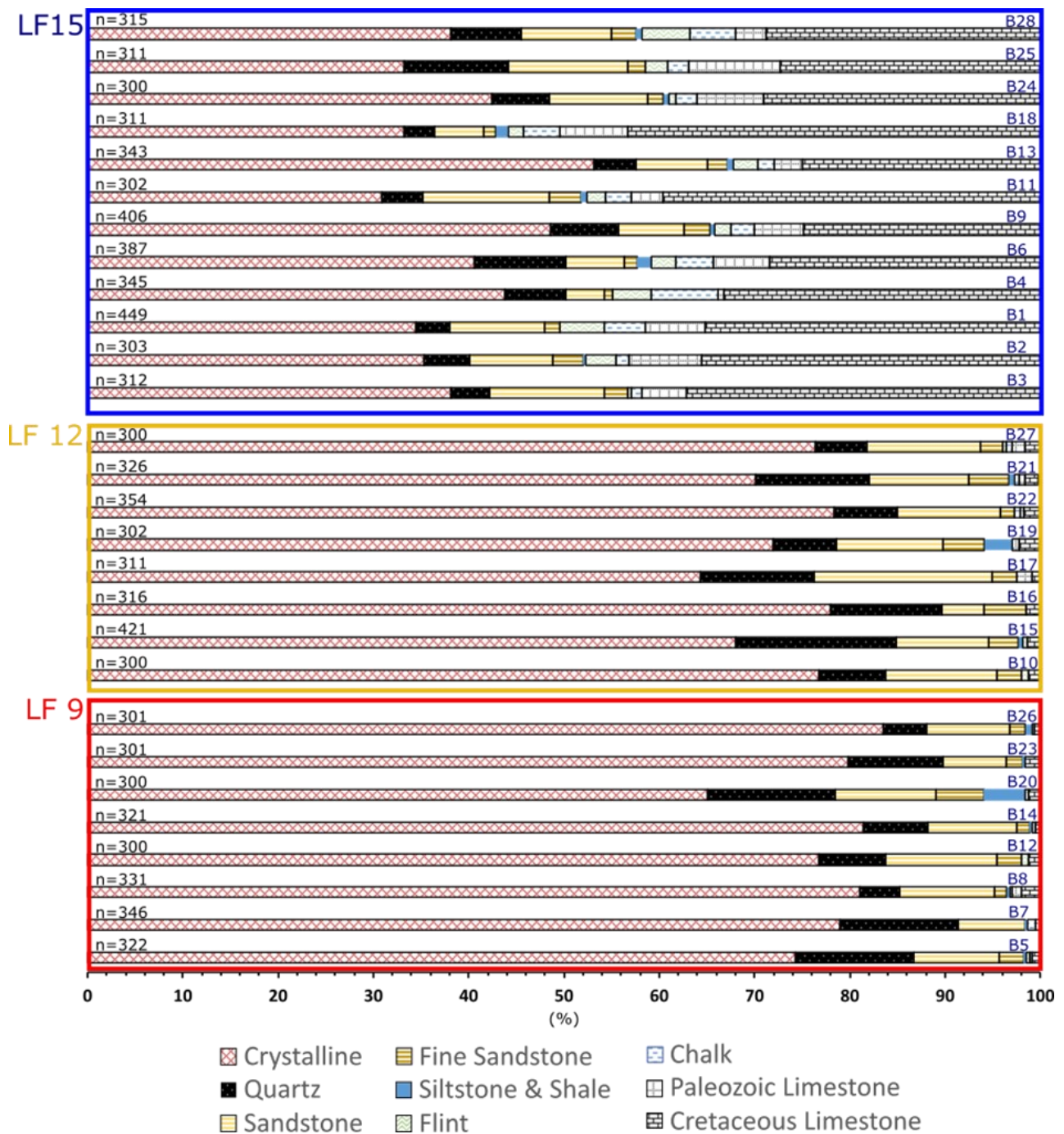


Figure 29. Percentages of different lithological categories of the fine gravel fraction (2-4 mm) of samples taken from LF9, LF12 and LF15 at various locations in section 1 and 2. The blue letter “B” followed by a number refers to the sampling location within the 2d-log seen in figure 7 and 8. “n” stands for the number of counted grains in each sample.

Through fine gravel analysis two distinct lithological assemblages can be identified where LF9 and LF12 share a similar lithological makeup dominated by crystalline grains compared to LF15 composed of larger quantities of limestone (Fig. 29). LF9 and LF12 both exhibit a significant quantity of crystalline grains that are seen to dominate the lithological assemblages between 64-83% in individual samples and averaging 75.2%. The second most common lithology in both LF9 and LF12 were quartz and sandstone with quartz varying between 4% and 17% in individual samples and an average of 8.2%, and sandstone ranging from 4% to 18% in individual samples with an average of 8.9%.

The remaining lithologies in LF9 and LF12 are highly diverse, although fine sandstone occurs at the highest average percentage at 2.3% with the highest percentage found in samples B19, B20 and B21 at roughly 4.3% respectively. The remaining lithologies being Palaeozoic limestone, Cretaceous limestone, siltstone and shale, flint, and chalk were all found to have an average percentage of <1% except for Cretaceous limestone that averaged 1.2%.

In contrast to this, LF15 has an average of 39% crystalline grains, with a peak of 53% and a minimum of 30% seen in B13 and B11, respectively. The second most prevalent lithology in LF15 is Cretaceous limestone with a composition pending between 25%-43% across individual samples and with an average of 32%. Sandstone followed by quartz are the third and fourth most common lithologies, with sandstone varying between 4%-12% (averaging 9%), and quartz varying between 3-10% (averaging 6%). Additionally, higher values of Palaeozoic limestone, flint and chalk are observed in LF15. Palaeozoic limestone is seen to occur at a frequency between 1-10% with an average of 5%, and flint between 1-5% and chalk pending between 0.4-5%, both with an average of 3%. The remaining lithologies, siltstone, shale and fine sandstone occurs at low frequencies, with fine sandstone averaging at 2% and siltstone and shale averaging at <1%.

## 7 Interpretation of depositional environments

### 7.1 Interpretation of LFA1

Based on homogeneity of the lithofacies LF1, 2, 3, 6, 7, and 11 they can be grouped together into one lithofacies association (LFA1). LF1-3 are seen between 296-336 m of section 1 while LF7 and 8 are seen between 97-103 m of section 1 (Fig.7). All lithofacies show a predominant mixture of fine-grained sediments such as silt, clay and fine sand which were deposited in a rhythmic and horizontal manner.

Rhythmic sequences of finer grained sediments con-

taining silt, clay and fine sand that is horizontally layered to laminated are often associated with slow gravitational deposition in calm standing water in glaciolacustrine or glaciomarine settings (Evans and Benn, 2010; Carrivick and Tweed, 2013). A few outsized clasts of varying sizes were found in LF3, 12 and 2 and are interpreted as drop stones, based on the bedding planes that are seen to be penetrated by the clast or they are bending around the clast, both of which are structures are a commonly seen in sediments with drop stones (Thomas and Connell, 1985). The presence of outsized clasts in laminated to massive fine-grained deposits are commonly linked to ice rafted debris (IRD) (Thomas and Connell, 1985; Evans and Benn, 2010). IRD can range from clay-sized particles to boulders and is linked to both glaciolacustrine and glaciomarine environments (Dowdeswell, 2009; Anderson et al., 1980). Thus, the presence of isolated, outsized clasts in LFA1 further suggests a glaciolacustrine or a glaciomarine origin of the sediments. Furthermore, the observed alternating beds of clay and silt in the sediments is thought to be connected to changes of the energy in the depositional environment or changes in debris transport.

### 7.2 Interpretation of LFA2

LF4 and LF5 are based on similarities in overall structure, facies, and stratigraphic position combined into LFA2. Both lithofacies exclusively seen in section 1 between 295-325m. LF4 and LF5 consists of coarser grained sediments compared to LFA1, but as previously mentioned finer grained sediments occur within the basal part of LF4.

A coarsening upwards sequence is observed in LF4 with the basal parts consisting of a mixture of fine sand and silty sand. In contrast the upper parts consist of medium to coarse-grained sand that is horizontally layered and occasionally cross-bedded with repeated thin bands of organics and occasional fine-grained bands of silty sand. LF5 has a gradual contact with LF4 as observed between 314-319 m of section 1 and consists of horizontally layered sandy gravel and gravelly sand. LFA2 is interpreted to represent a change in the depositional environment from a glaciolacustrine to a glaciofluvial setting. This interpretation is based on the observed coarsening upwards sequence, from fine-grained horizontally layered sediments typical of glaciolacustrine setting, to coarse-grained sediments that are a mixture of horizontally layered and cross-bedded which are common for glaciofluvial settings.

The differences in sedimentary structures and grain size noted within the upper parts of LF4 and in LF5, alongside occasional sharp transitions, are believed to have been attributed by fluctuation in the energy conditions of the water, indicating a dynamic setting. Similar findings of a diverse set of sorting and sedimentary structures with inclusions of organic sediments are commonly found in outwash plains, where

the type of deposit is dependent on the flow competence (Salamon, 2009; Mleczka and Pisarska-Jamrozy, 2021; Nesje et al., 2023; Singh et al., 2023). Furthermore, the inclusion of recurring organic sediments such as coal have also been found in outwash plains and are thought to represent former river bars or floodplains in braided rivers. The coarser fraction and the organic sediment found in LF4 and LF5 are interpreted as an outwash sediment, as the internal structure and texture are commonly associated with a braided river environment (Miall, 1977, Bridge, 1993).

### 7.3 Interpretation of LF8

LF8 consists of a combined four smaller units including silty sand containing inclusions of fine to medium sand, followed by gravelly sand, and lastly fine to medium sand. All of the units are layered except for the silty sand unit with its sandier inclusions that are all massive. These lithofacies together make up a recumbent fold on the verge of becoming an enclosed fold and are located inside of LF9. Due to the high degree of ductile deformation, it is difficult to assess the initial internal structure before deformation. However, considering the sorted nature of the and the variations in grain size a glaciofluvial origin for the sediments is likely (Benn, 2009). Furthermore, the high degree of sorting alongside the occurrence of organic sediments in the form of bands of peat and the variations in facies, suggest a glaciofluvial environment possibly linked to a braided river system located on an outwash plain. As previously mentioned, the sedimentary characteristics of braided river system on an outwash plain features a wide array of different types of sediments, where inclusions of organic sediments can occur which may explain the different facies and the inclusion of organics in the sediment within LF8 (Boothroyd and Ashley, 1975; Pochocka-Szware and Kryszkowski, 2015).

### 7.4 Interpretation of LF9

LF9 consists of a dark grey matrix supported, bimodal diamicton with a fine-grained matrix. Due to the high level of compaction and dimictic nature of the sediment, LF9 is interpreted as a sub glacial traction till, characterized as a primary glacial deposit with great variance in grain size distribution (Evans et al., 2006; Evans, 2017). Furthermore, the inclusion of different sand partings such as stringers and lenses are a common occurrence in subglacial tills, often linked to infills of subglacial water channels during periods of decoupling (Evans et al., 2006). Occasional fissility structures were observed in various parts of LF9, which is commonly found in subglacial tills and result from shear stress forming horizontal fractures within the till (Evans et al., 2006). Thus, the presence of stringers and lenses combined with the occasional fissile nature of the diamict further speaks for a subglacial

origin of the till. A clear dominance of crystalline and quartz grains was noted in the fine gravel section of the sediment with low variations between samples. These low variations indicate a homogenous and well mixed till matrix (Eyles and Menzies, 1983; Clarke 1987). The presence of lenses and stringers of sand suggests that the ice sheet that deposited the subglacial till was warm based due evidence of presence of flowing water in the subglacial zone (Piotrowski and Tulaczyk, 1999).

### 7.5 Interpretation of LF10

LF10 consist of a discontinuous gravel bed, which exhibits a fining upward sequence where the basal part consists of an poorly sorted massive gravel and the upper parts consists of a sorted horizontally layered sandy gravel. LF10 exhibits great lateral variations in the thickness of the layer and contains boulders with a

diameter of  $\leq 50$ cm. Given by the sorting and content of larger clasts LF10 may be interpreted as proximal outwash sediments deposited in a braided river environment. Proximal outwash sediments are deposited in the parts of the outwash plain located in the proximity of the ice margin, and subsequently characterised by coarse grain size fractions (Boothroyd and Ashley, 1975; Pochocka-Szware and Kryszkowski, 2015), due to the high flow rates. Furthermore, the internal structure and texture of the LF10 can also be associated with high energy braided river deposits (Miall, 1977, Bridge 1993). The fining upwards sequence are thought to represent the transition from a proximal setting to a more distal setting with a lower flow competence, based on the fining of the sediment in the upper parts as the ice sheet receded. An alternative interpretation for the LF10, is that it may be a subglacial channel fill due the presence of large boulders. However, as observed by Adrielsson (1984), LF10 is part of a more extensive unit that can be seen across large parts of the island. Due to the lateral extent of this deposit, it is thus unlikely to be part of a subglacial channel fill.

### 7.6 Interpretation of LF12

LF12 is composed of a matrix supported, bi-modal diamiction, with a light taupe-coloured fine to medium grained matrix. The diamicton was found to have a great lateral variance in exposure and thickness and contains several sheared and folded partings of sand. LF12 is interpreted as a primary glacial deposit, due to the diamictic nature of the sediment (Evans et al., 2006; Evans, 2017). Due to the dimictic nature, LF12 is labelled as a subglacial till.

## 7.7 Interpretation of LF13

LF13 mainly consist of a well-sorted, layered, medium sand with occasional inclusions of bands consisting of coarse sand, but between 182-237 m are inclusions of finer grained sediments such as silty sand and clay. LF13 can be intermittently traced near the upper parts of stratigraphic succession at section 1,2 and 3. LF13 is interpreted as a glaciofluvial outwash sediment likely deposited in a low energy braided river environment. The horizontally layered medium sand is believed to be a braided river deposit, and the finer grained sediment such as silty sand and clay found between 182-237 m in section 1 are commonly associated with stagnant water or very low energy currents which allows gravitational deposition to occur (Boothroyd and Ashley, 1975; Pochocka-Szwarc and Kryszkowski, 2015). The stagnant water may be the result of a channel abandonment or a transition into a proglacial lake environment. However, it is difficult to assess if the inclusions of the finer grained sediments are isolated inclusions or if they are a part of a much larger system, due to the erosion and deformation of the lithofacies. Although, it is unlikely that the sediments are derived from an abandonment of a channel due to the alternating beds of fine sand and clay which suggest periods of influx in sediments, which would not be expected in an abandoned channel (Miall, 1977). Instead, a transition into a proglacial lake is more likely considering the alternating facies (Carrivick and Tweed, 2013). Alternatively, the finer grained material may also be the result of a markedly decrease in flow competence in the outwash plain allowing finer grained material to be deposited (Mlecza and Pisarska-Jamroz, 2021). The gradual contact between the coarse sediments and the finer grained material suggests a gradual transition of the depositional environment.

## 7.8 Interpretation LF15

LF15 is composed of a light brown massive, matrix-supported bi-modal diamict, with a medium grained matrix. The diamict is located at the top of the stratigraphy throughout all examined sections. Considering the strong fabric ( $S_1 > 0.70$ ) coupled with a high level of compaction and the unsorted nature of the sediment, LF15 is interpreted as a subglacial till (Evans, 2017). Compared to LF9 and LF12, LF15 exhibits a larger variance in the fine gravel section of the till matrix which indicates a poorer degree of mixing in traction zone (Eyles and Menzies, 1983; Clarke, 1987), compared to LF9 and 12.

LF15 is seen to extend downwards in a wedge-like shape into LF3 intersecting preexisting bedding structures. Given wedge-like shape of the external structure this part of LF15 is interpreted as a till injection. Similar occurrence where LF15 are seen to extend downwards into the substrate has also been observed in section 2 but at a much smaller scale. Till injections are a

form of water-escape structure and are often initiated by hydrofracturing (Van der Meer et al., 1999; Phillips et al. 2013). Hydrofracturing is caused when high porewater pressure caused by the glacial overburden exceeds the tensile strength of the host material causes a fracture which is subsequent filled by sediment (Van der Meer et al., 1999). However, clastic injections may also be initiated by pressurized sediment and water through the exploitation of preexisting fractures (Rijsdijk et al. 1999). The presence of till injections in LF15 supports the notion of a subglacial origin of the till.

## 8 Lithostratigraphy of Ven

As previously discussed, the examined cliff sections located on the northern parts of Ven exhibits 15 distinct lithofacies, with a complex lateral distribution. However, field observations alongside eight vertical profiles taken at various locations in sections 1 and 2 (Fig.7; Fig. 8), and fine gravel analysis of various diamictions, are synthesized to present an interpreted overview of the vertical and lateral connection of the various lithofacies. Figure 30A illustrates this interpretation also forming the basis for the composite vertical profile, seen in figure 30B, which shows the interpreted lithostratigraphic succession of the studied cliff sections.

The oldest sediments in the stratigraphy are LF1, 2, and 3 belonging to LFA1 which was interpreted as glaciolacustrine sediments. These glaciolacustrine sediments are then overlain by LF4. with the basal part interpreted as a glaciolacustrine deposit transitioning into a outwash deposit towards the top. LF9 is later superimposed on these sediments, interpreted as a subglacial traction till. Important to mention is the fact the contact between LF9 and LF1, 2, 3, 4, and 5 could not be located in the field. However, the interpretation that these sediments predate LF9 stems from the glacial tectonic structures seen between 282-340 m of section 1 (Fig.7), interpreted as a thrust plane complex (see section 6.1).

Uncertainties regarding the positions of LF6 and LF7 in the stratigraphy are worth noting, due to buried contacts. However, since LF7 and LF6 are superimposed by LF9 between 101-104 m of section 1 (Fig. 7), I suggest that that these sediments predate the initial glacial advance that deposited LF9. LF7 and 6 are both interpreted as glaciolacustrine sediments and since they are thought to predate the onset of LF9 and due to the similarity in facies they are interpreted to be a part of the glaciolacustrine sediments LF1, 2, 3 and the basal part of 4. However, further analysis is needed to answer to which part of the sedimentary succession LF7 and 6 are connected, due to possible unconformities in the strata. Much like LF7 and 6, uncertainties regarding LF8 connection to the overarching stratigraphy is difficult to assess, due to the discontinuous na-

ture of the unit. LF8 is interpreted as a glaciofluvial deposit that forms the basis for a recumbent fold located inside of LF9. LF8 is interpreted to predate LF9 and be a part of the glaciolacustrine to glaciofluvial sediments previously explained.

On top of LF9 sits a complex discontinuous layer of poorly sorted gravel (LF10) and fine-grained sediments (LF11). LF11 was interpreted as a glaciolacustrine sediment while LF10 was interpreted as a proximal outwash deposit. LF10 and LF11 was predominantly located between LF9 and LF12, where LF12 was interpreted as a subglacial till. LF12 is seen to be superimposed by LF13 in section 2, 3 and large parts of section 1 with the notable exception between 55-67 m of section 1 (Fig. 6), where LF13 is seen to be deposited directly on top of LF9. LF13 is later superimposed by LF15. LF15 is interpreted as a subglacial till and is interpreted as the youngest sediment in the succession based on its place in the stratigraphy.

(A)

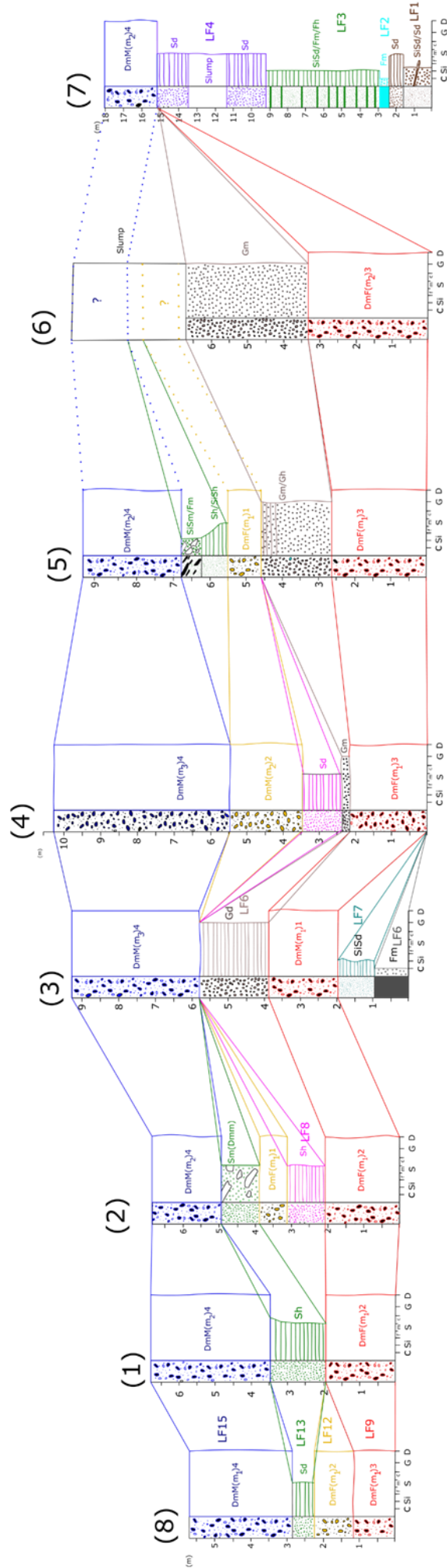


Figure 29. A) Vertical profile showing the interpreted lateral distribution/continuation of the lithofacies. A more detailed version of each vertical profile is presented in the Appendix. The number within the brackets refer to the location of the vertical profiles in the 2D-logs (Fig. 7, 8). B) Summarized vertical composite profile showing the interpreted sedimentary succession of the examined cliff sections and correlations to previous studies. The black arrows show the preferred clast long axis orientation inferred from fabric measurements.

(B)

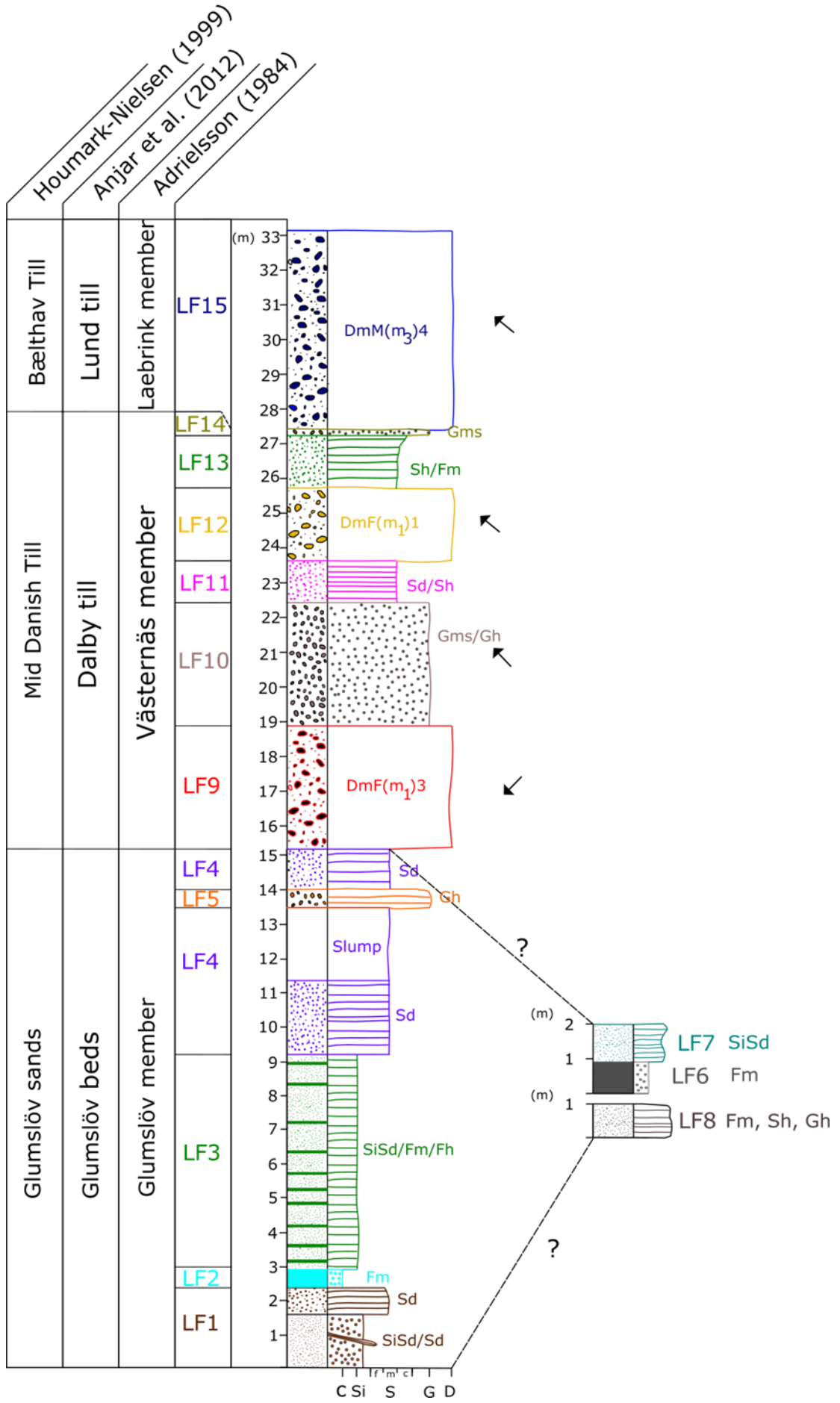


Figure 29. (Continued)



## 9 Tectonic evolution of Vens strata

### 9.1 Overview

The stratigraphy can be summarized to consist of three till beds LF9, LF12 and LF15 and 12 additional beds. The till beds are separated by sorted sediments interpreted as outwash deposits (LF4, 5, 8, 10, and 13) and glaciolacustrine deposits (LF1, 2, 3, and 11). A wide set of deformation structures are located within the sorted sediments. The deformation structures consist of a mixture of shear bands, faulting, folding, and boudinage, all which serves as a kinematic indicator to construct ice flow direction as well as granting a basis for interpreting the tectonic evolution of Ven's strata and give general ideas regarding the degree of deformation that may be present in the Alnarp valley fill located in the mainland. The glaciotectonic structures are related to glacial advances over the region and two types of deformation structures can be distinguished those caused by: (1) proglacial deformation characterised by compressional stress, and (2) subglacial deformation caused by pure but mainly simple shear. Below follows an interpretation of various deformation structures seen in different lithofacies following the interpreted stratigraphic order discussed above. These interpretations are then combined with the interpreted stratigraphy of the northern sections to construct a conceptual model of the tectonic evolution of the northern strata of Ven.

### 9.2 Interpretation of structural elements in LF1, 2, 3, 4, and 5

LF3, 4 and 5 sediments are characterized by a complex system of low angled normal faults which are most prominent in LF4 where the faults can be seen throughout the entire unit (Fig. 12A, 13, 14). These faults are interpreted as Riedel shears which are a brittle shear zone structure, consisting of a conjugate set of shear bands (Van der Wateren et al., 1999; Davis et al., 2000).

These types of structures are typically found underneath till beds and in push moraines (Van der Wateren, 1995). The Riedel fractures can be categorised into different groups of shears including R, R', P and Y-shears linked to the characteristics and orientation of the subglacial shear zone (Phillips, 2018). The Riedel shears of the examined sediments consist almost exclusively of Riedel shear planes (R), but inclusions of antithetic Riedel planes are present in the upper parts of LF4. These fractures can occur at any stage of the subglacial deformation but are most likely to form during the later phase of the subglacial deformation during low porewater pressures as the structure begins to solidify (Phillips, 2018). Furthermore, drag folds seen in small clay deposits in LF4 have been formed along some fracture planes and are linked to the sediment's rheological properties.

In total, 98 Riedel shears were measured in LF4 and then showed a strong preferred orientation towards the SE to S (Fig. 11), but local variations were also seen across different sections of LF4. Additionally, 103 bedding planes were measured in LF4 and 10 bedding planes were measured in LF3, which showed a strong tilt of the bedding planes towards the NW (Fig.11). These results indicate that the subglacial shearing must have been induced by an ice sheet flowing towards the SE to S.

Lastly, a series of step faults consisting of normal faults were found throughout LF1 and showed two sets of orientations, one toward the NE and one toward the SW (Fig.11). Normal faults are caused when the extensional stress exceeds the cohesive strength of the sediment. Thus, the orientation of these are thought to represent the directions of the greatest extensional stress. These two directions observed within LF1 are not in agreement with the other measurements. However, within any given deformation system there will be variations in the stress fields of the sediments which will create an array of different orientations in folds and fractures within the same system. This phenomenon is also used to explain the local variations in the directions of the Riedel shears measured in LF4.

The interval between 295-340 m of section 1 is characterised by a complex external shape of the sedimentary layers which are steeply inclined and have a repeating nature (Fig. 7). Two possible explanations can be employed to explain this structure. Either this unit represents a thrust complex where older units have been thrust to a higher plane through proglacial deformation, or the units represent a complex system of folding. The notion of a complex system of folding is unlikely due to the lack of ductile deformational structures in LF4 and 5 and a folding of the layers would not yield the repeating sedimentary structures observed within this interval. The more likely and simplest explanation for the observed structures is that it represents a thrust complex. Thrust complexes are a common proglacial to ice marginal deformation structure that is a result of progressive pushing by an advancing ice sheet (Phillips 2018; Benn and Evans, 2010). The nature of the presumed thrust complex is difficult to assess due to the unconformity caused by the deposition of LF15 and the large amount of thick, vegetated slump in key locations that could not be removed during fieldwork. However, the morphology of the sedimentary structures suggests the presence of at least two thrust planes within this section. The orientation of the thrust plane is unknown since it could not be located underneath slumped material, but the directions of the shearing inferred from the Riedel shears and the orientation of the bedding planes suggest it is highly likely that the thrust plane is dipping towards the N to NW since the inferred ice flow direction from the Riedel shears is towards the SE-S.

Furthermore, large scale folding is evident by the fold

seen in LF3 which is the result of ductile deformation where the bedding planes were plastically deformed. The fold type and the extent of the fold is difficult to assess due to the unconformity formed due to the deposition of LF15. However, large-scale folds are commonly associated with proglacial deformation and can form complex 3D-structures (Benediktsson et al., 2010; Bennet et al., 2004; Harris et al., 1997). The measured fold axis of the observed fold in LF3 has a dip towards the NW (Fig. 11), which suggests that the deformation was caused by an ice sheet moving from the NW to SE, which corresponds well with the other kinematic indicators seen in the internal structure of the units, thereby confirming an overall interpretation that units LF5, 4, 3, 2, and 1 were deformed post-depositionally by an ice sheet flowing over the sediments from a north to north-westerly direction.

### 9.3 Interpretation of structural elements in LF7

A variety of faults and folds were observed within LF7. The faults were interpreted as a subsequent series of normal faults with two distinct directions, one towards the SW and the other towards the SE. A small sheath fold is seen in LF7 in section 1 between 100-102 m (Fig.7). Sheath folds can occur both in ice-marginal and subglacial settings and are typically associated with high cumulative-strain shear zones in bedrock, but in glacial settings they can be developed at much lower strains due to the unconsolidated nature of glacial sediments exposed to high porewater pressures (Phillips, 2018). The orientation of the axial planes for two measurements in the sheath folds dip towards the SE and one showed a dip towards the NE (Fig. 16). The discrepancy in the measurement of the one toward the NE is identified to be caused by a measurement error given that all three measurements were taken of the same sheath fold, therefore it would be unlikely that one of the axial planes dips in another direction. This deviating measurement are considered a result of difficulties in tracing individual beds of the fold and the fact that only 3 measurements compared to the five taken at the other folds. Thus, this measurement should be excluded due to the unreliable measurements and the low number of measurements.

The sheath folds indicate a SW direction of ice movement towards the SW, and the faults suggests ice movement towards the SE and from towards the NW. This discrepancy in the results of the measurements may be attributed that they are formed during two subsequent ice advances separated in time which would yield two superimposed deformation structures.

The bedding planes of the LF7 were found to vary where parts where the bedding planes were dipping downwards and parts where the bedding planes were more horizontal with a slight dip. The bedding planes

that were dipping downwards were tilted towards the W and the bedding planes that were more horizontal had a slight dip towards the NW (Fig. 16). These variations in the bedding plane's structure are best explained with LF7 being a part of a fold system, which is then superimposed by a pinch and swell structure.

A pinch and swell structure were observed in the unit. This type of structures is commonly attributed to the beginning stages of boudinage, which is the result of progressive simple shear in the subglacial zone (Phillips, 2018; Hart, 2013; Van Deer Wateren et al., 2000; Benn and Evans, 2010). No measurements were taken of the boudins so the direction of ice sheet movement that caused the deformation is unknown.

### 9.4 Interpretation of LF8

LF8 consists of several different facies which was interpreted as outwash deposits and is interpreted to be connected to LF4. The bedding planes and the morphology of the internal beds combined makes up a recumbent fold which is in the beginning stages of becoming enclosed. Three measurements were taken inside of the recumbent fold which showed axial planes tilted towards the SE which indicates that the ice movement towards the SE (Fig. 18).

### 9.5 Interpretation of LF9

LF9 is interpreted as a subglacial traction till and its structural data are represented by seven A-axis fabric measurements. These showed a great lateral variation in preferred A-axis orientation and fabric strength (Fig.10). However, the seeming lack of a uniform preferred direction of the A-axis fabrics is not interpreted as the absence of a fabric. This is due to the clustered nature of the data points in all fabric measurements (Fig.10), which could result from very local differences within the direction of strain in the subglacial zone in the ice sheet that deposited the till, or it may be a post depositional effect caused by the realignment of the clast long axis.

Two distinct preferred A-axis orientations can be observed in LF9: one with a preferred clast orientation with a general direction of NE-SW (F1, F4, F12, and F14; Fig.10), followed by SE-NW direction of the clasts (F8, F9, and F16; Fig. 10). The discrepancy in the lack of a uniform direction of the long axis orientations are either attributed to very local variations in the subglacial strain signature of the icesheet, or post depositional realignment of the clasts, as a result of pure shear (Benn and Evans, 2010).

A combination of these explanations accounts for the observed phenomenon. The fabric which indicates a SE-NW direction is most likely caused by clast rea-

alignment as they are observed to mirror the strain signature seen in LF15, which has a clear SE-NW trend (Fig. 10). Meanwhile, F1, F4, F12, and F14 show minor differences in trends of the preferred clast orientation, but still have a general direction of roughly NE to SW (Fig.10). These minor discrepancies are thought to be attributed to minor variations in the direction of shear in the subglacial zone of the ice sheet over the pre-existing, likely undulating land surface that particular ice sheet encountered. Thus, to conclude the interpreted direction of movement of the ice sheet that deposited LF9 is NE to the SW, where parts of the unit have been affected by clast realignment, most likely caused by the deposition of LF15.

Nothing in regard to the external shape of the unit can be said, due to the large amount of slump covering the lower parts of LF9. However, a small part of LF9 extends upwards above LF7 and LF6 in a wedge like manner. This structure is interpreted as part of a fold system which has been cut by erosion and the section is viewing one of the fold limbs at an angle. LF7 and LF6 are interpreted as part of the fold core.

## 9.6 Interpretation of LF10

One a-axis fabric measurement was taken LF10 and showed a strong clustering of the clasts towards the NW and SE (Fig.10). The orientation of the clasts in gravel are commonly attributed to the direction of water flow (Krumbein 1939; Rust, 1972), which in this case would be towards the NW. However, considering that LF15 was interpreted as proximal outwash after the onset of LF9, whereas the ice sheet that deposited LF9 was interpreted to be flowing towards the SW would be unlikely to disperse water in a NW direction, instead a southern direction would be more likely for the water to be dispersed during the recession of the icesheet. Instead, the NW direction of the clast long axis is interpreted to be the consequence of clast realignment during the deposition of LF15 much like what is observed within LF9, whereas the overriding of the sediment would cause increased pore water conditions which have been found to allow the mobilization of the clasts due to the loss inter grain contacts (Rensbergen et al., 2003). During this state, the clast would be susceptible to realign in accordance with the direction of strain in the subglacial zone caused by the overriding of the ice sheet that deposited LF15, much like what is documented by Evans (2000). Due to the scarcity of fabric measurements in LF10, it is difficult to assess if this was a localized instance or if it occurred throughout the entire unit.

LF10 between 107-182 m of section 1 consists of several smaller isolated lenses. This feature is interpreted as boudinage where the gravel unit has been subjected to extensional shear in subglacial zone (Phillips, 2018; Hart, 2013; Van Deer Wateren et al., 2000; Benn and Evans, 2010), much like LF7, causing the gravel unit to be separated to smaller lenses. Furthermore, LF10

between 97-106 m of section 1 shows a part of the unit which extend upwards into LF15 in flame-like anticlines which overall resembles the structure observed in of LF11 between 170-175 m of section 1 (Fig, 7). This structure is interpreted to be derived from density contrast between the two units during the overriding of LF15, which is caused by liquefaction- induced soft deformation (Swiatek et al., 2023)

## 9.7 Interpretation of LF11

LF11 is characterized by a wide array of different deformational structures derived from both brittle and ductile deformation. The brittle deformation consists of reverse faults. These reverse faults show different orientations at different parts of the section. Between 65-68 m of section 1, several reverse faults are observed of which 15 were measured and have a dip towards SW (Fig.16), which indicates deformation caused by shearing from an ice sheet moving from the SW to NE. Furthermore one fold measurement and 10 bedding plane measurements were taken which showed that the axial plane and the bedding planes both tilted towards the NE (Fig.16), which further speaks for deformation caused by and ice sheet moving towards the SW from the NE. Unlike the bedding planes measured between 65-68 m the bedding planes measured between 70-80 m in section 1 (Fig. 6), showed a clustering towards the NNE (Fig. 16). Overall, this structure between 65-80 m is interpreted to be a part of a fold given by the difference in the bedding planes orientation. However, due to slump covering the distance between the two sections this theory could not be verified in the field but is still considered to be the most likely explanation. The reverse faults observed between 65-68 m, where the bedding planes are observed to be the most folded most likely caused when the shear stress during the folding event exceeded the tensile strength of the sediments causing brittle deformation (Phillips, 2018). Given by the orientation of the reverse faults this would indicate that the orientation of shearing occurred towards the NE which is further supported by the fold measurement.

LF11 located between 167-182 m of section 1, shows signs of both ductile and brittle deformation, with inclusions of reverse faults and asymmetrical and sheath folds. These deformation structures are commonly found in subglacial shear zones and are caused by extensional shear (Phillips, 2018). All but one axial planes are tilted towards the SE, the one axial plane that had a different direction towards the NW and was taken in the sheath fold (Fig. 25). However, this is attributed to a possible bad measurement. Eight fault planes were measured, and all had a dip towards the SSE, and 15 bedding planes were measured and showed a predominant tilt towards the NW (Fig. 25). All these measurements suggest that the deformation was caused by extensional shearing by an ice sheet moving from the SE to the NW.

The external structure of LF11 is characterized by smaller lateral discontinuous exposures in section 1. The lack of lateral continuation of the sediments is interpreted to be a result of subsequent advancements of two different ice sheets which caused partial erosion and deformation of the lacustrine sediments. Furthermore, a highly irregular morphology of the external structure of LF11 is observed between 170-175 m of section 1 (Fig. 6), where parts of LF11 are seen to extend upwards into LF12. Density derived structures commonly share this external characteristic that is found in LF11 and most likely caused by density differences in the subglacial zone when high density fluids are introduced to or mixed with low density fluids, which causes the uplift of the low-density fluid to reach a new internal equilibrium (Benn and Evans, 2010). Likewise, the irregular shaped exterior of LF11 in the given interval is interpreted as the product of density differences between the fine-grained material of LF11 and the subglacial till are both saturated, which leads to the expansion of LF11 into the overlying subglacial till.

To summarize, LF11 contain different deformational structures that are caused by shearing and density contrasts. These deformational structures can based on structural measurements can be concluded to have been caused by an ice sheet flowing from the SW.

## 9.8 Interpretation of LF12

LF12 was interpreted as a subglacial till, and two fabric measurements were taken within this unit, F5 and F17, which showed a great variation in the preferred orientation of the clast long axes (Fig.10). F5 showed a great variation in the clast orientation and F17 had a clear preferred clast long axis orientation towards the NW (Fig.10). However, this does not simply imply that the till was deposited by an ice sheet moving from the SE to NW, as LF12 have most likely also been affected by clast realignment much like LF9. The fabric measurement F17 is seen to mirror the strain signature of LF15, similar to what is observed in the fabric measurements of F8, F9 and F16 taken within LF9 (Fig.10).

Due to the low number of fabric measurement within LF12 it is difficult to assess the direction of the ice sheet which deposited the till. However, given the identical lithological makeup in both the fine gravel section (Fig. 29), a strong case can be made that LF9 and LF12 were deposited by the same ice sheet, and that LF12 either represents a readvancement of the same ice sheet that deposited LF9, and would thus share a similar direction of advance. Additionally, the discrepancy in the lithological makeup between LF9 and LF15 are vast (Fig. 29), which does not suggest that LF12 was deposited by an ice sheet moving from the SE to NW as their lithological makeup would in that case share a stronger resemblance with one and

another.

Moreover, sheared and folded sand lenses were found throughout LF12. A singular fold measurement was taken at Section 2 and shows an axial plane dipping towards the NW, indicating simple shear likely caused by an ice sheet moving from the SE to the NW. Furthermore, fabric measurements taken in LF9 and LF12 both show a mirror image of the fabric measurement of LF15 (Fig. 9), which suggests that the entire sedimentary sequence of section 2 underwent deformation influenced by LF15. This in turn strengthens the conclusion of clast realignment caused by LF15 in both LF9 and LF12.

The LF12 shows great variation in thickness and exposures throughout all studied sections. As LF12 and LF9 both share the same lithological make up and share the same similar internal textural and structure as LF9. Two interpretations can be drawn: either LF9 and LF12 are the same unit deposited during the same ice advance and parts of LF9 were stacked on top of each other through piggyback thrusting as described by Alsopa et al. (2018), or LF12 represents a readvance of the same ice sheet that deposited LF9.

Overall, LF12 represents a subglacial till deposit of which the ice flow direction could not be pinpointed due to the scarcity of fabric measurements and clast realignment. However, it is proposed that LF12 represents the same unit as LF9 and is the effect of till stacking through piggyback thrusting or that LF12 represents a readvance of the same ice sheet that deposited LF9.

## 9.9 Interpretation of LF13

Several different deformation structures are observed within LF13 which are predominantly connected to subglacial shearing. LF13 between 77-87 m and 252-262 m of section 1 (Fig.7), consists of a complex sequence of irregularly shaped lenses imbedded with LF12 and LF15. This structure is interpreted as a melange zone (Cowan 1985), which is a subglacial deformation structure caused by progressive simple shear (Hoffmann and Piotrowski 2001).

Furthermore, in the upper parts of LF13 between 183-237 m of section 1 (Fig 6), clay and sand were found to have been mixed in a complex manner, while the basal parts of LF13 were found to be seemingly unaffected. This structure seen in the upper parts of LF13 in this interval is interpreted to have been caused by simple shear in the subglacial shear zone, in line with findings by Waller et al. (2009), Lee and Phillips (2008), and Van der Wateren (1999). Additionally, signs of simple shear is not constricted to the aforementioned parts of LF13, but are seen throughout the entire upper parts of LF13 in all the observed sections that exhibit varying degrees of deformation caused by simple shear.

At roughly 228 m a small section of LF13 is seen to extend down into LF12 in a wedge-like manner (Fig. 27C, D). Wedge-like structures like these are commonly interpreted as ice wedges, are formed as an effect of repeated thawing and freezing of ice that causes hydrofracturing of sediments that can later be infilled by sediment through flowing or slumping which creates an ice wedge cast (Harry and Gozdzik 1988; Black, 1976). Furthermore, ice wedge structures have previously been described in fine grained sediments in the periglacial zone (Svensson, 1990; Worsley, 2014), and have also been proposed that they may be able to form in subglacial tunnel environments (Pisarska-Jamróży and Zielinski, 2012). However, even though similar in morphology to ice wedges, this structure is interpreted as a water escape structure. The observed structure does not display a slumping or flowing structure which is a defining trait for ice wedge casts (Harry and Gozdzik 1988; Black, 1976). Instead, a lateral dissipation and distribution of the finer-grained sediments in a fan like shape and irregular shape are seen, that is not connected to any surface feature other than the rupturing contact between the two units. The internal layering resembles a dendritic to pseudo-dendritic pattern, typical of water escape structures (Van der Meer et al. 1999; Phillips et al., 2013), and not ice-wedge casts. The water escape structure is connected to elevated porewater conditions during the continued advancement of the ice sheet that deposited LF15.

Lastly, deformed bedding planes are wrapped and compressed beneath boulders from LF15 that protrudes downwards into LF13. This type of deformational structures is in soft sediments located beneath a bed of subglacial traction till and are caused by lodgement. Lodgement is defined as the subglacial deposition of debris caused by friction and can quickly accrue in the soft substratum, where bigger boulders plough down into the lower unit and get stuck (Boulton, 1970), during which the bedding planes become progressively deformed and contort to the shape of the boulder. A total of 40 of bedding planes were measured within LF13 which showed a slight dip towards the NW between 55-65m of section 1, and SE between 222-237m in section 1 (Fig. 16; Fig. 28). This faint dip may either be connected to the direction of water flow, or it may have been caused by the onset of LF15.

Evident from section 2 and 3 is that LF13 displays a very heterogeneous bed geometry where the thickness and structure of LF13 in the two exposures varies greatly even though the two sections are only located a few m apart. LF13 in section 2 consist of a set of isolated lenses (Fig. 7), which is interpreted to be the result of extensional shearing which led to the boudinage, likewise LF13 in section 3 is observed to display a pinch and swell structure and is in the begging phase of boudinage (Phillips, 2018; Hart, 2013; Van Deer

Wateren et al., 2000). It is unclear whether LF13 in section 1 exhibits the same degree of variation seen between section 2 and 3. However, LF13 in section 1 shows a lack of vertical continuation which may be a direct result of boudinage, or it may be related to erosion or attenuation.

Overall, LF13 displays two types of deformational structures caused by simple shear and over pressurised water. These structures are all connected to the advancement of the ice sheet that deposited LF15.

#### 9.10 Interpretation of LF15

A total of eight a-axis fabric measurements were taken within LF15, whereas all show a preferred clast long axis orientation towards the NW (Fig.10). This suggests that the ice sheet that deposited LF15 came from the SE and move towards the NW. Small variations within the NW to SE trend of the clast long axes, which may be explained by local variations in the direction of strain in the subglacial shear zone, alternatively they may be derived from operational errors during the measuring process. However, operational error is an unlikely explanation due to the clustered nature of the fabric plots, and therefore the minor variations is most likely attributed to local variations of maximum strain.

## 10 Conceptual model for the tectonic evolution of the northern cliff exposures of Ven

The structural analysis revealed a complex system of deformation which can be separated into different phases of deformation connected to the advances of two separate ice sheets over the study area. Due to the uncertainty of the evidence caused by thick, vegetated slumps in key locations, two different scenarios are possible, and these are outlined below.

### 10.1 Conceptual model 1

**Stage 1-** Deposition in glaciolacustrine environment followed by gradual transition into a proglacial environment. The oldest sediments featured in the northern cliff exposures consist of glaciolacustrine sediments (Fig.30). A gradual transition from a lake environment to a proglacial environment occurred towards the end of this period (LF4; section 4).

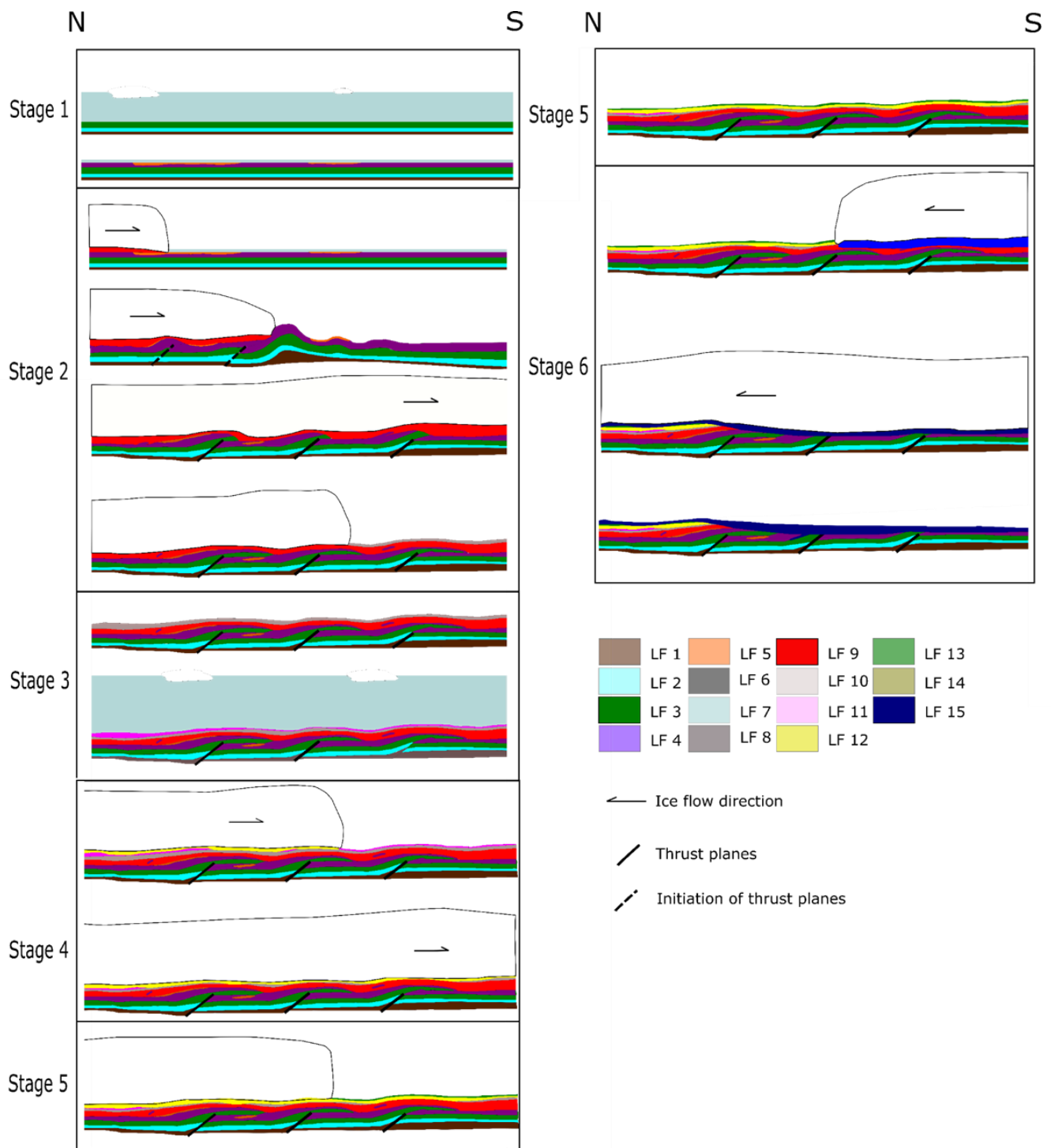


Figure 30. Conceptual model 1.

**Stage 2-** Phase 1 deformation and deposition of subglacial till. Phase 1 deformation was initiated by the ice sheet flowing from the NE to SW. The subsequent advance of the ice sheet deposited LF9 and caused ice marginal and proglacial deformation structures (see section 6.1), which was overridden at a later stage during this advance. The production of Riedel shears (LF4; section 6.1) and cannibalisation and deformation of the stratified sediments (stage 1; section 5) would have occurred during this stage as well, producing the folded complex seen in LF8 (Fig.30). It is possible that the lenses of sand observed within LF9 (103-128 m; Fig. 7) are also the effects of cannibalisation rather than ice-sediment decoupling and infilling.

**Stage 3-** retreat of ice sheet and subsequent transition into glaciolacustrine environment. After the initial phase of deformation, the ice receded northwards to an unknown location. During this recession large amounts of sediments would have been deposited in the outwash plain and in the ice marginal zone. This gave rise to proximal outwash sediments (LF10) deposited directly at the top and in places also caused some erosion of the subglacial till deposited in the early stage (LF9) (Fig.30). The formation of a proglacial lake of an unknown size should have occurred during this stage and deposited fine grained sediments (LF11).

**Stage 4-** Readvance of ice sheet and deformation phase 1.5. A readvance of the same ice sheet in stage 2 and deposited LF12. This occurred shortly after the deposition of the outwash sediments and the lacustrine deposit (LF10, LF11) (Fig.30). The flow of the ice sheet during the readvance is unknown. However, it is possible that the ice flow would resemble that of the previous advance (see section 6.6). During the readvance, preexisting lithofacies would have been subjected to deformation and erosion (Fig.30). The deformation that occurred during this stage is labelled as phase 1.5, but the extent and the character of the deformation and the lack possibly due to overprinting of the phase 3 deformation.

**Stage 5-** retreat of ice sheet followed by deposition of outwash sediments- (transition into proglacial lake?). During the retreat of the ice sheet an outwash plain formed in the area depositing glaciofluvial sediments (LF13) and possibly glaciolacustrine sediments linked to a proglacial lake (see section 5.7). Due to the lack of exposure and erosion it is difficult to assess the size and character of this proposed lake environment.

**Stage 6-** Advancing of ice sheet from the SE. During the last stages of the tectonic evolution of the strata an ice sheet approached from the SE with a flow towards the NW, which is 180 degrees change in ice flow direction from that seen in stage 2 (Fig.30). During the advance the basal sediments were deformed, producing folds, faults and boudins (LF11, 13, 10 and 7; Section 6), but also the density derived structures (LF11 and 10; Section 6) and the erosion. Additionally, at

this stage boulders in the subglacial zone would have been deposited through lodgement causing deformation of the upper bedding planes of the glaciofluvial deposits (LF13). Till injection and the dewatering structures would also have occurred during this stage (LF13, LF15; Section 6). The deformation that is linked to this stage is labelled as phase 2.

## 10.2 Conceptual model 2- Piggy backing of LF9

**Stage 1-** follows the same continuous events as outlined in the conceptual model 1.

**Stage 2-** Like the previous model, an ice sheet would have advanced from the NE and caused the thrusting and shearing and cannibalizing of the glaciolacustrine and the glaciofluvial sediments deposited in stage 1 (LF1, 2, 3, 4 and 5; Section 6.1) (Fig. 31).

However, unlike stage 2 of the other conceptual model, this model adopts a different method to explain LF12. In this model LF12 is interpreted to be the result of detachment from the same basal unit LF9, as proposed by the nearly identical fine gravel result (see Section 6.6), initiated by proglacial tectonism. The detachment resulted in the piggybacking of the subglacial traction till (LF9) to effectively doubling up on itself (Fig.31). During the ice advance outwash sediments in the proglacial setting would have been picked up and cannibalised into the subglacial till (LF10, LF11). Where after ramps would have formed within this sedimentary stack and eventually through piggyback thrusting caused parts of LF9 to stack on top of each other producing a complex till sequence that would greatly vary in thickness based on the thrusting. The thrustured parts would have later been overridden by the ice sheet and been deformed alongside the other constituents of the sedimentary pack. The deformation that is linked to this stage is labelled as phase 1.

**Stage 3** and **Stage 4** mirror the events depicted in Stage 5 and Stage 6 of Conceptual Model 1. Additionally, Deformational Phase 2, as described in Conceptual Model 1, transpires during Stage 4 instead of Stage 5 and 6 in Conceptual Model 2.

## 10.3 Summary of conceptual models

Above features two conceptual models of the tectonic evolution of the strata. The two models are largely the same but are differentiated by interpretations regarding the origin of LF12. The first model is based on the interpretation that LF12 represents a readvance of the same ice sheet that deposited the LF9, while the second model is based on LF12 not being caused by a readvance but instead through the stacking of LF9 through piggyback thrusting. No firm conclusions regarding which of the two conceptual models can be concluded based on structural and sedimentological data presented from this study alone.

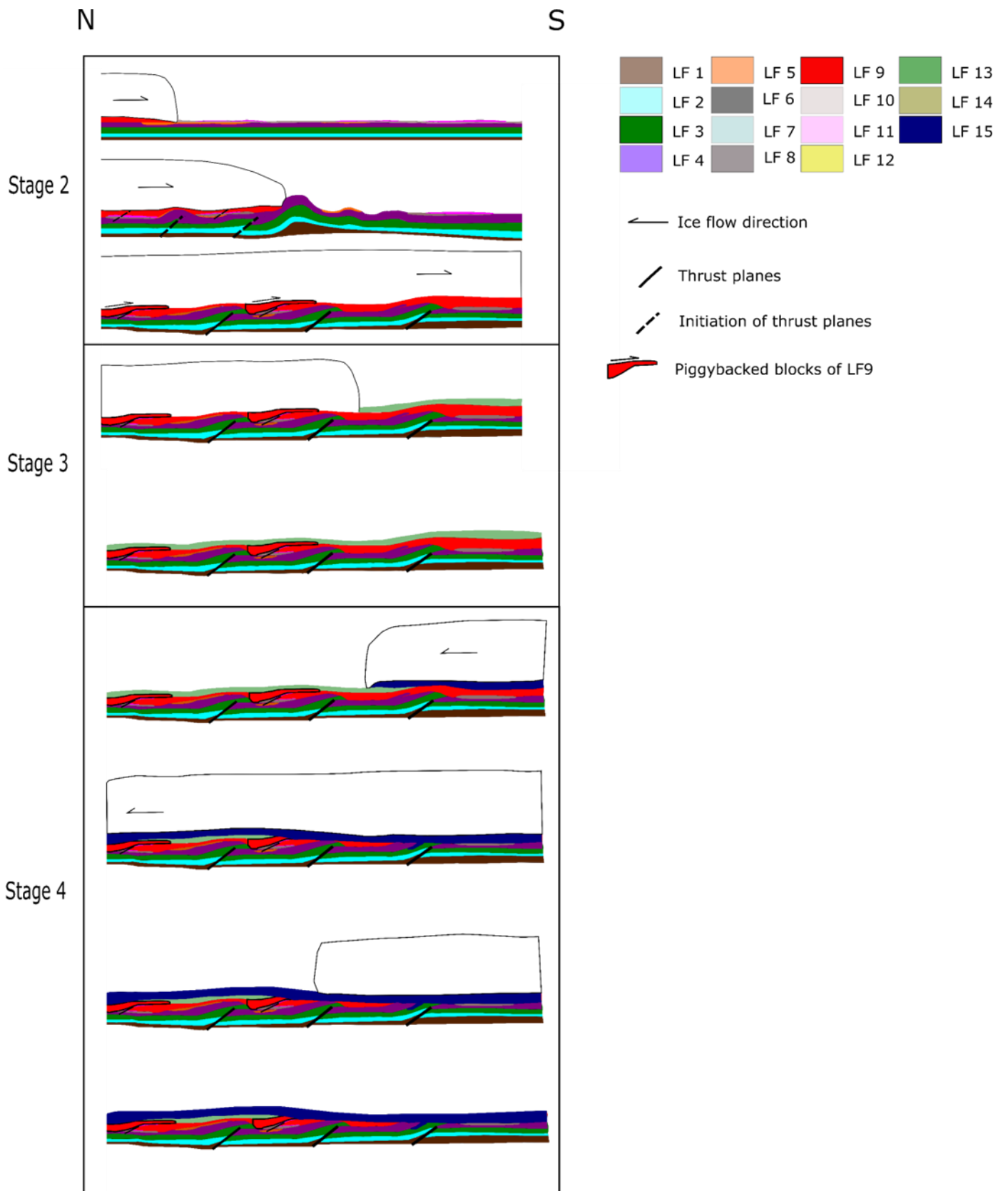


Figure 31. Conceptual model 2. Note that stage 1 is the same as stage 1 in the first model and that stage 2 in this model is followed by stage 5 and 6 presented in the first model.



## 11. Discussion

### 11.1 Sedimentological correlation with previous local studies

Three till beds have been distinguished in this study, all of which have been interpreted as subglacial tills. These units can confidently be correlated with the aforementioned studies on Ven based on the textural, structural, stratigraphical, and lithological correlations. The lower till LF9 observed with in this study is correlated to the basal till beds named the Västernäs till member by Adrielsson (1984) but are also correlated to the basal till beds discussed by Holmström (1879) and Erdmann (1883). However, Adrielsson (1984) located three different till beds in the northern sites that were interpreted to be connected to the main glacial advance during the late Weichselian, which differs from this study. Here, the field evidence only provides the basis for two till beds in the basal part of the exposure.

Two explanations could explain this phenomenon, either small incremental changes in the till makeup were missed during the logging or small incremental changes in the till beds may have been overscrutinized by Adrielsson (1984), interpreting them as individual till beds rather than one cohesive unit (splitting versus lumping; Evans and Benn, 2021). It is impossible to conclude which explanation is correct, only confidence in the analysis of this study can be expressed. Either way Adrielsson (1984) interpreted the stratigraphic sequence of the basal part of the northern cliff in line with the presented conceptual model 1, where the basal part of the section represents an initial advance followed by sediments linked to the deglaciation and later a readvance of the ice sheet depositing another till bed. However, the three till beds expressed by Adrielsson (1984) can exclusively only be occurring side by side in a small part of the northern part of the island while the other parts only contain one till bed that relates to the Västernäs till member. This raises the question regarding why the other till beds are not visible in the other sites Adrielsson (1984) described. Either this is explained by extensive deformation of the preexisting units during the emplacement of the upper till bed, or it further supports the validity of conceptual model 2. This model points out that LF12 and subsequently the other till beds explained by Adrielsson (1984) are a result of piggyback thrusting where the basal till bed have been stacked on top of each itself.

Based on the small section that was studied in great detail in this study, combined with Adrielsson's (1984) broader focus, there is a great opportunity to compare very local deviations in fabric orientation and fine gravel composition, inferred from the multitude of measurements taken over short distances along the

cliffs, to fewer measurements of fabric and fine gravel that Adrielsson (1984) took over a much larger area, i.e. a larger spacing between samples. Therefore, small deviations in terms of fabric and fine gravel can now be compared to see if they differ from that of the of a broader region, which allows for testing of possible heterogeneities or homogeneities in the till beds of LF9 and LF15.

The fine gravel lithological assemblage of the basal till in this study to contain very minor changes and are dominated by crystalline grains. Incidentally, the same trend was observed by Adrielsson (1984) and Holmström (1879). Considering that the fine gravel composition is seen to be homogenous in all three studies supports the notion of ample mixing of the till matrix within the subglacial traction zone.

Furthermore, three fabric measurements ( $n=25$  each), taken within the basal till bed of the Västernäs till member in the northern cliff sections by Adrielsson (1984), showed a preferred orientation towards the NW which were perpendicular to the inferred ice flow direction based on the orientation of striated boulders by Adrielsson (1984). This discrepancy between the orientation of the fabric and the striated boulders was interpreted by Adrielsson (1984) as evidence for the lack of shear strain by intergranular movement in the final stages of deformation. A similar trend NW preferred clast axis orientation was also noted within this study. However, the fabric can clearly be shown to vary significantly in orientation within the basal diamict (LF9). Despite this variation, most of the samples still had a broad NE to SW trend. The fabrics that showed a NW to SE trend are here attributed to be a post depositional effect caused by clast reorientation in response to pure shear during the emplacement of the upper till bed (LF15). The SW to NE trending fabrics in the basal till bed were most likely missed by Adrielsson (1984), given the lack of fabric measurements made in the lower till beds located in the northern sites. Thus, considering that the fabric is found to be aligned with the ice flow direction casts significant doubt on Adrielsson's (1984) initial hypothesis of this being a result of a lack of shear strain by intergranular movement during the later stages of the deposition.

The upper till bed of the Laebrink till member was found by Adrielsson (1984) to be located on top of the deformed sediments with an unconformity, and this observation is in large agreement with what was found in LF15. Based on similarities in texture, fine gravel content, and stratigraphic positioning between that of the upper till bed in the Laebrink till member reported by Adrielsson (1984) and that of the upper till bed of this study, the two units can confidently be correlated to be the same till. However, Adrielsson (1984) found additional sediments on top of the upper till bed consisting of debris flow deposits ("flow tills") and minor sand and gravel deposits. These sediments were not present along the cliffs logged during this study. One

complication here is that the upper part of the cliff section could not be reached for a majority of the studied cliff section due to the overhanging nature of the cliffs and may thus have been missed; alternatively, previously-existing pockets of such sediments may have been lost by cliff erosion. Adrielsson (1984) documented a number of partially imbedded lodged clasts located in the lower units of the till bed which were seen to deform the substrate in a comparable fashion to those observed in the upper parts of LF13. This suggests that the lodged clasts located within this study are perhaps not an isolated occurrence, but instead a common deformational structure.

Fine gravel analysis of the upper till bed was found to vary within the studied section, and is in agreement with what is presented by Adrielsson (1984). This speaks for a poor mixing of the till matrix in comparison to the lowest till unit. Furthermore, small variations in the local to regional clast orientation was seen in the upper till bed by Adrielsson (1984), however all the fabrics yielded a NW trend for the clast long axis. The same variations can also be seen in the local setting of the till expressed by the multitude of measurements taken in this study over a small span of the cliff sections.

The Glumslöv beds can be confidently correlated with the LF5, 4, 3, 2 and 1, based on overall likeness in regard to the internal structure and facies combined with the stratigraphic position. Drop stones were observed throughout the exposure of Glumslöv members, comparable to what was found in this study. Adrielsson (1984) interpretation of the Glumslöv member is that it represents a proglacial lake environment which gradually transitions into a braided river environment, which is also the case for this study.

To briefly summarize, the main discrepancies between this study and Adrielsson (1984) regarding the sedimentology, revolves around the interpretation of LF12 inferred from the conceptual model 2 and the fabric of the lower till unit. Two explanations regarding the origin of LF12 was presented in this study, where the conceptual model 1 is in line with what is envisaged by Adrielsson (1984). However, the conceptual model 2 offers a new perspective, and suggests that LF12 can be the result of piggybacking of lower till unit (LF9).

## 11.2 Stratigraphic correlations with regional studies

The stratigraphic correlation with Ven's stratigraphy and studies including Nilsson (1973), Miller (1977), Berglund and Lagerlund (1981), all conducted within the Alnarp valley have been established by Anjar et al. (2014) based on Ven's stratigraphy presented by Adrielsson (1984). These studies showed that the stratigraphic sequence observed on

Ven (Fig. 29B) represents the upper sedimentary succession of the Alnarp valley fill. Furthermore, a strong stratigraphic correlation with Ven's stratigraphy is also evident in other sites located outside of the Alnarp valley in Scania (Anjar et al., 2014) and in sedimentary cores from Kriegers Flak, located south of Scania in the Baltic Sea (Möller et al., 2020). Within these studies the Laebrink till was connected to the Lund till deposited during the Baltic advance (~18kya) and the Västernäs till member was connected to the Dalby till, deposited during the main advance (~23kya).

Ven's stratigraphy can also be compared to that of the general stratigraphic sequence of Denmark where the Västernäs tills corresponds to the mid Danish till bed and the Laebrink till corresponds to the Baelthav till bed, which respectively corresponds to the main glacial advance and the young Baltic advance during the late Weichselian (Houmark-Nielsen, 1999). The Glumslövs member corresponds to the Glumslöv sand in Denmark, but also to the Himmelev formation which represents proximal outwash sediments located found in Horsherred and in the Roskilde area (Houmark-Nielsen, 1999). These regional correlations with Ven's stratigraphy based on Adrielsson (1984), can further be extended to the stratigraphy presented in this study as the Laebrink till and the Västernäs till bed have been shown to correlate with the till beds of LF9, 4 and 16 and the Glumslövs beds have been correlated with LF5, 4, 3, 2 and 1 (Fig. 29B).

Based on dating by Möller et al. (2020) the Glumslöv beds and subsequently LF5, 4, 3, 2 and 1, are found to correspond to the interstadial period of MIS 3, and began to be deposited around 30 ka, where a large proglacial lake had formed in the southern parts of the Baltic, caused by damming of the Baltic basin due to the Kattegat advance; this advance has previously also been interpreted to be responsible for the deposition of the Ålabodarna till on Ven (Adrielsson, 1984; Houmark-Nielsen; 2003) which in turn has regionally been correlated to the Kattegat till (Houmark-Nielsen, 1999; Anjar et al., 2014).

However, this till bed is not present in the cliffs as recorded today. OSL dating of the mid Danish till gives an approximate age of 23-20 ka (Larsen et al., 2009), suggesting that the deposition of LF9 occurred around this time. These two dates of the lower till bed and the glaciolacustrine sediments suggest that the span between Stage 1 and 2 of both conceptual models represents 7000 years considering the dates presented above.

The oldest dates for the deglaciation of the main glacial advance dates to 19 ka. However, most of the dating lie around 17 ka (Houmark-Nielsen & Kjaer, 2003). The Young Baltic advances are dated to have occurred during the deglaciation after the NE advance dated to roughly 18 ka (Houmark-Nielsen & Kjaer 2003). This implies that stage 3, 4 and 5 in the conceptual model 1 where sorted sediments LF10 and LF11 were deposited on top of LF9, followed by a readvance depositing LF12, and later by the deposition of LF13, all took place before the young Baltic ice advance reached the island. This strongly implies a highly dynamic glacial depositional environment near an oscillating ice margin with response times on the order of decades, thus much more dynamic than previous models entertained.

Studies examining the glaciotectonic features connected to the last two advances of the SIS during the late Weichselian conducted in Germany, Denmark, and Sweden, have shown various degrees of influence caused by these two different advances. Glaciotectonic structures examined through a magnitude of well logs and the distribution of glaciotectonic landforms and features in Denmark shows a widespread glaciotectonically induced dislocation of both the Quaternary and pre-Quaternary strata, varying in size and intensity (Jakobsen, 1996; Jakobsen, 2003). The glaciotectonic structures seen along Danish cliff sections show largescale complex deformation structures like thrust faulting and folding induced and influenced by the main glacier advance but also by the young Baltic advances (Pedersen, 1996; Pedersen, 2000;

Pedersen and Gravesen, 2009; Madsen and Piotrowski, 2012). Furthermore, these types of structures are also observed in cliff sections in Germany (e.g. Gehrman et al., 2022; Van der Wateren, 1999).

Additionally, deformation structures linked to these two glacial advances have been observed in smaller exposures located in southern Sweden (Anjar et al, 2014; Barth 2011; Mattsson, 1997), but are generally found to be of smaller scale compared to that commonly found across Denmark. Clast reorientation caused by the Baltic advance have also been observed through the investigation of Quaternary sediments from the Hardeberga quarry (Mattsson, 1997), much like those observed in LF12 and LF9. This suggests that this clast realignment may be more widespread than hitherto acknowledged.

Despite there being good claims for an extensive influence of these two ice advances in the southern part of Scandinavia based on the findings from the surrounding region, there is a lack of observed deformation phenomena in the Alnarp valley observed in the previous borehole studies by Nilsson (1973), Miller (1977), Berglund and Lagerlund (1981), but also in locations outside of the Alnarp valley. However, a large scale thrust fault complex has been seen in the upper parts of the Alnarp valley resting on the heavily faulted pre-Quaternary strata in the northeastern parts of Sjælland, based on borehole and seismic data from Esrum Sø (Pedersen et al., 2020). The lack of deformation structures may either be explained by the fact that the upper sedimentary succession of the Alnarp valley is largely unaffected by the glaciotectonism, or at least unaffected by large scale deformation, with Ven and Esrum Sø being exceptions. This explanation is deemed to be unlikely, given the ubiquity of these larger scale glaciotectonic structures seen throughout the surrounding wider region and the prevalence of glaciotectonic processes in modern glacial environments more broadly (e.g. Aber and Ber, 2006; Phillips, 2018). Therefore, a more realistic explanation for the apparent lack of

deformation structures is that they have not been observed due to a combination of a lack of suitably sized exposures that enable tracing of large-scale folding patterns etc. Likewise, large-scale deformation structures are not visible in sedimentary cores, on which the majority of studies in southern Sweden has relied; or it could be the result of a combination of both factors.

### 11.3 Glaciotectonic correlation with previous local studies

The glaciotectonic features on the island were described by Erdmann (1883), Holmström (1883), Markgren (1961), Rasmussen (1973) and Adrielsson (1984). These authors all found complex conditions evidenced by a multitude of steeply inclined beds of sediment, complex folding, shearing and thrust faulting. The stratigraphy on the island is found to be complicated as a result with some locations containing highly disrupted and dislocated strata while other places contain a much more undisturbed sedimentary sequence (Rasmussen, 1973; Adrielsson 1984). The stratigraphy of the northern sites on Ven was found by Adrielsson (1984) to be particularly dislocated, consisting of discontinuous and laterally restricted beds. The glaciotectonic structures seen along the entire island were traced to three tectonic events connected to the advance of the SIS by some authors (Adrielsson, 1984; Rasmussen, 1973). Two of these tectonic events, which Adrielsson (1984) calls the Västernäs and the Laebrink glaciotectonic events, can be correlated to the different phases of deformation that occurred in combination with the deposition of the different till beds (LF9, 12 and 15). The third event is called the Möllebeck glaciotectonic event, which predates all the sediments that are presented in this study and will subsequently not be further discussed.

The Västernäs glaciotectonic event corresponds to deformation during phase 1 of the conceptual model 1 and 2, but also to the phase 1.5 in the conceptual model 1. The Laebrink glaciotectonic event corresponds to the deformation linked to the deposition of LF15 which corresponds to the deformation phase 2 in both conceptual models.

The structural analysis of these deformation phases reveals a greater variation in the direction of shearing

in each phase compared to Adrielsson's (1984) findings for the Västernäs glaciotectonic event. Adrielsson (1984) inferred a strict shear stress direction of the Västernäs glaciotectonic event with a north to north-easterly trend, while the direction of shear is noted to be more variable in this study with inclusions of shear directions toward the SW. On the other hand, the inferred shear stress direction of the Laebrink glaciotectonic event observed by Adrielsson (1984) are much more in line with what is observed in the phase 2 deformation of this study, where the direction of shear is exclusively towards the NW.

A lack of structural measurements within the northern cliff exposures are presented by Adrielsson (1984), where only a handful of fold and fault measurements, and some occasional bedding plane measurements of an unknown quantity have been taken in the sorted sediments of the Västernäs member. The measurements by Adrielsson (1984) indicate that the deformation signature in these sediments is solely connected to phase 1. However, this study presents evidence that the northern sites have been subjected to more extensive glaciotectonism that is linked to a second phase of deformation that resulted in a different style of overprinting of pre-existing sedimentary units. The difference to the findings of Adrielsson (1984) may be the result of the much-smaller sample number of structural measurements in the northern cliff sections that are the focus of this study.

Several low-angled thrust faults were observed by Adrielsson (1984) inside the Glumslöv beds in the northern cliff exposures and these thrust planes are presumably connected to the thrust planes that were observed here towards between 295-340 m of the section 1. A small number of bedding plane measurements were taken by Adrielsson (1984) at an undisclosed location within these beds which showed a dip towards the N-NE. Additionally, shallow faults were seen at the sole of the Laebrink till member and high angle faults occurred in the foot wall. No fault measurements were taken, and the character of the faults were not described and can therefore not be compared to the findings of this study. However, it is possible that these faults are connected to the Riedel shears seen in LF4. The bedding planes were seen to differ from that of the measured bedding planes in the thrust complex of section 1 of this study, which showed a preferred dip towards the NW. In contrast, internal variations in the bedding planes orientations are noted within the thrust complex, and thus the small sample size of the bedding plane measurements by Adrielsson (1984) may be the cause of the difference between the measurements of the bedding planes.

### 11.4 Concluding remarks of geomorphological mapping

In Section 3.1 of this study, two proposed alternatives

for the origin of the ridges were discussed: the possibility that the ridges are drumlins or that they were ridges the result of agricultural activities such as ploughing.

Considering that LF15 was found to be derived from an ice sheet flowing from the SE to the NW and the fact that the landforms are located within LF15 makes it highly unlikely that the ridges are drumlins, since the majority the crest lines of most of the ridge's trends SW to NE. This conflict arises since drumlins are formed parallel with the ice flow of a region and therefore it can be concluded that these ridges are not drumlins based on the discrepancy in the ridges orientation and the ice flow. This suggest that the ridges may in fact be ridges formed through the agricultural activity on the island. However, based on the information presented from this study alone, no firm conclusion regarding the origin of the presented ridges can be concluded.

Despite the uncertain nature of the origin of the ridge, the cupola hill statement by Aber et al. (1989), is deemed to be unlikely solely based on the evidence presented in this study. This is since linear features in terms of subtle long-stretched ridges seen throughout the islands otherwise exceedingly flat surface, which is not in line with the irregular hill complex that characterise Cupola hills (Aber et al., 1989). Nevertheless, since the source of the ridges remains unidentified, they cannot serve as exclusive evidence to refute the cupola hill hypothesis. In summary, relying solely on the evidence derived from geomorphological mapping, it is not possible to unequivocally reject the assertion made by Aber et al. (1989). Nonetheless, this statement is considered an improbable explanation, necessitating a more comprehensive geomorphological investigation.

### 11.5 Questions for future studies

Overall, there is a lack of knowledge concerning the stratigraphy of the Alnarp valley, which needs to be improved to gain a better understanding of the sedimentary succession. This improvement is not only vital for better understanding of the glacial evolution of Scandinavia during the late Weichselian period but also crucial for improving existing groundwater models of the Alnarp valley (e.g. Erlström, 2022). This might partly be achieved through continued studies examining stratigraphic sequences combine with seismic or ground penetrating radar methods (GPR). GPR has been shown to be a great tool for the examination of glaciotectionic and sedimentological structures in Quaternary sediments (Jakobsen and Overgaard, 2002; Olsen and Andreasen, 1995; Lukas and Sass, 2011; Watts et al., 2022; Pasanen, 2009), and the same goes

for seismic based methods (Watts et al., 2022; Novak and Pedersen, 2000; Newton et al., 2024; Sun et al., 2020), especially when connected to real-world sedimentological data from sections.

These types of methods may also be used to further improve our understanding the internal structure of Ven, which is currently lacking, and may improve our knowledge regarding the true extent of the glaciotectionic influence. Several smaller individual studies with a structural focus may also be an idea, to further supplement the structural data taken by Adrielsson (1984), as it has been noted in this study that the lack of clustered data points by Adrielsson (1984), have yielded a more simplistic view of the glaciotectionic evolution of the northern sites and may thus also be the case for the other parts of the island. A significant lack of dating is also recorded in the region and may be a consideration for future studies, which may improve our knowledge of the speed of which the sediments where deformed. Lastly, geochemical analysis of the tills LF9 and LF12 could help conclude if these two tills are the same unit or two separate units. This analysis would greatly help narrow down which of the two presented conceptual models are correct.

## 12 Conclusion

The aim of this study was to close gaps in our knowledge and improve our understanding of the deformation history of the glacial sediments of Ven, and independently assess the cupola hill interpretation made by Aber et al. (1989). This was accomplished using a systematic structural geological sampling approach, combined with geomorphological mapping of surface features on the island.

The conclusion drawn by Aber et al. (1989), asserting Ven as a prime instance of a cupola hill complex, cannot be solely refuted based on the evidence provided in the geomorphological mapping process. Nevertheless, this interpretation is regarded as improbable and warrants further comprehensive investigation. Ten long linear ridges are observed throughout islands otherwise flat surface. Although this study does not definitively determine their origin, there is a hypothesis that these ridges may result from agricultural practices such as ploughing. However, considerable uncertainties persist regarding their precise origins.

Fifteen distinct lithofacies were identified throughout the northern cliff exposure. They can be summarized to consist of three subglacial till beds (LF9, 12, 15) located at different stratigraphic levels and twelve beds consisting of a mixture of glaciolacustrine and glaciofluvial deposits. LF9 is located at the base of the stratigraphy throughout most of the investigated sections. LF12 is seen in the middle, and LF15 is located at the top of the succession. Between these till beds are dis-

continuous layers of outwash and glaciolacustrine deposits. These lithofacies can easily be correlated to previous studies on the island and studies in the broader region representing the upper sedimentary succession of the Alnarp Valley fill.

Measurements of deformational structures alongside the sedimentological findings indicate a substantial glaciotectonic influence from the last two glacial advances, including the main glacial advance and a young Baltic advance. This study employs two conceptual models to explain the evolution of the glaciotectonic structures and the sedimentological findings seen in the northern cliff exposures. The main separating feature between the two models regards the interpreted origin of the discontinuous till bed (LF12) found in the middle of the stratigraphy.

The first conceptual model describes a sequence of a glacial advance from the NE which deposited LF9 and caused substantial deformation of the preexisting glaciolacustrine deposits before it retreated and later readvanced and deposited LF12. A third glacial advance occurred over the region by an ice sheet flowing from the SW, which partly deformed and eroded the preexisting sediments.

The second conceptual model suggests a different turn of events which suggests that the sedimentary succession and the glaciotectonic structures can be explained by only two glacial advances, during which the turn of events is initiated by an ice sheet flowing from the NE deforming preexisting sediments. In this phase, it is suggested that zones of detachment emerged within the lower till layer (LF9) due to progressive proglacial deformation. This process ultimately caused sections of LF9 to be thrust and to an elevated plane in the stratigraphy that effectively resulted in a 'doubling' up sequence of the till bed, consequently forming the intricate till sequence.

Based on evidence presented in this study alone it cannot be safely determined which of these models is correct. However, since this sequence of the three till beds is only located in the northern part of the island may imply that the second model is more likely. Overall, the structural investigation of this study shows that our current understanding of the structural evolution of Ven's northern sedimentary succession is limited and presents a more simplified view of the glaciotectonic evolution than what is presented in this study.

Moreover, the absence of glaciotectonic influence in the Alnarp valley fill in the southern mainland of Sweden contrasts sharply with the significant deformation noted in this study and others conducted in the northern sections of the Alnarp Valley and the broader region. However, the dearth of observed deformation structures in the Alnarp valley may be attributed to the

exclusive reliance on sedimentary coring and the scarcity of sedimentary exposures of considerable scale for investigating large-scale faulting and folding. Alternatively, the absence of observed deformation within the Alnarp valley in Scania could stem from variations in the regional bed conditions of the ice sheet.

This study encourages the continued investigation of the Alnarp valley using different means of investigations such as seismic or ground penetrating radar. Additionally, continued glaciotectonically focused investigations on Ven are recommended to fully comprehend the islands glaciotectonic evolution. Future studies may also incorporate geochemical analysis of the till beds, to conclude if LF9 and LF12 are the same till bed, which would enable the elimination of one of the models.

### 13 Acknowledgements

I would like to express my heartfelt appreciation to Sven Lukas and Åsa Sonjasdotter for their unwavering support during my fieldwork. Sven's guidance and supervision have been crucial in shaping this study, providing me with the necessary direction and insight. Åsa's gracious hospitality and provision of accommodation created an environment where I could fully immerse myself in my research, enabling me to conduct the study to the extent that I did.

Their contributions have been instrumental in the success of this project, and I am truly grateful for their kindness and support throughout. Thank you, Sven and Åsa, for your invaluable assistance. Lastly, I would like to express my gratitude to Tina Nilsson, whose assistance with the sampling of bulk samples was invaluable.

### 14 References

- Aber, J. S., & Ber, A. (2007). Glaciotectonism. In *Developments in Quaternary Sciences* (Vol. 6). Elsevier. [https://doi.org/10.1016/S1571-0866\(07\)00601-2](https://doi.org/10.1016/S1571-0866(07)00601-2)
- Aber, J.S., Croot, D.G., & Fenton, M.M. (1989). Cupola-Hills. In *Glaciotectonic Landforms and Structures* (pp. 71-90). *Glaciology and Quaternary Geology*, vol. 5. Springer. [https://doi.org/10.1007/978-94-015-6841-8\\_5](https://doi.org/10.1007/978-94-015-6841-8_5)
- Adrielson, L. (1984). Weichselian lithostratigraphy and glacial environment in the Ven-Glumslov area, southern Sweden. *Lundqua Thesis*, 16. Lund university
- Adrielson, L., Mohrén, E., & Daniel, E. (1981). *Jordarts Geologiska kartan 3C Helsingborg SV*. SGU Serie Ae nr 16.
- Allmendinger, R. W., Cardozo, N., & Fisher, D. (2012). *Structural geology algorithms: Vectors and*

- tensors in structural geology. Cambridge University Press.
- Alsopa, G. I., Weinberger, R., & Marco, S. (2018). Distinguishing thrust sequences in gravity driven fold and thrust belts. *Journal of Structural Geology*, *109*, 99-119. <https://doi.org/10.1016/j.jsg.2018.01.005>
- Anderson, J.B., Domack, E.W., & Kurtz, D.D. (1980). Observations of sediment-laden icebergs in Antarctic waters: Implications for glacial erosion and transport. *Journal of Glaciology*, *25*, 387–396.
- Anjar, J., Adrielsson, L., Larsen, N.K., Möller, P., & Barth, K. (2014). Weichselian history of the Fennoscandian ice sheet, S Sweden and SW Baltic Basin. *Boreas*, *43*, 608–626. <https://doi.org/10.1111/bor.12048>
- Barker, S., Starr, A., van der Lubbe, J., Doughty, A., Knorr, G., Conn, S., Lordsmith, S., Owen, L., Nederbragt, A., Hemming, S., Hall, I., Levay, L., & Party, I. E. S. S. (2022). Persistent influence of precession on northern ice sheet variability since the early Pleistocene. *Science*, *376*(6596). <https://doi.org/10.1126/science.abm4033>
- Barker, S., Starr, A., van der Lubbe, J., Doughty, A., Knorr, G., Conn, S., Lordsmith, S., Owen, L., Nederbragt, A., Hemming, S., Hall, I., Levay, L., & Party, I. E. S. S. (2022). Persistent influence of precession on northern ice sheet variability since the early Pleistocene. *Science*, *376*(6596), 961-+. <https://doi.org/10.1126/science.abm4033>
- Barth, K. (2011). Late Weichselian glacial and geomorphological reconstruction of South-Western Scania, Sweden (Examensarbeten i geologi vid Lunds universitet, Nr. 267, 28 pp.). Lund University.
- Batchelor, C. L., Margold, M., Krapp, M., Murton, D., Dalton, A. S., Gibbard, P. L., Stokes, C. R., Murton, J. B., & Manica, A. (2019). The configuration of Northern Hemisphere ice sheets through the Quaternary. *Nature Communications*, *10*, Article 3713. <https://doi.org/10.1038/s41467-019-11601-2>
- Batchelor, C. L., Margold, M., Krapp, M., Murton, D., Dalton, A. S., Gibbard, P. L., Stokes, C. R., Murton, J. B., & Manica, A. (2019). The configuration of Northern Hemisphere ice sheets through the Quaternary. *Nature Communications*, *10*, Article 3713. <https://doi.org/10.1038/s41467-019-11601-2>
- Benediktsson, I., Schomacker, A., Lokrantz, H., & Ingólfsson, O. (2010). The 1890 surge end moraine at Eyjabakkajökull, Iceland: a re-assessment of a classic glaciotectonic locality. *Quaternary Science Reviews*, *29*(3-4), 484-506. <https://doi.org/10.1016/j.quascirev.2009.10.004>
- Benn, D. I., & Evans, D. J. A. (2010). *Glaciers & glaciation* (2nd ed.). Hodder Education.
- Benn, D.I. (2009). Glaciofluvial Sediments. In V. Gornitz (Ed.), *Encyclopedia of Paleoclimatology and Ancient Environments* (Encyclopedia of Earth Sciences Series). Springer, Dordrecht. [https://doi.org/10.1007/978-1-4020-4411-3\\_98](https://doi.org/10.1007/978-1-4020-4411-3_98)
- Benn, D.I., & Lukas, S. (2021). Macrofabric. In Evans, D.J., & Benn, D.I. (Eds.), *A Practical Guide to the Study of Glacial Sediments* (2nd ed., Chapter 5). Quaternary Research Association.
- Bennett, M. R., Huddart, D., Waller, R. I., Cassidy, N., Tomio, A., Zukowskyj, P., Midgley, N. G., Cook, S. J., Gonzalez, S., & Glasser, N. F. (2004). Sedimentary and tectonic architecture of a large push moraine: a case study from Hagafellsjökull-Eystri, Iceland. *Sedimentary Geology*, *172*(3-4), 269-292. <https://doi.org/10.1016/j.sedgeo.2004.10.002>
- Berglund, B. E., & Rapp, A. (1988). Geomorphology, climate and vegetation in North—West Scania, Sweden, during the Late Weichselian. *Geographia Polonica*, *55*, 13-36.
- Berglund, B.E., & Lagerlund, E. (1981). Eemian and Weichselian stratigraphy in South Sweden. *Boreas*, *10*, 323-362. <https://doi.org/10.1111/j.1502-3885.1981.tb00494.x>
- Black, R. F. (1976). PERIGLACIAL FEATURES INDICATIVE OF PERMAFROST - ICE AND SOIL WEDGES. *Quaternary Research*, *6*(1), 3-26. [https://doi.org/10.1016/0033-5894\(76\)90037-5](https://doi.org/10.1016/0033-5894(76)90037-5)
- Boothroyd, J., & Ashley, G. (1975). Processes, bar morphology, and sedimentary structures on braided outwash fans, Northeastern Gulf of Alaska. *Glaciofluvial and Glaciolacustrine Sedimentation SEPM Spec. Publ.*, *23*, 192-222. <https://doi.org/10.2110/pec.75.23.0193>
- Boulton, G. S. (1970). On the deposition of subglacial and melt-out tills at the margins of certain Svalbard glaciers. *Journal of Glaciology*, *9*, 231-245.
- Brennand, T. A. (1994). MACROFORMS, LARGE BEDFORMS AND RHYTHMIC SEDIMENTARY SEQUENCES IN SUBGLACIAL ESKERS, SOUTH-CENTRAL ONTARIO - IMPLICATIONS FOR ESKER GENESIS AND MELTWATER REGIME. *Sedimentary Geology*, *91*(1-4), 9-55. [https://doi.org/10.1016/0037-0738\(94\)90122-8](https://doi.org/10.1016/0037-0738(94)90122-8)
- Bridge, J. S. (1993). The interaction between channel geometry, water flow, sediment transport and depo-

- sition in braided rivers. *Geological Society, London, Special Publications*, 75(1), 13- 71. <https://doi.org/doi:10.1144/GSL.SP.1993.075.01.02>
- Bridge, J. S. C. (1993). The interaction between channel geometry, water flow, sediment transport and deposition in braided rivers. *Geological Society, London, Special Publications*, 75, 13 - 71.
- Cardozo, N., & Allmendinger, R. W. (2013). Spherical projections with OSXStereonet. *Computers & Geosciences*, 51, 193–205. <https://doi.org/10.1016/j.cageo.2012.07.021>
- Cardozo, N., & Allmendinger, R. W. (2013). Spherical projections with OSXStereonet. *Computers & Geosciences*, 51, 193–205. <https://doi.org/10.1016/j.cageo.2012.07.021>
- Carrivick, J. L., & Tweed, F. S. (2013). Proglacial lakes: character, behaviour and geological importance. *Quaternary Science Reviews*, 78, 34-52. <https://doi.org/10.1016/j.quascirev.2013.07.028>
- Chandler, B. M. P., Lovell, H., Boston, C. M., Lukas, S., Barr, I. D., Benediktsson, Í. Ö., Benn, D. I., Clark, C. D., Darvill, C. M., Evans, D. J. A., Ewertowski, M. W., Loibl, D., Margold, M., Otto, J.-C., Roberts, D. H., Stokes, C. R., Storrar, R. D., & Stroeven, A. P. (2018). Glacial geomorphological mapping: A review of approaches and frameworks for best practice. *Earth-Science Reviews*, 185, 806-846. <https://doi.org/10.1016/j.earscirev.2018.07.015benn>
- Christensen, J. (2019). Exploring the Extent of Artificial Agricultural Drainage using GIS Tools (Soil and Water Conservation Society). Paper presented at the 2019 Annual Conference of the Soil and Water Conservation Society, Pittsburgh, PA.
- Clarke, C. D., Hughes, A. L. C., Greenwood, S. L., Spagnolo, M., & Ng, F. S. L. (2009). Size and shape characteristics of drumlins, derived from a large sample, and associated scaling laws. *Quaternary Science Reviews*, 28(7-8), 677-692. <https://doi.org/10.1016/j.quascirev.2008.08.035>
- Clarke, P. U. (1987). Subglacial sediment dispersal and till composition. *The Journal of Geology*, 95 (4), 527–541. <http://www.jstor.org/stable/30081084>
- Cowan, D. S. (1985). STRUCTURAL STYLES IN MESOZOIC AND CENOZOIC MELANGES IN THE WESTERN CORDILLERA OF NORTH-AMERICA. *Geological Society of America Bulletin*, 96(4), 451- 462. [https://doi.org/10.1130/0016-7606\(1985\)96<451:Ssimac>2.0.Co;2](https://doi.org/10.1130/0016-7606(1985)96<451:Ssimac>2.0.Co;2)
- Davis, G. H., Bump, A. P., García, P. E., & Ahlgren, S. G. (2000). Conjugate Riedel deformation band shear zones. *Journal of Structural Geology*, 22(2), 169-190. [https://doi.org/10.1016/s0191-8141\(99\)00140-6](https://doi.org/10.1016/s0191-8141(99)00140-6)
- de Boer, B., & van de Wal, R. (2021). Ice sheets in the Cenozoic. In A. Fowler & F. Ng (Eds.), *Glaciers and Ice Sheets in the Climate System* (pp. 415-430). Springer International Publishing. [https://doi.org/10.1007/978-3-030-42584-5\\_16](https://doi.org/10.1007/978-3-030-42584-5_16)
- Dewald, N., Lewington, E. L. M., Livingstone, S. J., Clark, C. D., & Storrar, R. D. (2021). Distribution, characteristics and formation of esker enlargements. *Geomorphology*, 392, Article 107919. <https://doi.org/10.1016/j.geomorph.2021.107919>
- Dowdeswell, J.A. (2009). Ice-Rafted Debris (IRD). In V. Gornitz (Ed.), *Encyclopedia of Paleoclimatology and Ancient Environments*. Encyclopedia of Earth Sciences Series. Springer, Dordrecht. [https://doi.org/10.1007/978-1-4020-4411-3\\_113](https://doi.org/10.1007/978-1-4020-4411-3_113)
- Earle, S. (2019). *Physical Geology – 2nd Edition*. Victoria, B.C.: BCcampus. Retrieved from <https://opentextbc.ca/physicalgeology2ed/>
- Ehlers, J., Gibbard, P. L., & Hughes, P. D. (2018). Quaternary glaciations and chronology. In *Past Glacial Environments* (pp. 77-101). Elsevier. <https://doi.org/10.1016/B978-0-08-100524-8.00003-8>
- Engel, O. D. (1914). Effects of Continental Glaciation on Agriculture. Part II. *Bulletin of the American Geographical Society*, 46(5), 336–355. <https://doi.org/10.2307/201815>
- Erdmann, E. (1883). Bidrag till kännedomen om de lösa jordaflagringerne i Skåne. *Geologiska Föreningen i Stockholm Förhandlingar*, 2(4), 101-116. <https://doi.org/10.1080/11035897409454004>
- Evans, D. J. A. (2000). A gravel outwash/deformation till continuum, Skálafellsjökull, Iceland. *Geografiska Annaler Series a-Physical Geography*, 82A(4), 499-512. <https://doi.org/10.1111/j.0435-3676.2000.00137.x>
- Evans, D.J.A. (2017). *Till: A Glacial Process Sedimentology*. John Wiley & Sons Ltd. <https://doi.org/10.1002/9781118652541>
- Evans, D.J.A., & Benn, D. (2010). *Glaciers and Glaciation* (2nd ed.). London: Routledge.
- Evans, D.J.A., & Benn, D.I. (2021). Facies description and the logging of sedimentary particles. In Evans, D.J., & Benn, D.I. (Eds.), *A Practical Guide to the Study of Glacial Sediments* (2nd ed., Chapter 2). Quaternary Research Association.
- Evans, D.J.A., Phillips, E.R., Hiemstra, J.F., & Auton,



- C.A. (2006). Subglacial till: Formation, sedimentary characteristics and classification. *Earth-Science Reviews*, 78(1–2), 115-176. <https://doi.org/10.1016/j.earscirev.2006.04.001>
- Eyles, N., & Menzies, J. (1983). The Subglacial Landsystem. In N. Eyles (Ed.), *Glacial Geology* (pp. 19-70). Pergamon. <https://doi.org/10.1016/B978-0-08-030263-8.50008-7>.
- Florén, K., & Ohlsson, M. (2006). Glacifluviala avlagrings- och erosionsformer i sydöstra Skåne – en sedimentologisk och geomorfologisk undersökning (Seminarieuppsats nr 124). Lund University.
- Freeze, R.A. and Cherry, J.A. (1979). Groundwater. Prentice-Hall Inc., Englewood Cliffs, Vol. 7632, 604.
- Gehrmann, A., Pedersen, S. A. S., & Meschede, M. (2022). New insights into the structural development and shortening of the southern Jasmund Glacitectonic Complex (Rügen, Germany) based on balanced cross sections. *International Journal of Earth Sciences*, 111(6), 1697-1715. <https://doi.org/10.1007/s00531-022-02216-y>
- Gustafsson, O. (1983). Beskrivning till hydrogeologiska kartbladet Trelleborg NO/ Malmö SO. SGU Serie Ag nr 6.
- Harris, C., Williams, G., Brabham, P., Eaton, G., & McCarroll, D. (1997). Glaciotectonized Quaternary sediments at Dinas Dinlle, Gwynedd, North Wales, and their bearing on the style of deglaciation in the eastern Irish Sea. *Quaternary Science Reviews*, 16(1), 109-127. [https://doi.org/10.1016/s0277-3791\(96\)00050-9](https://doi.org/10.1016/s0277-3791(96)00050-9)
- Harry, D. G., & Gozdzik, J. S. (1988). Ice wedges: Growth, thaw transformation, and palaeoenvironmental significance. *Journal of Quaternary Science*, 3, 39-55. <https://doi.org/10.1002/jqs.3390030107>
- Hart, J. K. (2013). Depositional processes. In J. F. Shroder (Ed.), *Treatise on Geomorphology* (pp. 113–126). Academic Press. <https://doi.org/10.1016/B978-0-12-374739-6.00199-8>
- Hoffmann, G., & Reicherter, K. (2012). Soft-sediment deformation of Late Pleistocene sediments along the southwestern coast of the Baltic Sea (NE Germany). *International Journal of Earth Sciences*, 101(1), 351-363. <https://doi.org/10.1007/s00531-010-0633-z>
- Hoffmann, G., & Reicherter, K. (2012). Soft-sediment deformation of Late Pleistocene sediments along the southwestern coast of the Baltic Sea (NE Germany). *International Journal of Earth Sciences*, 101(1), 351-363. <https://doi.org/10.1007/s00531-010-0633-z>
- Hoffmann, K., & Piotrowski, J. A. (2001). Till mélange at Amsdorf, central Germany: sediment erosion, transport and deposition in a complex, soft-bedded glacial system. *Sedimentary Geology*, 140, 215-234.
- Holmström, L. (1879). Bidrag til kändedomen af moränbildningarne på Hven och närliggande skånska kust. *Geologiska Föreningen i Stockholm Förhandlingar*, 2(4), 96-101. <https://doi.org/10.1080/11035897409454003>
- Houmark-Nielsen, M. (1994). Late Pleistocene stratigraphy, glaciation chronology and Middle Weichselian environmental history from Klintholm, Mon, Denmark. *Bulletin of the Geological Society of Denmark*, 41, 181-202.
- Houmark-Nielsen, M. (1999). A lithostratigraphy of Weichselian glacial and interstadial deposits in Denmark. *Bulletin of the Geological Society of Denmark*, 46, 101-114.
- Houmark-Nielsen, M. (2003). Signature and timing of the Kattégat Ice Stream: onset of the Last Glacial Maximum sequence at the southwestern margin of the Scandinavian Ice Sheet. *Boreas*, 32(1), 227-241. <https://doi.org/10.1080/03009480310001128>
- Houmark-Nielsen, M., & Kjær, K. H. (2003). Southwest Scandinavia, 40-15 kyr BP: palaeogeography and environmental change. *Journal of Quaternary Science*, 18(8), 769-786. <https://doi.org/10.1002/jqs.802>
- Jakobsen, P. R. (1996). Distribution and intensity of glaciotectionic deformation in Denmark. *Bulletin of the Geological Society of Denmark*, 42, 175-185.
- Jakobsen, P. R. (2003). GIS based map of glaciotectionic phenomena in Denmark. *Geological Quarterly*, 47(4), 331–338. Warszawa.
- Jakobsen, P. R., & Overgaard, T. (2002). Georadar facies and glaciotectionic structures in ice marginal deposits, northwest Zealand, Denmark. *Quaternary Science Reviews*, 21(8-9), 917-927, Article Pii s0277-3791(01)00045-2. [https://doi.org/10.1016/s0277-3791\(01\)00045-2](https://doi.org/10.1016/s0277-3791(01)00045-2)
- Johnsson G. (1956). *Glacialmorfologiska studier i södra sverige; med särskild hänsyn till glaciala riktningselement och periglaciala frostfenomen*. P. Lindstedts universitetsbokhandel.
- Juliusson, O. (2021). Följder av interaktioner mellan inlandsis och berggrund i Ullstorp, Skåne, södra Sverige. Examensarbeten i geologi vid Lunds universitet, Nr. 626, 53 sid. 45 hp.
- Krumbein, W. C. (1939). Preferred orientation of pebb-

- bles in sedimentary deposits. *Journal of Geology*, 47, 673–706.
- Krüger, J., & Kjær, K. H. (1999). A data chart for field description and genetic interpretation of glacial diamicts and associated sediments -: with examples from Greenland, Iceland, and Denmark. *Boreas*, 28(3), 386-402. <Go to ISI>://WOS:000082414100005
- Krzyszowski, D., & Koszka-Maron, D. (2018). Stratigraphic position and sedimentary environment of Late Pleistocene deposits along the cliffed coast of the middle part of the Polish Baltic coast. *Geological Quarterly*, 62(1), 48-68. <https://doi.org/10.7306/gq.1392>
- Lantmäteriet. (2019). *Laserdata\_NH\_2019\_laz\_Lidardata*. Retrieved from [https://www.geodata.se/geodataportalen/srv/swe/catalog/search#/search?resultType=swe-details&\\_schema=iso19139\\*&type=dataset%20or%20series&from=1&to=20](https://www.geodata.se/geodataportalen/srv/swe/catalog/search#/search?resultType=swe-details&_schema=iso19139*&type=dataset%20or%20series&from=1&to=20)
- Larsen, N. K., Knudsen, K. L., Krohn, C. F., Kronborg, C., Murray, A. S., & Nielsen, O. B. (2009). Late Quaternary ice sheet, lake and sea history of southwest Scandinavia - a synthesis. *Boreas*, 38(4), 732-761. <https://doi.org/10.1111/j.1502-3885.2009.00101.x>
- Lee, J. R., & Phillips, E. R. (2008). Progressive soft sediment deformation within a subglacial shear zone - a hybrid mosaic-pervasive deformation model for Middle Pleistocene glaciotectionised sediments from eastern England. *Quaternary Science Reviews*, 27(13-14), 1350-1362. <https://doi.org/10.1016/j.quascirev.2008.03.009>
- Lloyd, J.W. (1983). Hydrogeology in glaciated terrain. In N. Eyles (Ed.), *Glacial Geology* (pp. 349–368). Pergamon.
- Lukas, S., & Sass, O. (2011). The formation of Alpine lateral moraines inferred from sedimentology and radar reflection patterns: A case study from Gornergletscher, Switzerland. *Geological Society of London Special Publications*, 354, 77-92. <https://doi.org/10.1144/SP354.5>
- Maclachlan, J. C., & Eyles, C. H. (2013). Quantitative geomorphological analysis of drumlins in the Peterborough drumlin field, Ontario, Canada. *Geografiska Annaler Series a-Physical Geography*, 95A(2), 125-144. <https://doi.org/10.1111/geoa.12005>
- Madsen, T., & Piotrowski, J. (2012). Genesis of the glaciotectionic thrust-fault complex at Halk Hoved, southern Denmark. *Bulletin of the Geological Society of Denmark*, 60, 61-80. <https://doi.org/10.37570/bgdsd-2012-60-05>.
- Malmberg, C. (2022). *Mapping of Quaternary Geomorphology in Southern Dalarna: A LiDAR Study* (Bachelor of Science thesis Nr. B1172). University of Gothenburg.
- Markgren, M. (1961). Glaciotektoniken i Vens och Glumslövsområdets strandklingor. *Svensk geografisk årsbok, Volume Number(37)*, 115-123
- Mattsson, A. (1997). Glacial striae, glacial sediments and Weichselian ice movements in southernmost Sweden. *Sedimentary Geology*, 111(1-4), 285-311. [https://doi.org/10.1016/s0037-0738\(97\)00022-5](https://doi.org/10.1016/s0037-0738(97)00022-5)
- Mattsson, Å. (1997). Glacial striae, glacial sediments and Weichselian ice movements in southernmost Sweden. *Sedimentary Geology*, 111(1-4), 285-311. [https://doi.org/10.1016/s0037-0738\(97\)00022-5](https://doi.org/10.1016/s0037-0738(97)00022-5)
- Miall, A.D. (1977). A Review of the Braided River Depositional Environment. *Earth Science Reviews*, 13, 1-62. [http://dx.doi.org/10.1016/0012-8252\(77\)90055-1](http://dx.doi.org/10.1016/0012-8252(77)90055-1)
- Miller, U. (1977). Pleistocene deposits of the Alnarp Valley- Microfossils and their stratigraphic application. LUNDQUA thesis 4, 125pp.
- Mleczka, M., & Pisarska-Jamroz, M. (2021). A record of deglaciation-related shifting of the proximal zone of a sandur - a case study from the Gwda sandur, NW Poland (MIS 2). *Journal of Palaeogeography-English*, 10, Article 12. <https://doi.org/10.1186/s42501-021-00089-x>
- Möller, P., Alexanderson, H., Anjar, J., & Björck, S. (2020). MIS 3 sediment stratigraphy in southern Sweden sheds new light on the complex glacial history and dynamics across southern Scandinavia. *Boreas*, 49(3), 389-416. <https://doi.org/10.1111/bor.12433>
- Nesje, A., Røther, D.C., & Yde, J.C. (2023). Stratigraphy and age of a Neoglacial sedimentary succession of proglacial outwash and an alluvial fan in Langedalen, Veitastred, western Norway. *Boreas*, 52, 194-205. <https://doi.org/10.1111/bor.12608>
- Newton, A. M. W., Montelli, A., Batchelor, C. L., Bellwald, B., Harding, R., Huuse, M., Dowdeswell, J. A., Ottesen, D., Johansen, S. E., & Planke, S. (2024). Glacial seismic geomorphology and Plio-Pleistocene ice sheet history offshore NW Europe. *Geological Society, London, Special Publications*, 525(1), SP525-2023-2117. <https://doi.org/10.1144/SP525-2023-117>
- Nilsson, K. (1973). Glacialgeologiska problem i Sydvästskåne. Lund-qua thesis 1, 20pp. Lund university.
- Novak, B., & Pedersen, G. K. (2000). Sedimentology, seismic facies and stratigraphy of a Holocene spit-platform complex interpreted from high-resolution shallow seismics, Lysegrund, southern Kattegat,

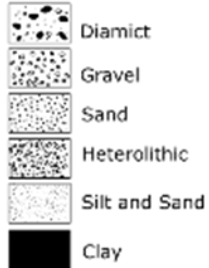
- Denmark. *Marine Geology*, 162(2-4), 317-335. [https://doi.org/10.1016/s0025-3227\(99\)00088-2](https://doi.org/10.1016/s0025-3227(99)00088-2)
- Olsen, H., & Andreasen, F. (1995). SEDIMENTOLOGY AND GROUND-PENETRATING RADAR CHARACTERISTICS OF A PLEISTOCENE SANDUR DEPOSIT. *Sedimentary Geology*, 99(1), 1-&. [https://doi.org/10.1016/0037-0738\(94\)00136-i](https://doi.org/10.1016/0037-0738(94)00136-i)
- Pasanen, A. (2009). Radar stratigraphy of the glacio-tectonically deformed deposits in the Isoniemi area, Haukipudas, Finland. *Bulletin of the Geological Society of Finland*, 81, 39-51. <https://doi.org/10.17741/bgsf/81.1.002>
- Pedersen, S. A. S. (1996). Progressive glacioteconic deformation in Weichselian and Palaeogene deposits at Feggeklit, northern Denmark. *Bulletin of the Geological Society of Denmark*, 42, 153-174. <Go to ISI>://WOS:000204235100003
- Pedersen, S. A. S. (2000). Superimposed deformation in glacioteconics. *Bulletin of the Geological Society of Denmark*, 46, 125-144.
- Pedersen, S. A. S., & Gravesen, P. (2009). Structural development of Maglevandsfald: a key to understanding the glacioteconic architecture of Mons Klint, SE Denmark. *Geological Survey of Denmark and Greenland Bulletin*(17), 29-32. <Go to ISI>://WOS:000272997100007
- Pedersen, S., Winslow, L., Boldreel, L., & Nørmark, E. (2020). Wrench-fault structures superimposed by glacioteconic complexes, interpreted from high-resolution reflection-seismic sections and boreholes along the western bank of Esrum Sø, north-east Sjælland, Denmark. *Bulletin of the Geological Society of Denmark*, 68, 171-193. <https://doi.org/10.37570/bgsd-2020-68-08>.
- Phillips, E., Everest, J., & Reeves, H. (2013). Micro-morphological evidence for subglacial multiphase sedimentation and deformation during overpressurized fluid flow associated with hydrofracturing. *Boreas*, 42 (2), 395-427. <https://doi.org/10.1111/j.1502-3885.2012.00261.x>
- Phillips, E.R. (2018). Glaciteconics. In J. Menzies & J.J.M. Van deerMeer (Eds.), *Past Glacial Environments* (Second Edition) (pp. 467-502). Elsevier. <https://doi.org/10.1016/B978-0-08-100524-8.00014-2>.
- Piotrowski, J. A., & Tulaczyk, S. (1999). Subglacial conditions under the last ice sheet in northwest Germany: ice-bed separation and enhanced basal sliding? *Quaternary Science Reviews*, 18(6), 737-751. [https://doi.org/10.1016/s0277-3791\(98\)00042-0](https://doi.org/10.1016/s0277-3791(98)00042-0)
- Piotrowski, J. A., Larsen, N. K., & Junge, F. W. (2004). Reflections on soft subglacial beds as a mosaic of deforming and stable spots. *Quaternary Science Reviews*, 23(9-10), 993-1000. <https://doi.org/10.1016/j.quascirev.2004.01.006>
- Pisarska-Jamroży, M., & Zielinski, T. (2012). Specific erosional and depositional processes in a Pleistocene subglacial tunnel in the Wielkopolska region, Poland. *Geografiska Annaler Series A Physical Geography*, 94, 429-443. <https://doi.org/10.2307/23254424>.
- Pochocka-Szwarc, K., & Krzyszkowski, D. (2015). The Outwash Plain Of The Rospuda River Valley – A Record Of Depositional Environments. *Studia Quaternaria*, 32, 63-78. <https://doi.org/10.1515/squa-2015-0006>.
- Rasmussen, L. A. (1973). The Quaternary stratigraphy and dislocations on Ven. *Bulletin of the Geological Institution of the University of Uppsala, New Series*, 5, 37-40.
- Raunholm, S., Larsen, E., & Sejrup, H. P. (2002). Weichselian sediments at Foss-Eikeland, Jæren (southwest Norway): sea-level changes and glaciation history. *Journal of Quaternary Science*, 17(3), 241-260. <https://doi.org/10.1002/jqs.674>
- Rensbergen, P., Hillis, R. R., Maltman, A. J., & Morley, C. K. (Eds.) (2003). *Subsurface sediment mobilization* (Vol. 216). Geological Society Special Publications. <https://doi.org/10.1144/GSL.SP.2003.216>
- Rijsdijk, K. F., Owen, G., Warren, W. P., McCarroll, D., & van deer Meer, J. J. M. (1999). Clastic dykes in over-consolidated tills: Evidence for subglacial hydrofracturing at Killiney Bay, eastern Ireland. *Sedimentary Geology*, 129(1-2), 111-126. [https://doi.org/10.1016/S0037-0738\(99\)00093-7](https://doi.org/10.1016/S0037-0738(99)00093-7)
- Ringberg, B. (1987). Beskrivning till jordartskartan 2C Malmö NO. SGU Serie Ae nr 85.
- Rust, B. R. (1972). Pebble orientation in fluvial sediments. *Journal of Sedimentary Petrology*, 42, 384-388. <https://doi.org/10.1306/74d7255e-2b21-11d78648000102c1865d>
- Saad D. A. (2008). Agriculture-related trends in groundwater quality of the glacial deposits aquifer, central Wisconsin. *Journal of environmental quality*, 37(5 Suppl), S209-S225. <https://doi.org/10.2134/jeq2007.0053>
- Salamon, T. (2009). Origin of Pleistocene outwash plains in various topographic settings, southern Poland. *Boreas*, 38(2), 362-378. <https://doi.org/10.1111/j.1502-3885.2008.00049.x>
- Singh, A. K., Dubey, C. A., Singh, D. S., Kumar, D., &

- Sharma, R. (2023). Sedimentary Parameters and Evolution of the Outwash Plain Deposits during Late Holocene in the Gangotri Glacier Region, Garhwal Himalaya, India. *Journal of the Geological Society of India*, 99(9), 1309-1316. <https://doi.org/10.1007/s12594-023-2465-z>
- Smith, M.J. (2011). Digital mapping: Visualisation, interpretation and quantification of landforms. *Geomorphological Mapping: Methods and Applications*, 15, 225-251. <https://doi.org/10.1016/b978-0-444-53446-0.00008-2>
- Spagnolo, M., Clark, C. D., & Hughes, A. L. C. (2012). Drumlin relief. *Geomorphology*, 153, 179-191. <https://doi.org/10.1016/j.geomorph.2012.02.023>
- Stokes, C. R., Spagnolo, M., & Clark, C. D. (2011). The composition and internal structure of drumlins: complexity, commonality, and implications for a unifying theory of their formation. *Earth-Science Reviews*, 107, 398-422.
- Sun, R., Kaslilar, A., & Juhlin, C. (2020). Reprocessing of high-resolution seismic data for imaging of shallow groundwater resources in glacial deposits, SE, Sweden. *Near Surface Geophysics*. <https://doi.org/10.1002/nsg.12101>
- Svensson, H. (1990). RELICT PERIGLACIAL STRUCTURES - OCCURRENCES, AGE AND DEVELOPMENT IN DIFFERENT MATRICES ON A COASTAL-PLAIN OF SOUTHWESTERN SWEDEN. *Geografiska Annaler Series a-Physical Geography*, 72(1), 79-91. <https://doi.org/10.2307/521239>
- Swiatek, S., Belzyt, S., Pisarska-Jamrozy, M., & Woronko, B. (2023). Sedimentary Records of Liq-uefaction: Implications From Field Studies. *Journal of Geophysical Research-Earth Surface*, 128(8), Article e2023JF007152. <https://doi.org/10.1029/2023jf007152>
- Thomas, G. S. P., & Connell, R. J. (1985). Iceberg drop, dump and grounding structures from Pleistocene glaciolacustrine sediments, Scotland. *Journal of Sedimentary Petrology*, 55, 243-249.
- Van der Meer, J. J. M., Kjaer, K. H., & Krüger, J. (1999). Subglacial water-escape structures and till structures, Slettjokull, Iceland. *Journal of Quaternary Science*, 14(3), 191-205. [https://doi.org/10.1002/\(sici\)1099-1417\(199905\)14:3<191::Aid-jqs436>3.0.Co;2-#](https://doi.org/10.1002/(sici)1099-1417(199905)14:3<191::Aid-jqs436>3.0.Co;2-#)
- Van der Wateren, F. M. (1995). Structural geology and sedimentology of push moraines - processes of soft sediment deformation in a glacial environment and the distribution of glaciotectionic styles. *Mededelingen Rijks Geologische Dienst*, 54, 1-168.
- Van der Wateren, F. M. (1999). Structural geology and sedimentology of the Heiligenhafen till section, Northern Germany. *Quaternary Science Reviews*, 18 (14), 1625-1639. [https://doi.org/10.1016/s0277-3791\(98\)00120-6](https://doi.org/10.1016/s0277-3791(98)00120-6)
- Van der Wateren, F. M., Kluiving, S. J., & Bartek, L. R. (1999, Sep). Kinematic indicators of subglacial shearing. *Geological Society Special Publication [Deformation of glacial materials]*. Conference on Deformation of Glacial Materials, Geol Soc London, London, England.
- Waller, R., Murton, J., & Whiteman, C. (2009). Geological evidence for subglacial deformation of Pleistocene permafrost. *Proceedings of the Geologists Association*, 120, 155-162. <https://doi.org/10.1016/j.pgeola.2009.08.009>
- Watts, H., Booth, A. D., Reinardy, B. T. I., Killingbeck, S. F., Jansson, P., Clark, R. A., Chandler, B. M. P., & Nesje, A. (2022). An Assessment of Geophysical Survey Techniques for Characterising the Subsurface Around Glacier Margins, and Recommendations for Future Applications. *Frontiers in Earth Science*, 10, Article 734682. <https://doi.org/10.3389/feart.2022.734682>
- Willeit, M., Ganopolski, A., Calov, R., & Brovkin, V. (2019). Mid-Pleistocene transition in glacial cycles explained by declining CO<sub>2</sub> and regolith removal. *Science Advances*, 5(4), Article eaav7337. <https://doi.org/10.1126/sciadv.aav7337>
- Worsley, P. (2014). Ice-wedge growth and casting in a Late Pleistocene, periglacial, fluvial succession at Baston, Lincolnshire. *Mercian Geologist*, 18, 159-170.
- Yrgård, A. (1980). *Geomorfologisk kartläggning för naturvärdesbedömning och planering: En flygbilds-metodisk studie i syd- och mellansvensk terräng*. Statens naturvårdsverk PM 1339.

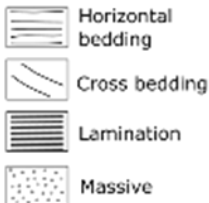
# 11 Appendix

## Legend:

### Lithology



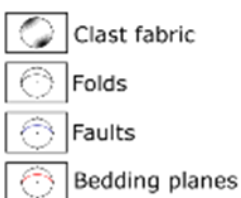
### Sorted sediments



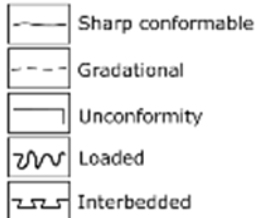
### Lateral distribution



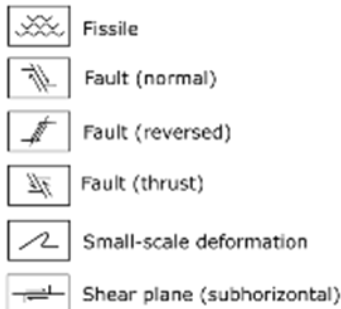
### Directional elements



### Basal contacts



### Structures



### Other structures



### Lithofacies code

#### Diamictic sediments

D Diamict

#### General appearance:

m Massive, homogenous  
h Heterogenous  
b Banded/stafified

#### Matrix:

M Medium-grained, silty-sandy  
F Fine-grained, clayey-silty

#### Clast/matrix relationship:

(m<sub>1</sub>) Matrix-supported, clast poor  
(m<sub>2</sub>) Matrix-supported, moderate  
(m<sub>3</sub>) Matrix-supported, clast-rich

#### Consistence when moist:

1 Loose  
2 Friable  
3 Firm, difficult to excavate  
4 Extremely firm

#### Sorted sediments

Gm Gravel, massive  
Gh Gravel, horizontal laminated  
Gd Gravel deformed  
Sm Sand, massive  
Sh Sand, horizontally laminated  
Sd Sand, deformed  
SiSh Silty sand, horizontally laminated  
SiSd Silty sand, deformed  
Fm Fines, massive  
Fh Fines, horizontally laminated

Figure A1. Symbology for the vertical profile logs featured below.

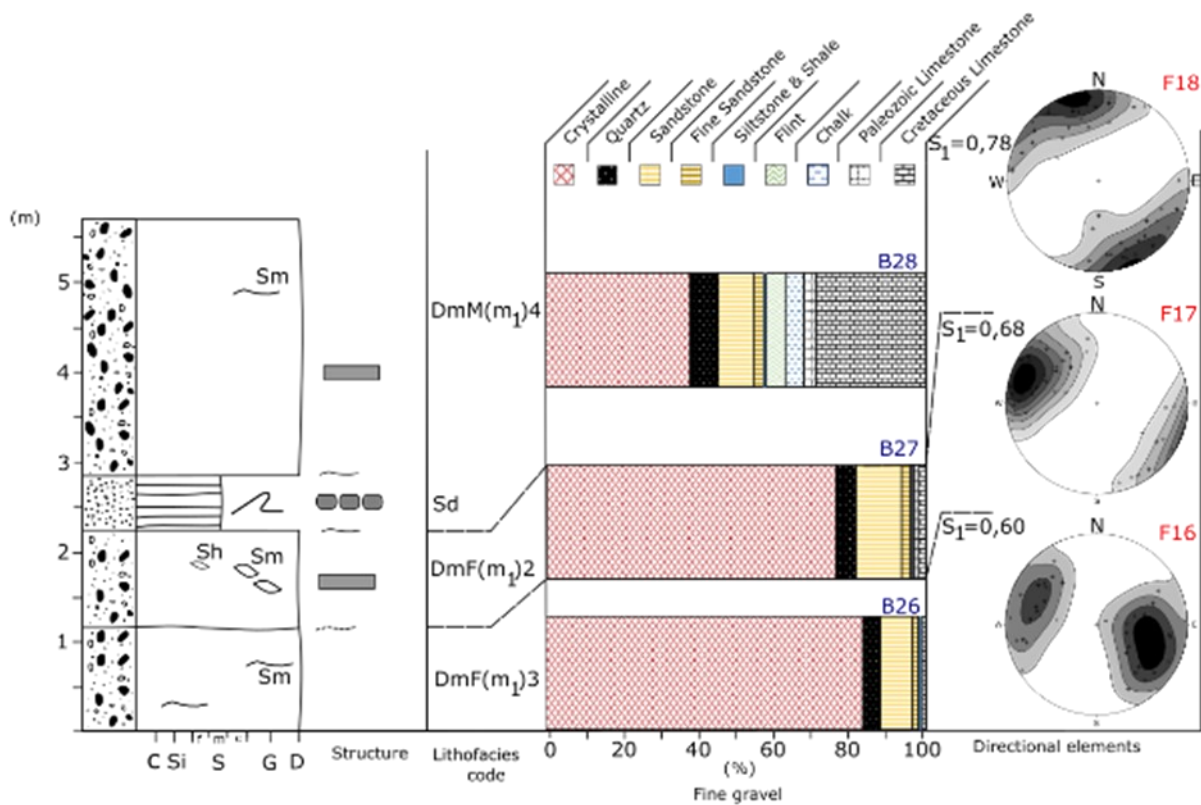


Figure A2. Vertical profile number 8 taken in the middle of section 2 seen in figure 8

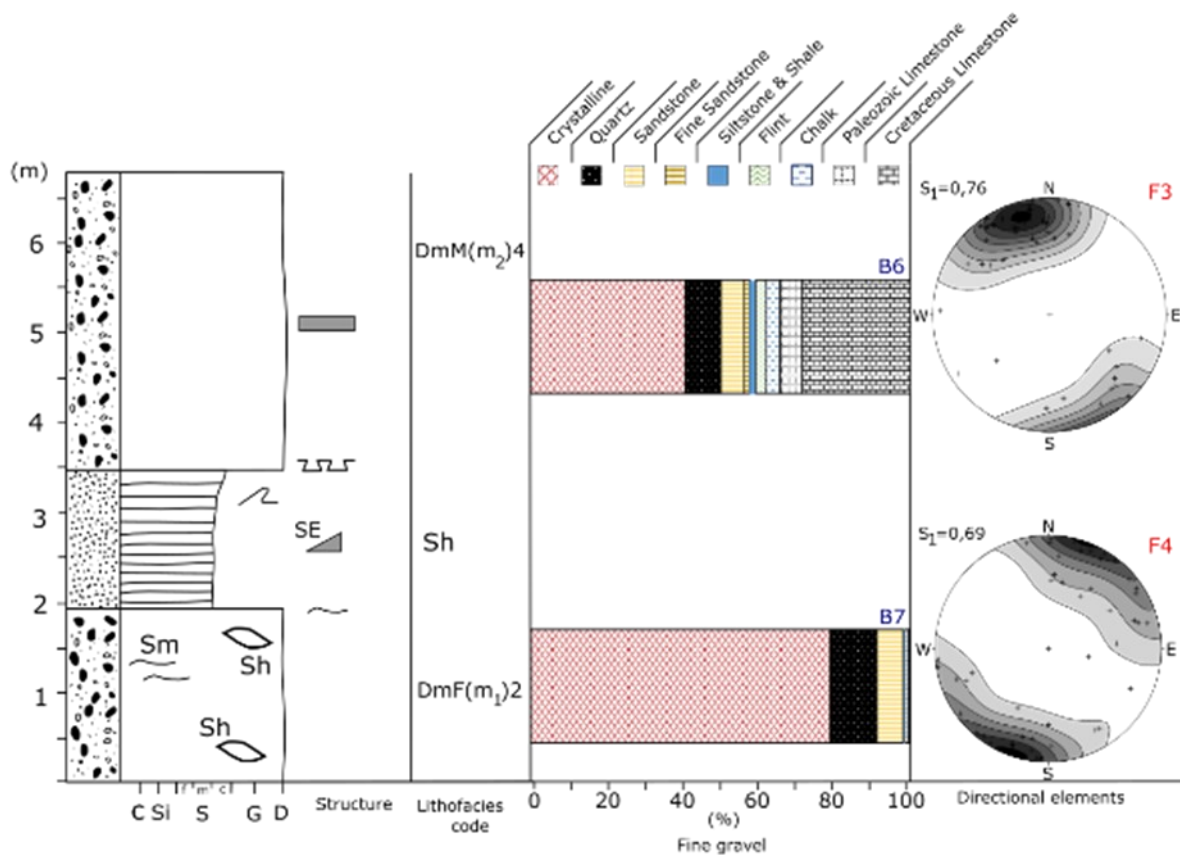


Figure A3. Vertical profile number 1 taken at 63.2 m in section 1 (Fig 7)

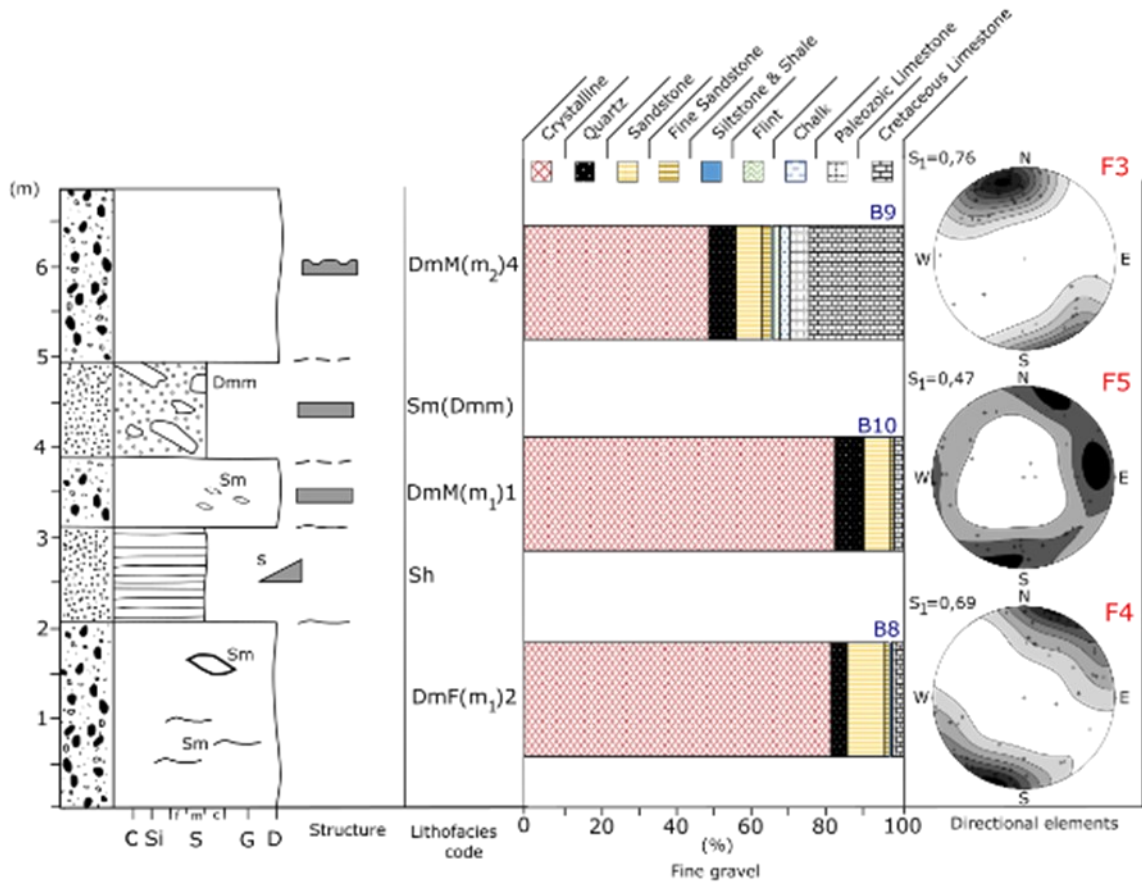


Figure A4. Vertical profile number 2 taken at 77.8 m of section 1 (Fig. 7)

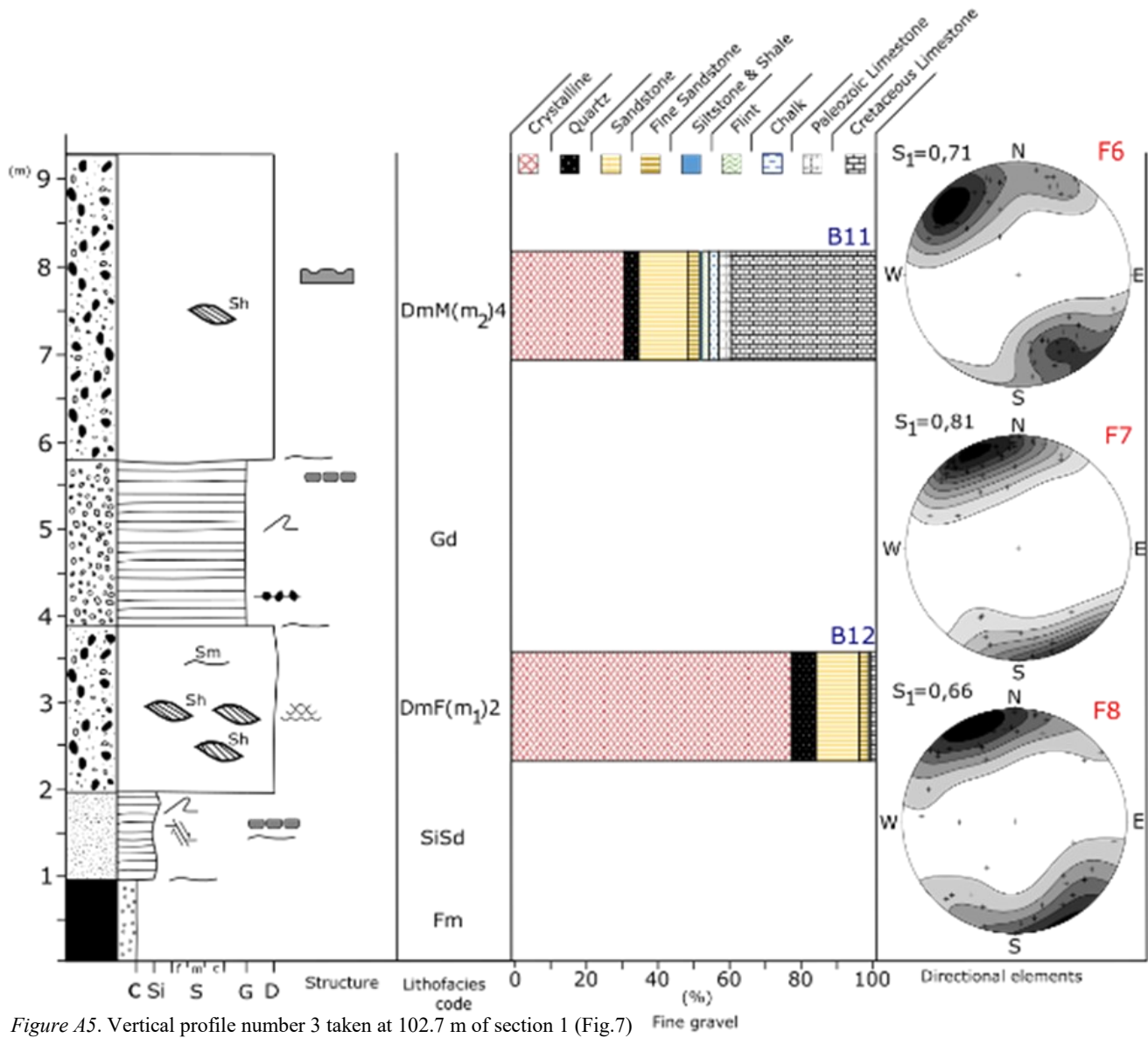


Figure A5. Vertical profile number 3 taken at 102.7 m of section 1 (Fig.7)



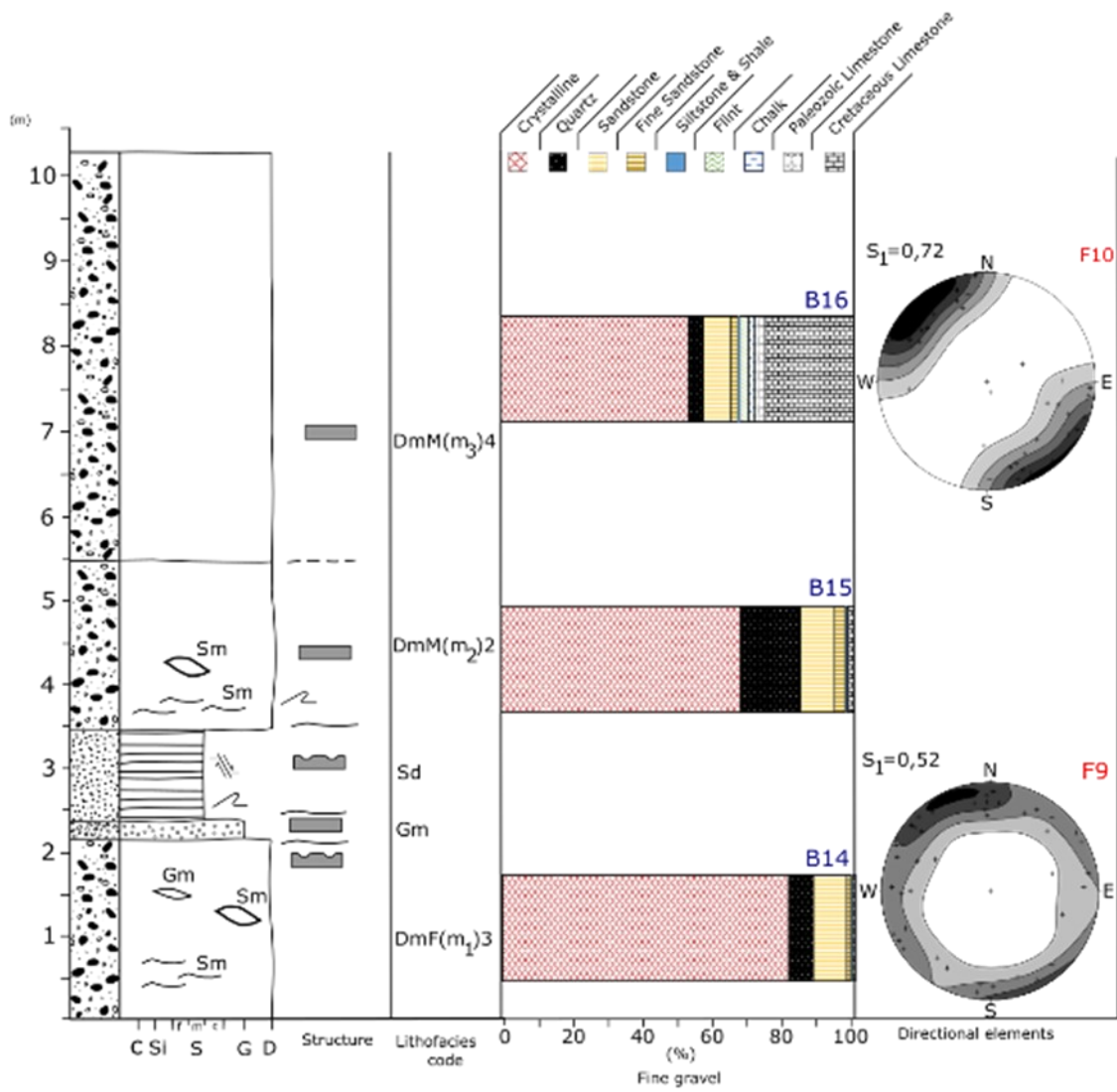


Figure A6. Vertical profile number 4 taken at 172 m of section 1 (Fig.7)

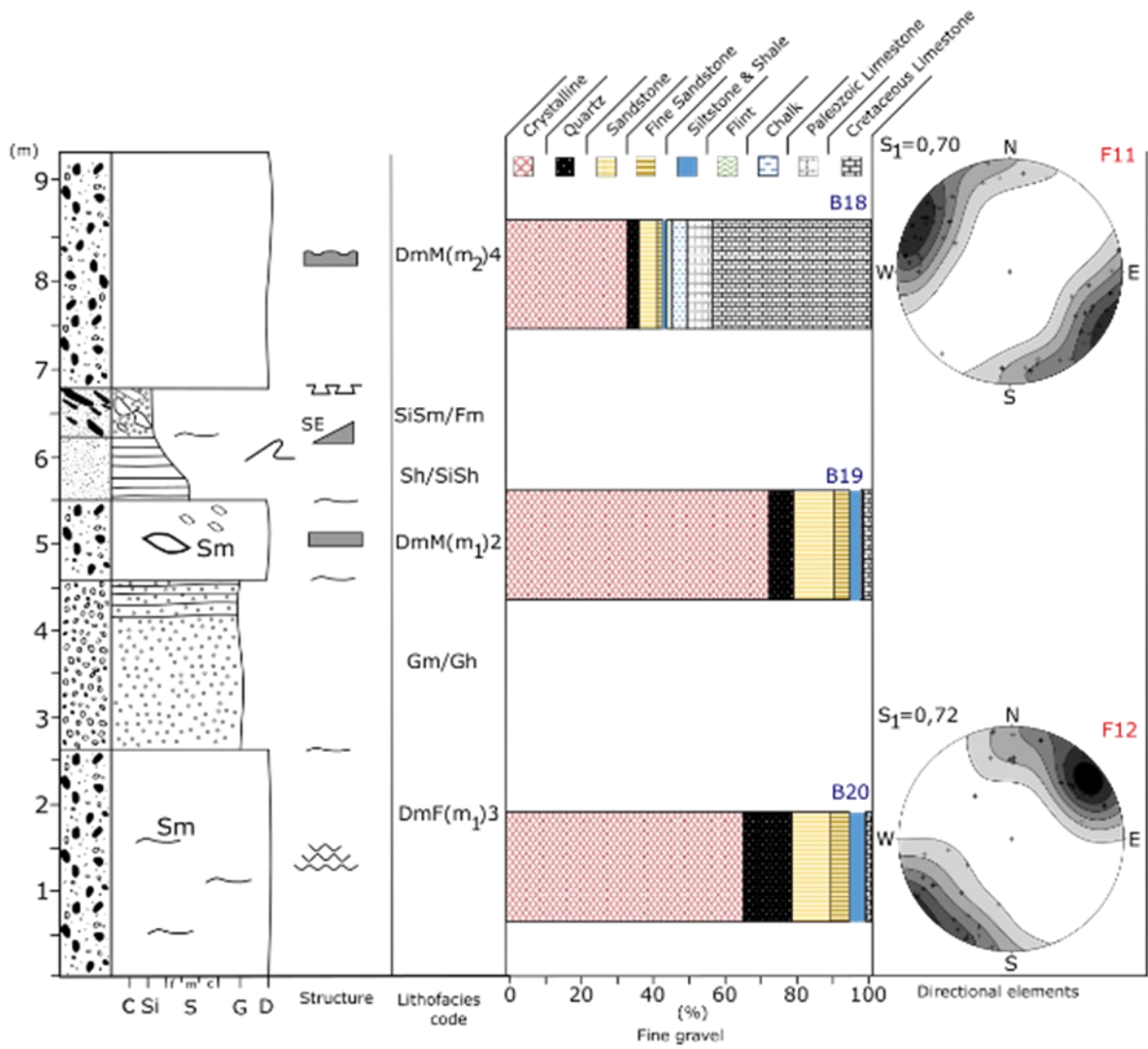


Figure A7. Vertical profile number 5 taken at 231.4 m of section 1 (Fig. 7)

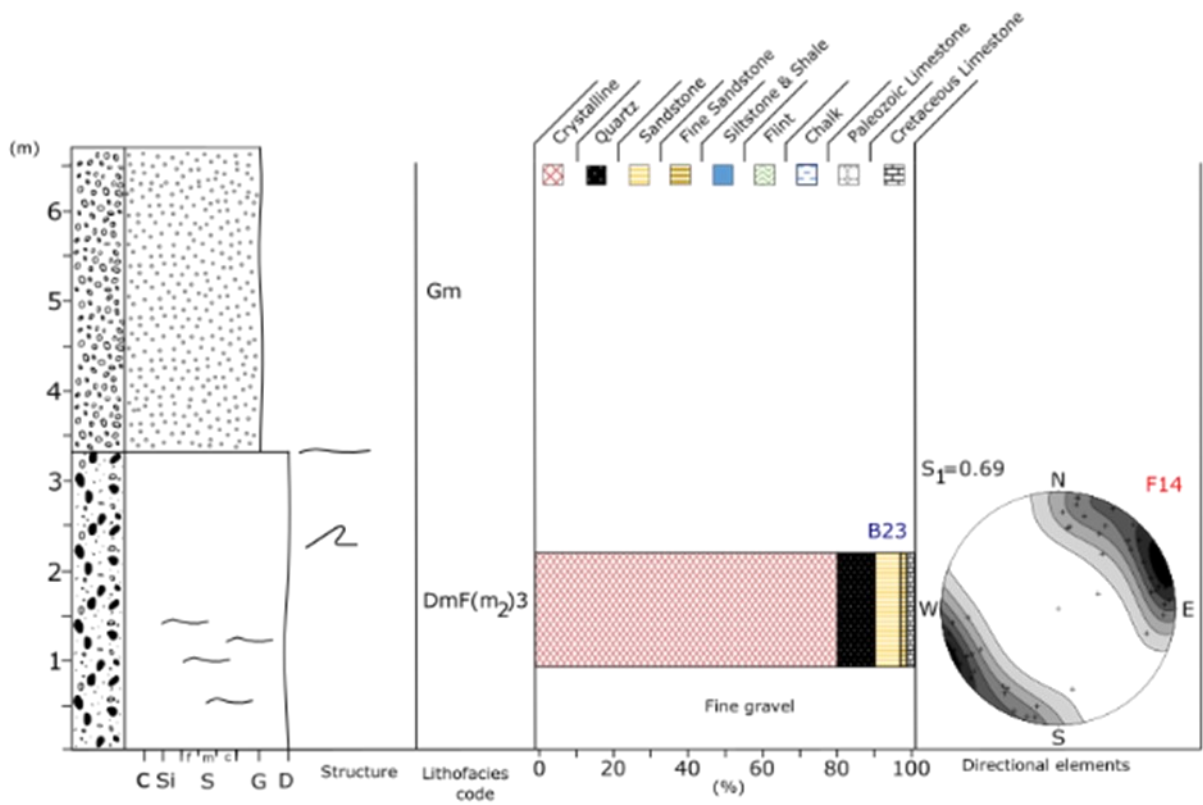


Figure A8. Vertical profile number 2 taken at 275.5 m of section 1 (Fig.7)

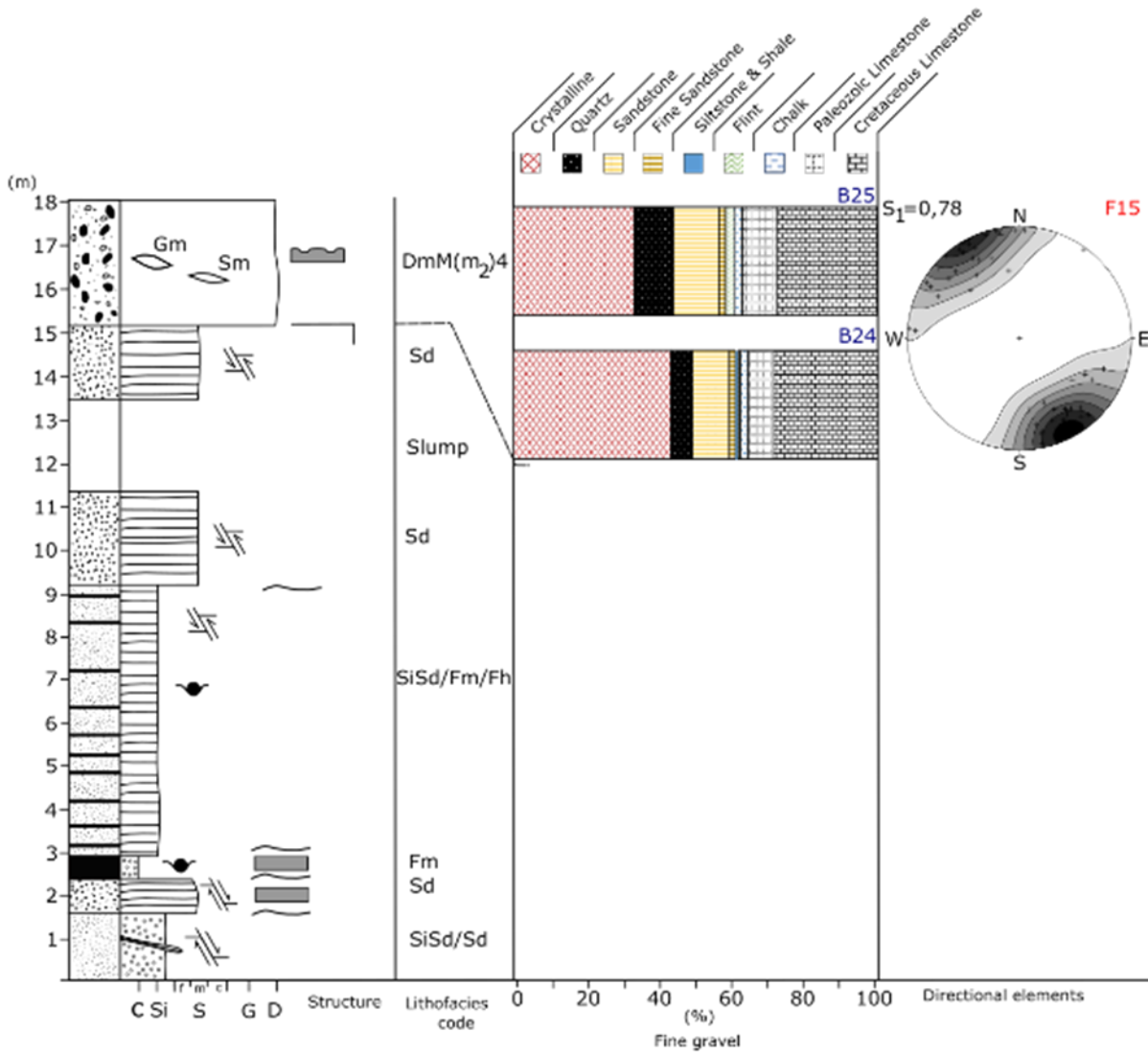


Figure A9. Vertical profile number 7 taken at 321.1 m of section 1 (Fig.7).

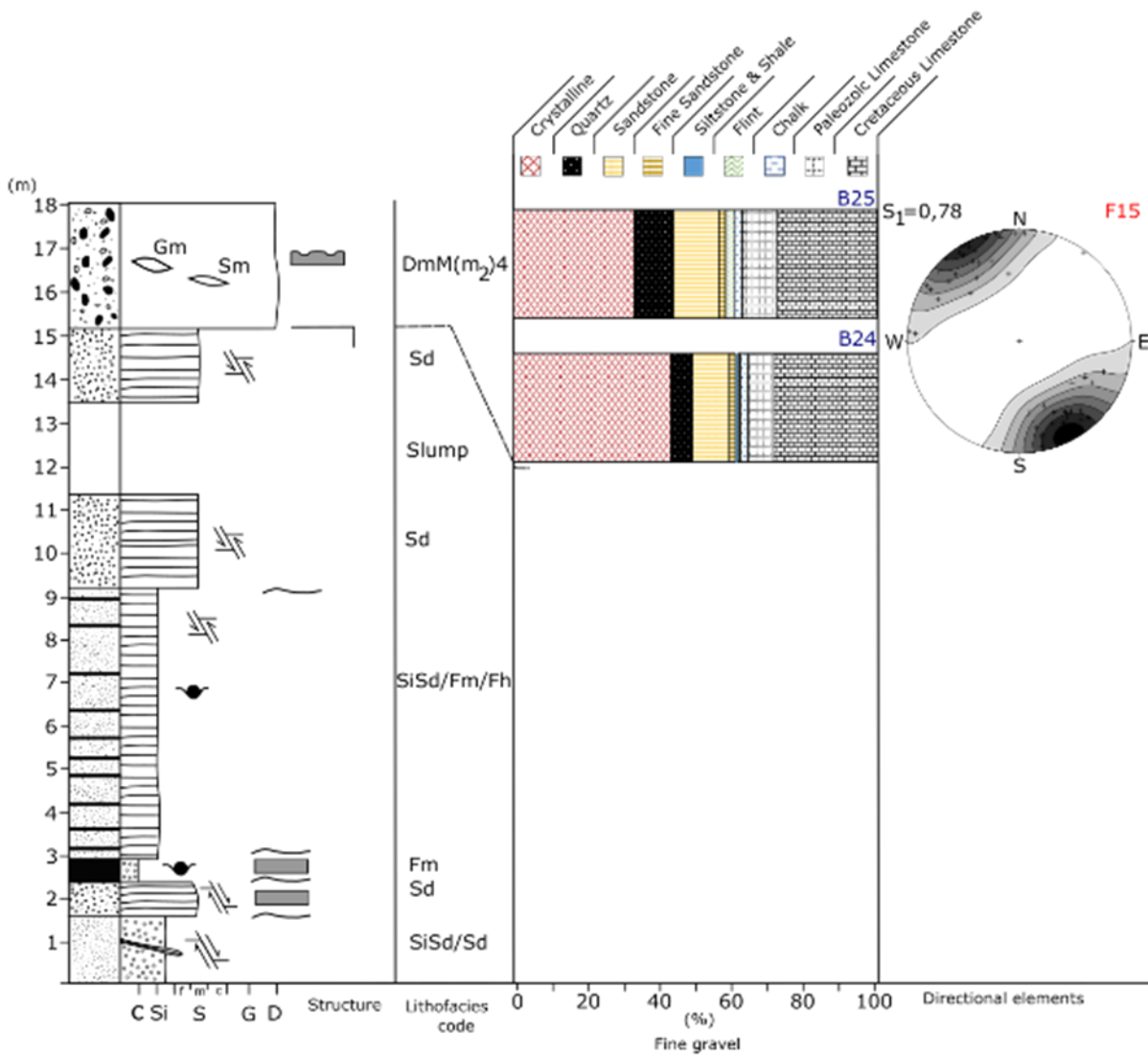


Figure A9. Vertical profile number 7 taken at 321.1 m of section 1 (Fig.7).





## Tidigare skrifter i serien

### ”Examensarbeten i Geologi vid Lunds universitet”:

619. Westberg, Märta, 2021: The preservation of cells in biomineralized vertebrate tissues of Mesozoic age – examples from a Cretaceous mosasaur (Reptilia, Mosasauridae). (45 hp)
620. Gleisner, Lovisa, 2021: En detaljerad undersökning av kalkstenslager i den mellanordoviciska gullhögenformationen på Billingen i Västergötland. (15 hp)
621. Bonnevier Wallstedt, Ida, 2021: Origin and early evolution of isopods - exploring morphology, ecology and systematics. (15 hp)
622. Selezeneva, Natalia, 2021: Indications for solar storms during the Last Glacial Maximum in the NGRIP ice core. (45 hp)
623. Bakker, Aron, 2021: Geological characterisation of geophysical lineaments as part of the expanded site descriptive model around the planned repository site for high-level nuclear waste, Forsmark, Sweden. (45 hp)
624. Sundberg, Oskar, 2021: Jordlagerföljden i Højeådalen utifrån nya borrhningar. (15 hp)
625. Sartell, Anna, 2021: The igneous complex of Ekmanfjorden, Svalbard: an integrated field, petrological and geochemical study. (45 hp)
626. Juliusson, Oscar, 2021: Implications of ice-bedrock dynamics at Ullstorp, Scania, southern Sweden. (45 hp)
627. Eng, Simon, 2021: Rödslem i svenska kraftdammar - Problematik och potentiella lösningar. (15 hp)
628. Kervall, Hanna, 2021: Feasibility of Enhanced Geothermal Systems in the Precambrian crystalline basement in SW Scania, Sweden. (45 hp)
629. Smith, Thomas, 2022: Assessing the relationship between hypoxia and life on Earth, and implications for the search for habitable exoplanets. (45 hp)
630. Neumann, Daniel, 2022: En mosasaurie (Reptilia, Mosasauridae) av paleocensk ålder? (15 hp)
631. Svensson, David, 2022: Geofysisk och geologisk tolkning av kritskollors utbredning i Ystadsområdet. (15 hp)
632. Allison, Edward, 2022: Avsättning av Black Carbon i sediment från Odensjön, södra Sverige. (15 hp)
633. Jirdén, Elin, 2022: OSL dating of the Mesolithic site Nilsvikdalen 7, Bjorøy, Norway. (45 hp)
634. Wong, Danny, 2022: GIS-analys av effekten vid stormflod/havsnivåhöjning, Morupstrakten, Halland. (15 hp)
635. Lycke, Björn, 2022: Mikroplast i vattenavsatta sediment. (15 hp)
636. Schönherr, Lara, 2022: Grön fältspat i Varbergskomplexet. (15 hp)
637. Funck, Pontus, 2022: Granens ankomst och etablering i Skandinavien under postglacial tid. (15 hp)
638. Brotzen, Olga M., 2022: Geologiska besöksmål och geoparker som plattform för popularisering av geovetenskap. (15 hp)
639. Lodi, Giulia, 2022: A study of carbon, nitrogen, and biogenic silica concentrations in *Cyperus papyrus*, the sedge dominating the permanent swamp of the Okavango Delta, Botswana, Africa. (45 hp)
640. Nilsson, Sebastian, 2022: PFAS- En sammanfattning av ny forskning, med ett fokus på föroreningskällor, provtagning, analysmetoder och saneringsmetoder. (15 hp)
641. Jägfeldt, Hans, 2022: Molnens påverkan på jordens strålningsbalans och klimatsystem. (15 hp)
642. Sundberg, Melissa, 2022: Paleontologiska egenskaper och syreisotopsutveckling i borrhkärnan Limhamn-2018: Kopplingar till klimatförändringar under yngre krita. (15 hp)
643. Bjeremo, Tim, 2022: A re-investigation of hummocky moraine formed from ice sheet decay using geomorphological and sedimentological evidence in the Vomb area, southern Sweden. (45 hp)
644. Halvarsson, Ellinor, 2022: Structural investigation of ductile deformations across the Frontal Wedge south of Lake Vättern, southern Sweden. (45 hp)
645. Brakebusch, Linus, 2022: Record of the end-Triassic mass extinction in shallow marine carbonates: the Lorüns section (Austria). (45 hp)
646. Wahlquist, Per, 2023: Stratigraphy and palaeoenvironment of the early Jurassic volcanoclastic strata at Djupadalsmölle, central Skåne, Sweden. (45 hp)
647. Gebremedhin, G. Gebreselassie, 2023: UPb geochronology of brittle deformation using LA-ICP-MS imaging on calcite veins. (45 hp)
648. Mroczek, Robert, 2023: Petrography of impactites from the Dellen impact structure, Sweden. (45 hp)
649. Gunnarsson, Niklas, 2023: Upper Ordovician stratigraphy of the Stora Sutarve core (Gotland, Sweden) and an assessment of the Hirnantian Isotope Carbon Excursion (HICE) in high-resolution. (45 hp)
650. Cordes, Beatrix, 2023: Vilken ny kunskap ger aDNA-analys om vegetationsutvecklingen i Nordeuropa under och efter Weichsel-istiden? (15 hp)
651. Bonnevier Wallstedt, Ida, 2023: Palaeocolour, skin anatomy and taphonomy of a soft-tissue ichthyosaur (Reptilia, Ichthyopterygia) from the Toarcian (Lower Jurassic) of Luxembourg. (45 hp)



652. Kryffin, Isidora, 2023: Exceptionally preserved fish eyes from the Eocene Fur Formation of Denmark – implications for palaeobiology, palaeoecology and taphonomy. (45 hp)
653. Andersson, Jacob, 2023: Nedslagskratrars inverkan på Mars yt-datering. En undersökning av Mars främsta ytdateringsmetod "Crater Counting". (15 hp)
654. Sundberg, Melissa, 2023: A study in ink – the morphology, taphonomy and phylogeny of squid-like cephalopods from the Jurassic Posidonia Shale of Germany and the first record of a loligosepiid gill. (45 hp)
655. Häggblom, Joanna, 2023: En patologisk sjöililja från silur på Gotland, Sverige. (15 hp)
656. Bergström, Tim, 2023: Hur gammal är jordens inre kärna? (15 hp)
657. Bollmark, Viveka, 2023: Ca isotope, oceanic anoxic events and the calcareous nannoplankton. (15 hp)
658. Madsen, Ariella, 2023: Polycykliska aromatiska kolväten i Hanöbuktens kustnära sediment - En sedimentologisk undersökning av vikar i närhet av pappersbruk. (15 hp)
659. Wangritthikraikul, Kannika, 2023: Holocene Environmental History of Warming Land, Northern Greenland: a study based on lake sediments. (45 hp)
660. Kurop, Anna, 2023: Reconstruction of the glacier dynamics and Holocene chronology of retreat of Helagsglaciären in Central Sweden. (45 hp)
661. Frisendahl, Kajsa, 2023: Holocene environmental history of Washington Land, NW Greenland: a study based on lake sediments. (45 hp)
662. Ryan, Cathal, 2023: Luminescence dating of the late Quaternary loess-palaeosol sequence at Velika Vrbica, Serbia. (45 hp)
663. Lindow, Wilma, 2023: U-Pb datering av zirkon i metasediment tillhörande Stora Le-Marstrand, SV Sverige. (15 hp)
664. Bengtsson, Kaisa, 2023: Geologisk karaktärisering av den kambriska Faluddensandstenen i Östersjön och dess lämplighet för koldioxidlagring. (15 hp)
665. Granbom, Johanna, 2023: Insights into simple crater formation: The Hummeln impact structure (Småland, Sweden). (45 hp)
666. Jonsson, Axel, 2023: Datering av vulkanen Rangitoto, Nya Zeeland, genom paleomagnetiska analysmetoder. (15 hp)
667. Muller, Elsa, 2023: Response of foraminifera *Ammonia confertitesta* (T6) to ocean acidification, warming, and Deoxygenation An experimental approach. (45 hp)
668. Struzynska, Patrycja, 2023: Petrography, geochemistry, and origin of deep magmatic cumulates in the Canary Islands – the xenolith record. (45 hp)
669. Krätzer, Tobias, 2023: Artificiella torskrev i Hanöbukten: Förstudie. (15 hp)
670. Khorshidian, Farid, 2023: 3D modelling and resistivity measurements for hydrogeological assessments in the northern part of Vombsänkan. (45 hp)
671. Sundberg, Oskar, 2023: Methodology for Stored Heat "Heat In Place" (HIP) assessment of geothermal aquifers – Exemplified by a study of the Arnager Greensand in SW Scania. (45 hp)
672. Haraldsson, Emil, 2023: Kan akademien hjälpa industrin utveckla mer robusta grundvattenmodeller? En studie av moderna Svenska industriframtagna grundvattenmodeller. (15 hp)
673. Barabas, Ricky, 2024: Kan chockmetamorfof i okonventionella mineral hjälpa till att identifiera nedslagskratrar? (15 hp)
674. Nilsson, Sebastian, 2024: The glaciotectonic evolution of Ven, Sweden: insights from a comprehensive structural, sedimentological, and geomorphological analysis. (45 hp)



## LUNDS UNIVERSITET

Geologiska institutionen  
Lunds universitet  
Sölvegatan 12, 223 62 Lund